# POLITECNICO DI TORINO

DEPARTMENT OF ENVIRONMENT, LAND AND INFRASTRUCTURE ENGINEERING
Master's Degree Programme in Environmental and Land Engineering


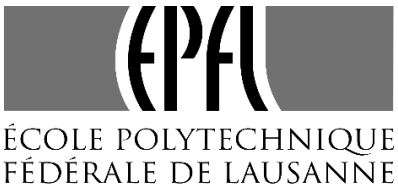


# PERFORMANCE OF RETAINING WALLS IN UNSATURATED SOILS

**Supervisors:**
Prof. Ph.D. Alessio Ferrari
Prof. Ph.D. Guido Musso
**Co-supervisor:**
Eng. Gianluca Speranza

**Candidate:**
Andrea Caldirola

**November 2018**

# Abstract

Retaining structures are built to support excavation or stabilize slope. These geostructures usually retains soils that are in partially saturated condition and their performance is influenced by the environmental actions. Current geotechnical analyses consider the soils totally dry or totally saturated. In geoengineering applications in the vadose zone, unsaturated soils may be present during part or all of their design lives (SIEMENS, 2017). This thesis works deals to investigate the interactional behaviour between retaining structures and unsaturated soils for both ultimate and serviceability conditions. A tempting challenge is the consideration of the hydro-mechanical behaviour of geomaterials for the geotechnical analysis of the geostructures.

The thesis work firstly recalls some fundamentals of unsaturated soils' principles, then, the employed materials are introduced and described. Their retention properties are investigated and, for one of the treated material, the Soil Water Characteristic Curve (SWRC) has been determined experimentally. After an analysis of the current standards (NTC 2018 and Eurocode 7), in this work an approach for the investigation of retaining walls performances during rainfalls events is illustrated.

Analytical analyses are performed, by mean of steady state and transitory solutions for Lateral Earth Pressure (LEP) and a Limit Equilibrium Method (LEM), to compute the active earth thrust on a gravity wall of three meters high. Subsequently a Finite Element Model (FEM) allowed to evaluate the global stability and the displacement of the structure, via coupled hydromechanical analysis.

The results highlight the wall to remain into operative conditions (FS=2.15), also afterwards an exceptional raining event of a hundred years period of returns. Furthermore, the same scenario, but with a malfunction of the drainage system, got the structure to limit conditions (SF=1.2).

Concluding, the presented hydromechanical analysis provides reasonable solutions to evaluate the existing pore water pressure distribution and the exerted thrust force on retaining structures, interacting with an unsaturated soil. Anyway, their performances can

be guaranteed only by a careful analysis of the precipitations event, and by a meticulous planning of the maintenance interventions.

# Sommario

Le opere di sostegno sono costruite per supportare scavi o per stabilizzare versanti. Solitamente, queste geostrutture sostengono terreni in condizioni di parziale saturazione e il loro funzionamento è influenzato dalle azioni ambientali. Le analisi geotecniche odierne considerano il terreno in condizioni totalmente sature o totalmente secche. Le applicazioni di tipo geo ingegneristico che si trovano a contatto con la zona vadosa, possono durante la loro vita progettuale, interagire con terreni insaturi (SIEMENS, 2017). L'obbiettivo di questa tesi è studiare le interazioni tra opere di sostegno e terreni non saturi, sia per gli stati limite ultimi che quelli di esercizio.

Nel seguente lavoro, vengono richiamate le basi dei principi sui terreni insaturi ed in seguito, sono presentati e descritti i materiali adottati. Se ne sono studiate le loro proprietà di ritenzione e per uno dei materiali utilizzati, si è determinata sperimentalmente la curva di ritenzione idrica (SWRC). Segue un'analisi delle normative tecniche vigenti (NTC 2008 ed Eurocodice 7) e la descrizione di una metodologia orientata a valutare le azioni e le prestazioni delle strutture di sostegno, in seguito ad eventi pluviometrici intensi.

Si sono effettuate analisi analitiche per mezzo di soluzioni stazionarie e transitorie basate sul metodo dell'equilibrio limite (LEM) e sul teorema statico (LEP) per calcolare la forza di spinta attiva agente su un muro a gravità alto tre metri. Successivamente, con un'analisi idromeccanica accoppiata, si sono valutati gli spostamenti e la stabilità globale dell'opera di sostegno su di un modello degli elementi finiti (FEM).

I risultati mostrano che il muro rimane in condizioni operative (FS=2.15), anche in seguito a precipitazioni di carattere eccezionale calcolate su un periodo di ritorno di cent'anni. Inoltre, si è evidenziato come un eventuale malfunzionamento dei dreni possa compromettere la funzionalità dell'opera (FS=1.2).

Concludendo, le analisi idromeccaniche adottate forniscono soluzioni ragionevoli per valutare le pressioni e le forze agenti a tergo di un'opera di sostegno interagente con terreni insaturi. Ciononostante, il corretto funzionamento della struttura può essere garantito solamente in seguito a un'accurata analisi delle precipitazioni e a un'altrettanta attenta pianificazione degli interventi di manutenzione.

# Contents

# List of Figures

# List of Tables

# Introduction

Retaining structures are built to support excavation or stabilize slope. These geostructures usually retains soils that are in partially saturated condition and their performance is influenced by the environmental actions. The main feature of unsaturated soils is the contemporary presence of a gaseous and a liquid phase in contact whit the solid skeleton; their interaction creates a phenomenon named suction, that act on the soil originating tension stresses. Current geotechnical analyses consider the soils totally dry or totally saturated. This assumption can be justified by its conservativism and by the major grade of difficulty encountered measuring property of multiphase media. Nowadays the increasing technologies allow to adequately characterize soils properties and the last decades studies furnished solid foundations above the unsaturated soil's behaviour. Furthermore, a conservatism approach induces higher costs and material consumption.

This aim of this work is to investigate the interactional behaviour between retaining structures and unsaturated soils, for both ultimate and serviceability conditions. This is done through the six chapters here briefly summarized.

In Chapter One are described the basics concepts of unsaturated soils, firstly is described the physical interaction between the different phases and the origin of the suction phenomena, then the hydraulic features, such as SWRC and flow equations, are explained, and finally the Bishop's stress definition, and its application in stress state and strength criteria, are illustrated.

In Chapter Two are illustrated the main techniques adopted to obtain the soil water retention curve, subsequently the materials involved in this work are presented. Then the method and the results, of the experimental determination of the SWRC, for one of the used soil, are presented.

In Chapter Three, the classical method for computing the lateral earth thrust on retaining structures are discussed and described. After analytical steady state and transitory solutions, for Lateral Earth Pressure (LEP) and a Limit Equilibrium Method (LEM), are presented.

In Chapter Four, the Italian (NTC 2018) and European (Eurocode 7) standards are analysed. In light of this an approach for the investigation of retaining walls performances during rainfalls events is illustrated.

In Chapter Five, the case of study is presented, subsequently hydrological analysis are performed and thus the active earth thrust is evaluated by mean of the analytical solutions described in Chapter Three

In Chapter Six, coupled hydromechanical analysis are introduced, subsequently the adopted geometry, mesh and boundary conditions of the Finite Element Model, are described. Then the results for six different scenarios, are commented in order to assess the reliability of the structure under critical rainfall event and by taking in to account the efficiency loss of the drain system.

Finally, in Chapter six a summary of the results is given.

# Chapter 1 Basic Concepts of unsaturated soils

An unsaturated soil is a media constituted by three phases: solid particle, a liquid one (generally is water but can be also another liquid such as petroleum) and a gaseous one (normally air but it can also be for instance, a natural gas). The presence of these two fluids, inside the interparticle voids, and the interactions that hose have in-between them and with the solid skeleton, highly influence the tensional state and the hydraulic behaviour.

Water in to a soil media can be grouped into three categories whose proportions are function of the pore dimension and of the kind of interaction with the solid interparticle. Gravitational water is the portion of water that can drain by mean of the only gravitational force (e.g. the water that naturally drain from the sand you can pick up by the foreshore). Capillary water is the water portion that gravity is not able to mobilize, it is hydraulically connected to the ground water table (GWT) and move through minute pores used as capillary tubes, to rise against the gravity force; it defines the so-called capillary fringe located above the GWT. Finally the adsorbed water is the one held by soil's particle by mean of molecular attraction by forces of five orders of magnitude bigger than the gravity, it can be removed from a soil just by warming it up to 100°C (DI MOLFETTA & SETHI, 2012).

Soils that covers our lands are mainly unsaturated (or at least they do experience this stage), that's easy to infer by thinking, at the water cycle (**Figure 1-1**). Indeed, vapour rise from a water body (also from others surface as plants and ground), condense into the atmosphere, it falls on the land under the form of rain, it infiltrates through the soil until it reaches an aquifer and it close the circle by filtrating till a water body.

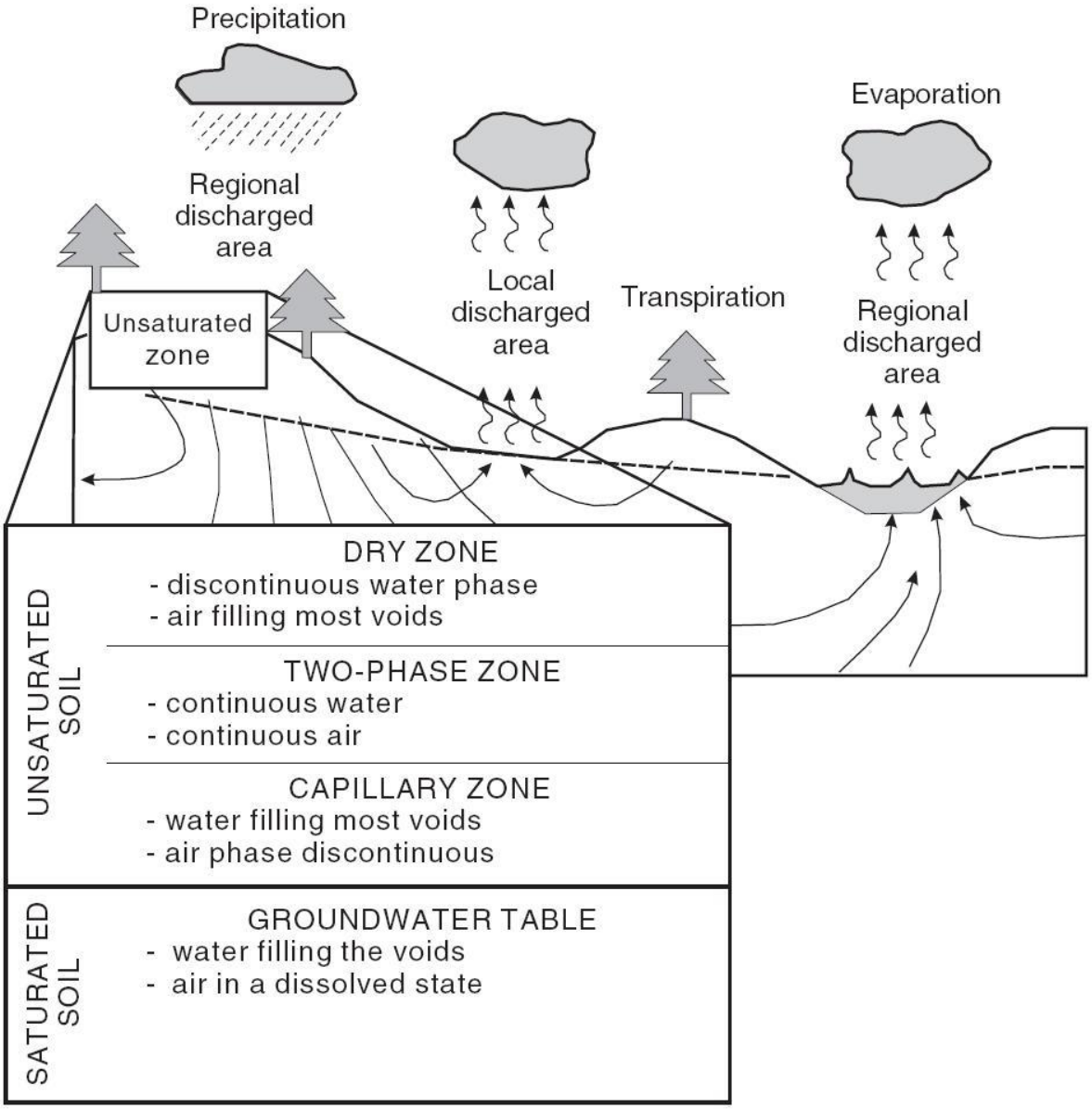


***Figure 1-1;*** *Water cycle (FREDLUND, et al., 1993)*

Despite, as shown we deal mainly with unsaturated soil, the classical engineering approach, is to study its behaviour considering it either fully saturated or fully dry neglecting its three-phase nature. This is generally justified by the conservativism of the approach (LU & LIKOS, 2004), but since knowledges and technologies have been improved in the past decade, it is worth where possible, to consider the real unsaturated nature of the soil.

The fundamental aspect of interest that concern unsaturated soils, are the negative pressure that develop when the soil is placed in contact with pure free water at atmospheric pressure. This negative pressure is called total suction ($\psi_t$) and can be divided in to two components: matric suction ($\psi_m$) due to the capillary rise phenomenon and osmotic suction ($\psi_o$) induced

by the electrochemical potential, that develops due to the difference of salt concentration in between the pure water and the interparticle water.

In the following pages of the chapter, are reported the basics concepts (mechanicals and hydraulic) necessary to understand the behaviour of the unsaturated soil media.

## 1.1 Phases interactions

The peculiarity of the unsaturated medias is the compresence of three different phases: solid, liquid and gaseous. And since the fluids move in to the interparticle voids, it is easy to infer their importance, in the role of establishing the amount of water and air that can be contained in the pore of the solid matrix.

To describe the relations between void and the respective fillings are normally used the following ratios (**Figure 1-2**): Void ratio (e), defined as the ratio of the volume of voids ($V_v$) to the volume of solids ($V_s$):

$$e = \frac{V_v}{V_s} \tag{1.1}$$

Porosity (n), defined as the ratio of the volume of voids ($V_v$) to the total volume ($V_t$):

$$n = \frac{V_v}{V_t} \tag{1.2}$$

Saturation ratio (Sr), defined as the ratio of the volume of water ($V_w$) to the volume of voids ($V_v$):

$$Sr = \frac{V_w}{V_v} \tag{1.3}$$

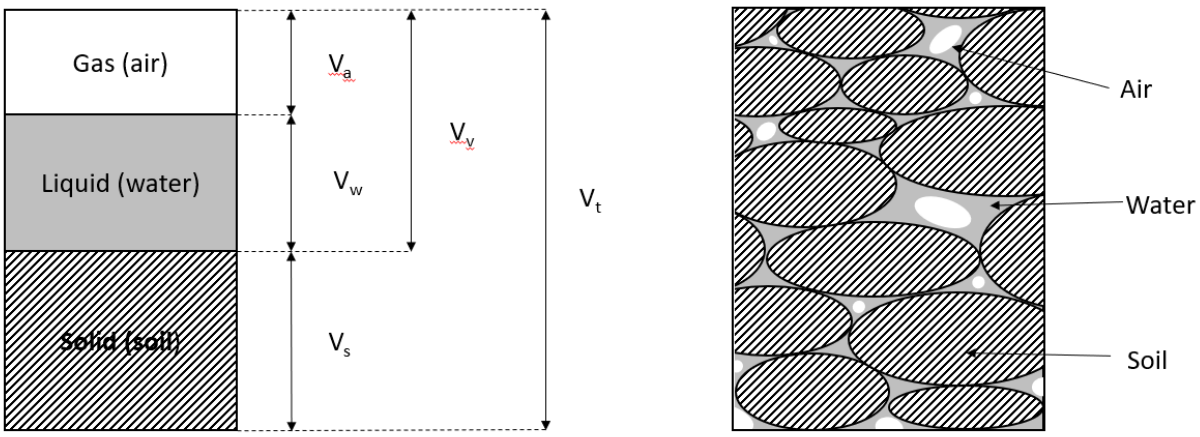


*Figure 1-2; Three phases of a soil element and representation of its natural state*

Another common index is the volumetric water content (ϑ) defined as the ratio of water volume ($V_w$) to the total volume of the element ($V_t$):

$$\vartheta = \frac{V_w}{Vt} \tag{1.4}$$

The previous indexes allow to describe the relative amount of the three phases but, it is mandatory to understand how they do interact because, by that, depend the liquid and air static distribution in to the media. To do so, it is necessary, to better analyse the interfacial equilibrium in between liquid-gas and liquid-gas-solid phases.

The liquid-gas equilibrium is the one that describe the amount of liquid that can exist in the liquid phase and the amount of gas present as solute in the liquid one. Basically, what happen in to any sparkling drink, where the carbon dioxide is dissolved in to the drink is in balance with the undissolved one. This equilibrium can be described by the Henry's law (1.5) that state that at equilibrium the amount of dissolved gas is proportional to its partial pressure in the gas phase.

$$\frac{M_i/\omega_i}{V_l} = k_{Hi}u_i \tag{1.5}$$

Where: $M_i$ is the mass of the gas [kg], $\omega_i$ it's molecular mass [kg/mol], $V_l$ the volume of the liquid [$dm^3$], $k_{Hi}$ the Henry's law constant [$mol*dm^{-3}*bar^{-1}$] and $u_i$ the partial gas pressure [bar]; the i stay for the i-th gas.

Whereas the amount of vapour of the liquid phase can be evaluated by mean of the ideal gas law (Equation 1.6)

$$\rho_v = \frac{\omega_v u_v}{RT} \tag{1.6}$$

Where: $u_v$ is the saturated vapour pressure in [kPa], $\omega_v$ the vapour molecular mass [kg/mol], R=8.314 [$J*mol^{-1}*K$], T is the temperature [K].

The saturated vapour pressure can be computed with the following empirical formula (1.7):

$$u_v = 0.611exp\left(\frac{T-273.2}{T-36}\right) \tag{1.2}$$

Where: $u_v$, the saturated vapour pressure is computed in [kPa], and T is in [K].

The shape of the contact between air and water is determined by their relative pressures and their surface tensions. Where surface tension can be defined as the elastic capacity of a fluid surface to store energy, for instance, this is the phenomena that allows some insects to walk on the water. And since the air surface tension can be ignored then just three are

the variables that define the geometry and the pressure. Those conditions lead to the concavity pointing towards the fluid with a higher pressure.

In the case of the additional presence of the solid phase, things became more complicated as it is necessary to consider also the shape of the solid and the solid-liquid-gas contact angle. The contact angle (α) is a characteristic that define the wettability of a solid with respect two phases liquid and gaseous (**Figure 1-3**). It can be defined as the angle, determined by the tangent to the fluid surface in contact with the solid, measured starting from the solid and passing through the liquid phase.

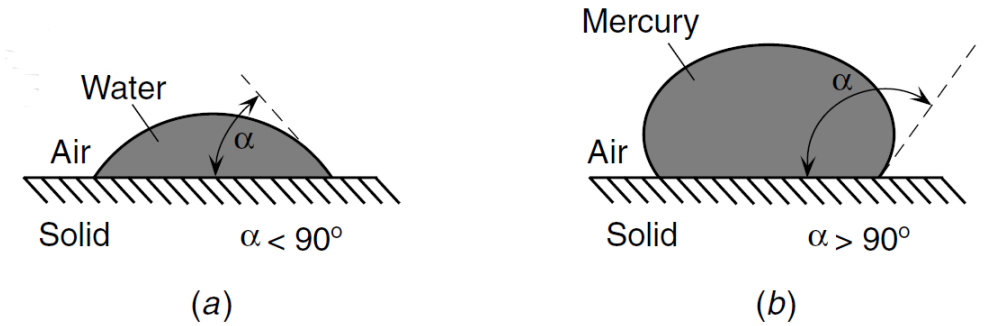


***Figure 1-3**; An example of wetting interaction (a) and a repelling one (b), (LU & LIKOS, 2004).*

Thus, depending on the angle there are different behaviours:

- 0° < α < 90°: partially wetting surface, (air-water-glass)
- α = 90°: neutral surface (air-water)
- 90° < α < 180°: partially repellent surface (air-mercury-glass)

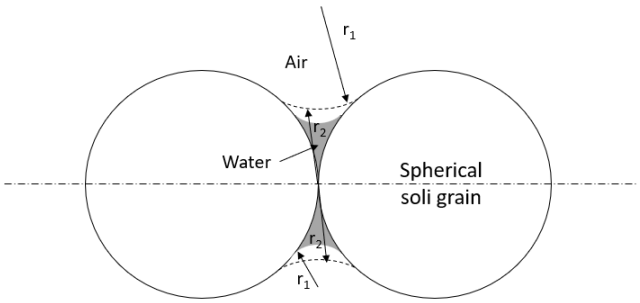


***Figure 1-4**; Idealized spherical soil grain in unsaturated conditions; $r_1$ and $r_2$ are the distances between the particle's axis*

This is a general case, characterized by 2D unsaturated soil (**Figure 1-4**), the behaviour is determined by solving the horizontal equilibrium of the force acting on the water that connect two spherical soil grains, is possible to obtain (1.8):

$$u_a - u_w = T_s\left(\frac{1}{r_1} - \frac{1}{r_2}\right) \tag{1.8}$$

Where: $T_s$ is the surface tension [N/m], $r_1$ and $r_2$ are the distance between the particle's axis and the radius of curvature of the water surface, respectively. The quantity on the left side of the Equation 1.8 ($u_a$-$u_w$) is named matric suction and is the pressure that drive most of the water movement in to unsaturated soils.

Considering the air pressure constant is possible to see how the water pressure is affected by a change in the two value of the radius: if $r_1$ is greater than $r_2$ (situation that happen in general unsaturated condition) than the water pressure decrease and consequently, the first term of the Equation 1.8, called suction, will increase, while if $r_2$ is greater than $r_1$ (situation close to saturation) the suction decrease.

The decrease of the water pressure drives the capillarity phenomena, a process that is possible to experience in to our everyday life, for example when walking in a rainy day the hem of your pants gets wet and this wet spot expand till the calf-length. Well that's the same phenomena that occur into a soil above the Ground Water Table (GWT), where water rise above it saturating heterogeneously a certain area called capillary fringe. This can be explained with the capillary tube and the Young-Laplace equation (1.9) that furnish a relation between the matric suction and a 3D surface:

$$u_a - u_w = T_s\left(\frac{1}{R_1} + \frac{1}{R_2}\right) \tag{1.9}$$

Where $R_1$ and $R_2$ are the main two radii of curvature of the interface surface.

Assuming that the surface is an ellipsoid with main radii $\rho_1=r_1\cos\alpha$ and $\rho_2=r_2\cos\alpha$ than the Equation 1.9 can be rewritten as:

$$u_a - u_w = T_s\cos\alpha\left(\frac{1}{r_1} + \frac{1}{r_2}\right) \tag{1.10}$$

The above equation 1.10 can be rewritten in terms of only one diameter (d) and because at equilibrium the water pressure is equal to the weight of the water ($\gamma_w$) times it's high (h) we get:

$$u_w = u_a - 4T_s\cos\alpha\left(\frac{1}{d}\right) = \gamma_w * h \tag{1.11}$$

And rearranging:

$$h = 4\frac{T_s cos\alpha}{d * \gamma_w} \tag{1.12}$$

For example is possible to compute h for a sand in drying conditions (LU & LIKOS, 2004), using one of the Surface tension values reported in **Table 1**, using water at 20°C is possible to simplify the equation 1.12 just as a function of the meniscus diameter (d):

$$h = \frac{0.3}{d} \tag{1.13}$$

***Table 1**; Surface tension of some common liquids in contact with air (SPEIGHT, 2005)*

| Liquid | Temperature [°C] | Surface tension [N/m] |
|---|---|---|
| Acetic acid | 20 | 0.028 |
| Acetone | 20 | 0.024 |
| Ethanol | 20 | 0.022 |
| Mercury | 20 | 0.559 |
| Olive oil | 20 | 0.032 |
| Sodium chloride 6.0 M aqueous solution | 20 | 0.083 |
| Sucrose (55%) + water | 20 | 0.076 |
| Water | 0 | 0.076 |
| Water | 20 | 0.073 |
| Water | 50 | 0.068 |
| Water | 100 | 0.059 |

In literature are also available some empirical equations that relates, for instance, the $D_{10}$ (size of the sieve through which pass the 10% weight of the soil) and the void ratio with the capillary rise:

$$h_c = \frac{C}{e * D_{10}} \tag{1.14}$$

Where: C is a constant ranging from 0 to50 [$mm^2$].

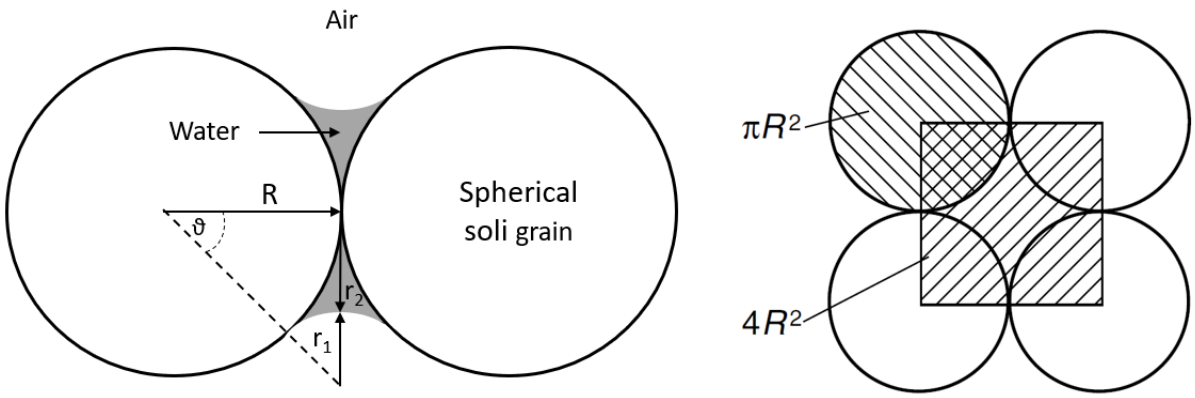


***Figure 1-5**; Air-water-solid interaction and unit areas for a primitive cubic system (BISHOP, 1959) modified.*

The net force acting on the spherical grains due to the particle's interaction can be written as (BISHOP, 1959):

$$F_e = u_a \pi R^2 - (u_a - u_w)\pi R^2 - T_s 2\pi r_2 \tag{1.15}$$

Thus, the stress contribution on the surface $\pi R^2$ can be written as:

$$\sigma_w = u_a - \frac{r_2^2}{R^2}(u_a - u_w) - \frac{2r_2^2 r_1}{R^2(r_2 - r_1)} \tag{1.16}$$

Adjusting and substituting in to the effective stress definition:

$$\sigma' = \sigma - u_w = \sigma - u_a + \frac{r_2^2}{R^2}\frac{r_1 + r_2}{(r_2 - r_1)}(u_a - u_w) \tag{1.17}$$

That is the same effective stress definition introduced by (BISHOP, 1959):

$$\sigma - u_a + \frac{r_2^2}{R^2}\frac{r_1 + r_2}{(r_2 - r_1)}(u_a - u_w)\sigma' = \sigma - u_a + \chi(u_a - u_w) \tag{1.18}$$

In this case and as well if the surface $4R^2$, the effective stress parameter $\chi$ depends on the degree of saturation since when $r_2$ rise $r_1$ decrease approaching the unitary value, this happened when the soil is close to the saturation, analogously when the soil is nearly dry $r_2$ becomes close to zero so the whole fraction goes at zero.

## 1.2 Hydraulic Features

The motion of a liquid fluid in to an unsaturated soil, is governed by the total potential ($\mu_t$) measured as an energy per unit of mass [J/kg]. It could be written also in terms of total suctions ($\psi_t$) or total head $h_t$ [m], as follows:

$$\mu_t = \frac{\psi_t}{\rho_w} = \frac{1}{\rho_w}(\psi_g + \psi_o + \psi_m) = g * h_t = g * (h_g + h_m + h_o) \quad (1.19)$$

Where: $h_g$ is the position head ($h_g$=z), $h_m$ is the matric head and $h_o$ the osmotic head. The matric head has the same meaning of the matric suction s=($u_a$-$u_w$) but instead of being written in terms of pressure is described in terms of length, the relation that link the two notation is the following:

$$h_m = \frac{(u_a - u_w)}{g * \rho_w} = \frac{s}{g * \rho_w} \quad (1.20)$$

The osmotic head ($h_o$) is the head due to a different concentration of the solute in an aqueous solution, is the cause of the osmosis phenomena; the position head $h_g$ is given by the height of the liquid with respect the chosen reference system. Different concentration in to the interparticle void are due to Cation-exchange capacity (CEC) of the soil, that is directly proportioned with the clay content of the soil (RHOADES, et al., 1976).

Forasmuch as in the application of interest the contribute of the osmotic component is widely lower, if compared with the suction one, in most of the geotechnical engineering problems that involve unsaturated soils, with low CEC, the osmotic head can be neglected. Hence this is the reason of the importance of the suction in the description of any flow in to unsaturated soils.

As shown in the previous paragraph the matric suction (s) and the amount of water filling the voids are directly linked. This behaviour can be trapped by the Soil Water Retention Curve (SWRC), where the amount of water can be described by the volumetric water content (ϑ) or by the degree of saturation (Sr).

The SWRC is generally depicted in to a semilogarithmic plane with the matric suction in a logarithmic scale on the y axis and a variable describing the amount of water in to the soil on the x axis.

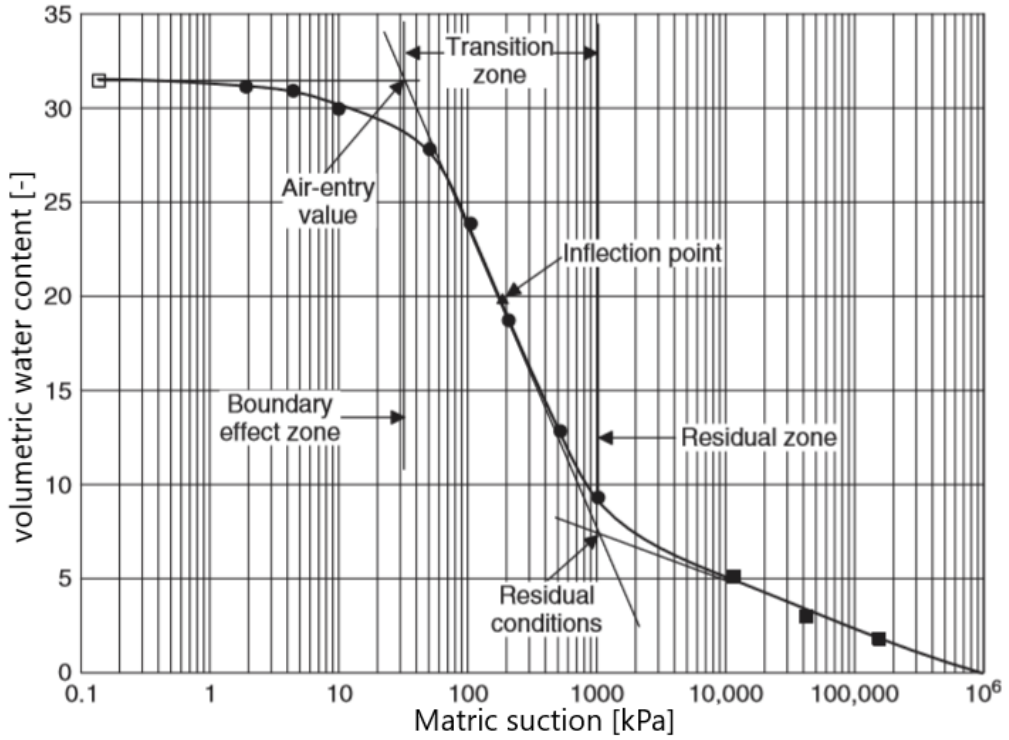


*Figure 1-6; Typical SWRC trend and main characteristics (FREDLUND, et al., 1993)*

In **Figure 1-6** is shown the typical trend of a SWRC: on the left (boundary effect zone), for low values of suction, the soil is saturated and an increment of the values of suctions don not induce any significant variation of the volumetric water content. This part finish with the formation of the first air bubbles in to the soil's voids, the corresponding value of suction is named Air Entry Value (AEV). In the middle (transition zone), the amount of water presents in to the soil decrease considerably and the liquid phase become discontinuous. On the right part (residual zone of saturation), to big increment of suction correspond small variation of the water content. The value of the suction related with the transition between the middle and right side of the curve, describes the residual conditions and the corresponding amount of water is named residual volumetric water content or residual degree of saturation, depending on the used variable to describe the water changes in to the soil.

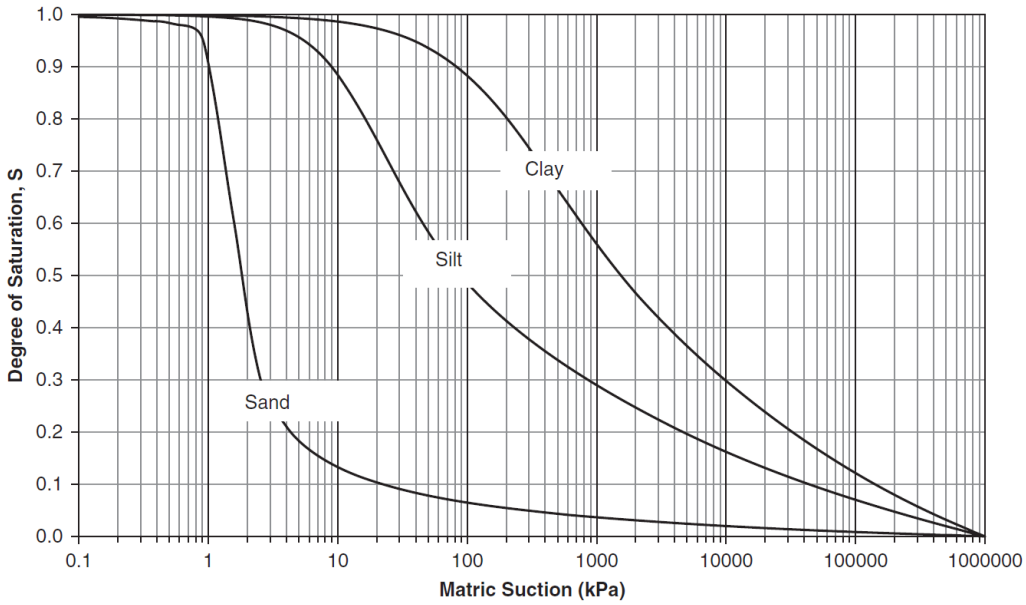


*Figure 1-7; Typical SWRC for sand, silt and clay (ZAPATA & HOUSTON, 2008)*

As is possible to infer from **Figure 1-7**, the shape of the retention curve depends by the pore size and the granulometric curve: in coarse soils (sands and gravels) the pore are interconnected and their sizes are big, thus are characterized by low AEV, low residual conditions and a steep curve in the transition zone. Indeed, in fine soils (clays) particles have a high specific surface and thus strong electro-chemical bond with water, so they have high AEV and a lower tilt of the curve in the transition zone. The former soils are named Low Air Entry Value soils (LAEV) while the latter High Air Entry Value soils (HAEV).

During the process of decreasing the water content (by increasing suction) starting from saturated condition, the soil follow a retention curve named main drying that is different from the one obtained by the inverse process. The latter one, named main wetting, do not reach a fully the saturation of the soil because a certain amount of air remains trapped in to the voids. In order to remove it is necessary to apply a positive water pressure. This phenomenon characterized by two different shape of the SWRC during a wetting and a drying process is named hysteresis.

A flow in to a porous media such as a soil is mainly controlled by the total potential as previously said but as show the Darcy's law its velocity is corrected by a constant called Hydraulic conductibility. In to unsaturated soils the hydraulic conductivity depends on the Matric suctions and on the amount of water inside the pores as illustrate the **Figure 1-8**.

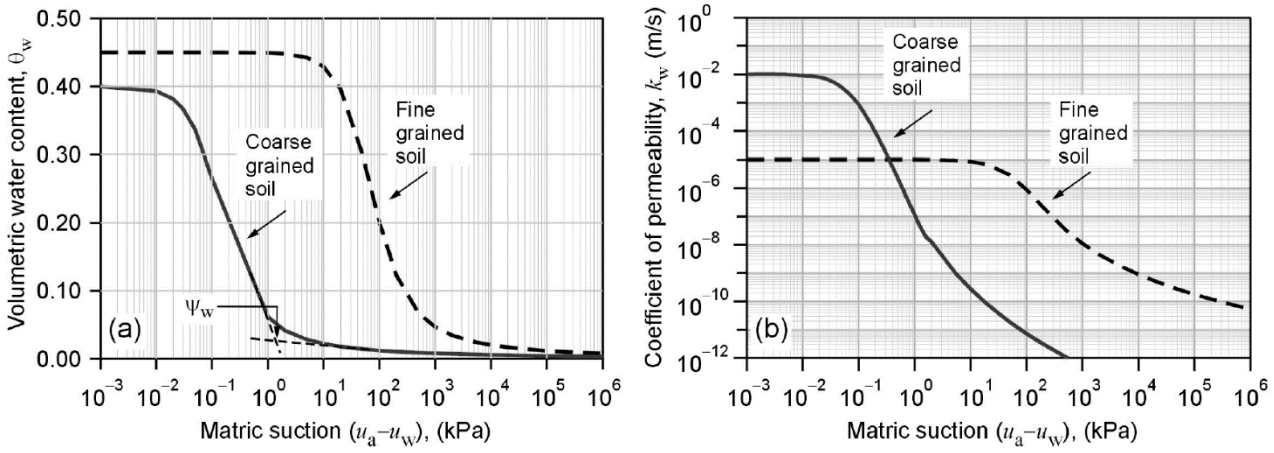


*Figure 1-8; Matric suction dependence of volumetric water content (a) and hydraulic conductibility (b) (EICHENBERGER, 2013)*

**Figure 1-8** shows a decrease of the hydraulic conductivity with the rise of matric suction and hence with the volumetric water content ; especially it has the maximum value that corresponds with the saturation of the soil. That means that the maximum value of the hydraulic conductivity in to unsaturated soils coincides with the saturated hydraulic conductivity ($k_s$). Therefore, it is a common practice to normalize the unsaturated hydraulic conductivity with the saturated one, in this case the values will range from zero and one and is named relative hydraulic conductivity.

As for saturated soils, the water flow in to unsaturated one is steered mainly by total potential and hydraulic conductivity, two variables of the Darcy's law (1.21), thus, it is possible to substitute the total head (1.19) in to the (1.21) to describe the steady flow in to unsaturated conditions (1.22):

$$v = -k\Delta h \tag{1.21}$$

$$\boldsymbol{q} = -k_x(h_m)\frac{\partial h_t}{\partial x}\boldsymbol{i} - k_y(h_m)\frac{\partial h_t}{\partial y}\boldsymbol{j} - k_z(h_m)\frac{\partial h_t}{\partial z}\boldsymbol{k} \tag{1.22}$$

Where: $k_x$, $k_y$, $k_z$ are the hydraulic conductivity [m/s] in the directions x, y and z respectively, **i**, **j** and **k** are the versors of the coordinates system.

Let's take the opportunity to remark the difference between intrinsic permeability (K) and hydraulic conductivity (k): Besides the fact that they are measured with two different units $m^2$ and m/s respectively, the former is an intrinsic characteristic of the porous media while the latter is also fluid dependent. The hydraulic conductibility is linked to the intrinsic permeability by the following relation:

$$k = \frac{\rho g K}{\mu} \tag{1.23}$$

Where: μ is dynamic viscosity of the fluid [Pa*s] or [kg*m$^{-1}$*s$^{-1}$] and ρ is the density [kg/m$^3$] of the fluid. Intrinsic permeability is often measured in darcy where 1 darcy = 0987*10$^{-2}$ m$^2$ and using the value listed in **Table 2**, for water, 1 darcy ≈ 10$^{-3}$ m/s.

***Table 2**; Density and dynamic viscosity of water function of temperature (DI MOLFETTA & SETHI, 2012) modified and corrected.*

| *Temperature [°C]* | *Density [kg/m$^3$]* | *Dynamic viscosity [Pa*s]* |
|---|---|---|
| 0 | 999.8 | 1.781 |
| 10 | 999.7 | 1.307 |
| 20 | 998.2 | 1.002 |
| 50 | 988 | 0.547 |
| 100 | 958.4 | 0.282 |

If the flow is steady, then the net flow at any point is null for the principle of mass conservation and not dependent from time; neglecting the osmotic contribution of the total head and the third dimension (y) the 1.22 becomes:

$$\frac{\partial k_x}{\partial x}\frac{\partial h_m}{\partial x} + \frac{\partial k_z}{\partial z}\left(\frac{\partial h_m}{\partial z} + 1\right) + k_x\frac{\partial^2 h_m}{\partial x^2} + k_z\frac{\partial^2 h_m}{\partial z^2} \tag{1.24}$$

As for the steady conditions, it is possible to derive the equation that control a transient flow, referring to **Figure 1-9**, is possible to write the net mass flow through the soil element as:

$$\begin{aligned} q_{in} - q_{out} &= \rho\left(q_z dxdy + q_y dxdz + q_x dzdy\right) \\ &- \rho\left[\left(q_z + \frac{\partial q_z}{\partial z}dz\right)dxdy + \left(q_y + \frac{\partial q_y}{\partial y}dy\right)dxdz \right. \\ &\left. + \left(q_z + \frac{\partial q_x}{\partial x}dx\right)dzdy\right] \end{aligned} \tag{1.5}$$

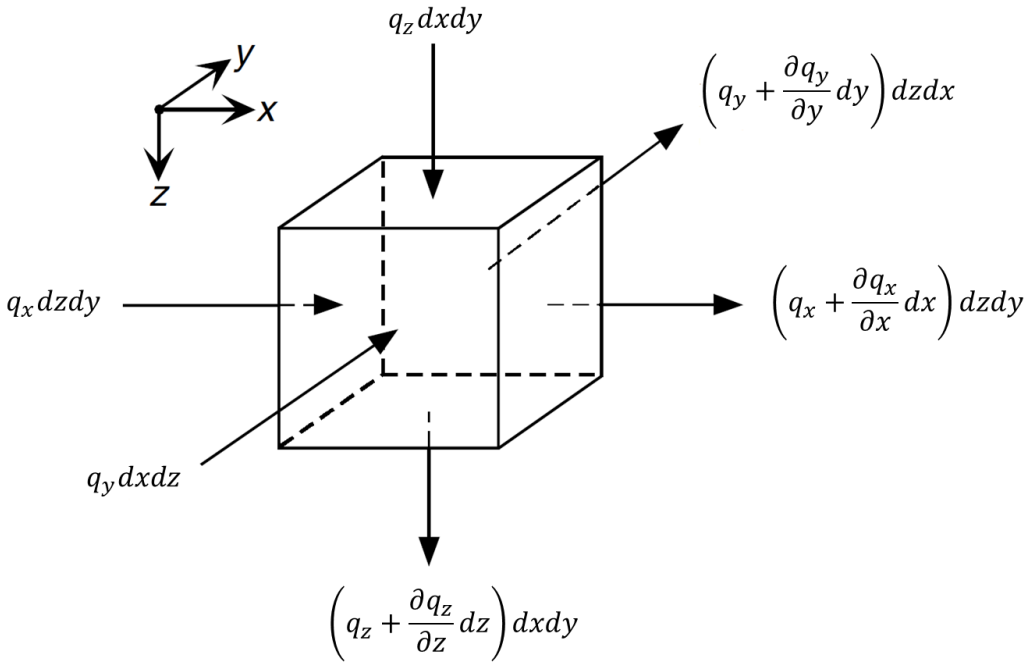


*Figure 1-9; Soil's volume of control and fluid flux*

The change of mass inside the box can be written in terms of water content variation:

$$\frac{\partial(\rho\theta)}{\partial t}dxdydz \tag{1.26}$$

For the conservation of the mass the quantities 1.26 and 1.25 are equal, and considering the density constant over the time, simplifying:

$$-\left(\frac{\partial q_x}{\partial x}+\frac{\partial q_y}{\partial x}+\frac{\partial q_z}{\partial x}\right)=\frac{\partial\vartheta}{\partial t} \tag{1.7}$$

Because the water content is a function of the matric head, it is possible to write its derivative as the derivative of a function composition:

$$\frac{\partial\theta}{\partial t}=\frac{\partial\theta}{\partial h_m}\frac{\partial h_m}{\partial\vartheta}=C(h_m)\frac{\partial h_m}{\partial t} \tag{1.28}$$

Where: $C(h_m)=\partial\Theta/\partial h_m$ is called specific moisture capacity.

Substituting the 1.27 an the 1.26 in to the 1.28:

$$\frac{\partial}{\partial x}\left[k_x(h_m)\frac{\partial h_m}{\partial x}\right]+\frac{\partial}{\partial y}\left[k_y(h_m)\frac{\partial h_m}{\partial y}\right]+\frac{\partial}{\partial z}\left[k_z(h_m)\frac{\partial h_m}{\partial z}+k_z\right]=C(h_m)\frac{\partial h_m}{\partial t} \tag{1.29}$$

That is the Richard's equation that can be written in the more compact notation:

$$C(h_m)\frac{\partial h_m}{\partial t} = div[k(h_m)\nabla h_t] \tag{1.30}$$

It is a nonlinear partial differential equation, and a possible one-dimensional solution will be given in chapter three.

The variations of the hydraulic conductibility and the water content can be written as functions of the matric suction. There are several models in literature but just the one used ahead will be reported. For simplicity let's write normalize the water content and the saturation ratio as follow:

$$\Theta = \frac{\theta - \theta_{res}}{\theta_{sat} - \theta_{res}} = \frac{S_r - S_{r,res}}{1 - S_{r,res}} \tag{1.31}$$

The water content distribution can be described by using the Van Ghenuchten three parameters model (VAN GENUCHTEN, 1980):

$$\Theta = \left[\frac{1}{1 + (\beta h_m)^n}\right]^m \tag{1.32}$$

$$\theta = e^{\beta h_m} \tag{1.33}$$

Where: a is a parameter related to the air entry value and is equal to β [$m^{-1}$] if it multiplies the matric head or equal to α [$kPa^{-1}$] if suction is used in place of matric head; n is related to the granulometric curve and m to the symmetry of the curve's model.

In the presented work, the Hydraulic conductibility the mono parameter Gardner's exponential model is used (GARDNER, 1958):

$$k = k_s * e^{\beta h_m} \tag{1.34}$$

Where β has the same meaning as for the equations 1.32 and 1.33.

## 1.3 Mechanical Features

During 1936 when Karl Von Terzaghi formally introduced the effective stress principle laying the groundwork for the modern geotechnics (BERARDI, 2009). The introduction of this principle allowed to compute the real stress acting in to a soil, also in saturated condition by mean of taking in to account the pore water pressure ($u_w$). That was done subtracting to the total stress the pore water pressure (TERZAGHI, 1936) as shown in equation (1.35):

$$\sigma'_{ij} = \sigma_{ij} - \delta_{ij} u_w \tag{1.35}$$

Or in the explicit matrix form:

$$\begin{bmatrix} \sigma_x & \tau_{xy} & \tau_{xz} \\ \tau_{yx} & \sigma_y & \tau_{yz} \\ \tau_{zx} & \tau_{zy} & \sigma_z \end{bmatrix} = \begin{bmatrix} \sigma'_x & \tau_{xy} & \tau_{xz} \\ \tau_{yx} & \sigma'_y & \tau_{yz} \\ \tau_{zx} & \tau_{zy} & \sigma'_z \end{bmatrix} + \begin{bmatrix} u_w & 0 & 0 \\ 0 & u_w & 0 \\ 0 & 0 & u_w \end{bmatrix} \tag{1.36}$$

In 1959, Alan Wilfred Bishop a British geotechnical engineer, extended the Terzaghi's effective stress definition (1.35) in order to take into account also negative pore water pressure and the presence of two liquid phases (**Figure 1-1**): a liquid one (water) and a gaseous one (air).

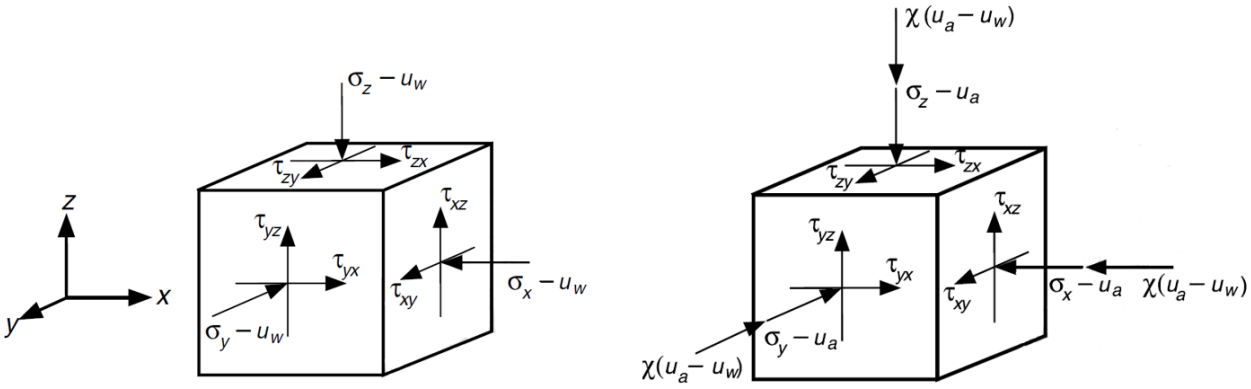


*Figure 1-10; Stress representation on a cubic soil element: Terzaghi's approach on the left and Bisop's one on the right.*

The equation introduced by Bishop (1.37) represent the stress state shown in the right side of **Figure 1-10**,

$$\sigma'_{ij} = \sigma_{ij} - \delta_{ij} u_a + \chi \delta_{ij} (u_a - u_w) \tag{1.37}$$

Or in the explicit matrix form:

$$\begin{bmatrix} \sigma_x - u_a & \tau_{xy} & \tau_{xz} \\ \tau_{yx} & \sigma_y - u_a & \tau_{yz} \\ \tau_{zx} & \tau_{zy} & \sigma_z - u_a \end{bmatrix} = \begin{bmatrix} \sigma'_x & \tau_{xy} & \tau_{xz} \\ \tau_{yx} & \sigma'_y & \tau_{yz} \\ \tau_{zx} & \tau_{zy} & \sigma'_z \end{bmatrix} + \chi \begin{bmatrix} u_a - u_w & 0 & 0 \\ 0 & u_a - u_w & 0 \\ 0 & 0 & u_a - u_w \end{bmatrix} \tag{1.38}$$

Where: $\sigma'_{ij}$ is the effective stress, $\sigma_{ij}$ is the total stress, $\sigma_{ij} - \delta_{ij} u_a$ is the net stress, $\chi$ is the effective stress parameter (a material property that later on has been placed equal to the

effective saturation ratio), $\chi(\delta_{ij}u_a - \delta_{ij}u_w)$ is a parameter that represent the interparticle stress due to suction.

Passing from a 3 dimensions stress state in to a 2 dimensional one as shown in **Figure 1-11**, considering a generical plane (AB), who's normal is rotated of an angle Θ from the z axis.

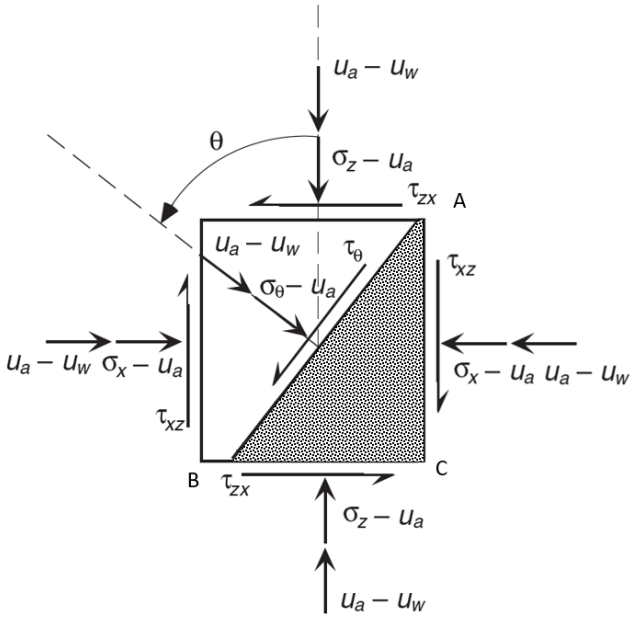


*Figure 1-11; 2D state of stress (LU & LIKOS, 2004) modified*

To compute the net ($\sigma_\vartheta - u_a$) and shear ($\tau_\vartheta$) stresses acting on this plane, considering the triangle with the vertex A, B and C, identified by the plane AB and let's do the balance to translation of the forces in the normal and perpendicular directions to the plane AB:

$$\begin{aligned}(\sigma_\theta - u_a + u_a - u_w)AB \\ = (\sigma_x - u_a + u_a - u_w)cos(\theta)AC \\ + (\sigma_z - u_a + u_a - u_w)sin(\theta)CB + \tau_{zx}\cos(\theta)\,CB \\ + \tau_{xz}\sin(\theta)CB\end{aligned} \tag{1.38}$$

$$\begin{aligned}\tau_\theta AB = (\sigma_x - u_a + u_a - u_w)sin(\theta)AC + (\sigma_z - u_a + u_a - u_w)cos(\theta)CB - \\ \tau_{zx}\sin(\theta)\,CB + \tau_{xz}\cos(\theta)CB;\end{aligned} \tag{1.39}$$

Where: AC and CB are the projections of the unitary side on the side AB, thus AB=1, AC=cos(ϑ) and CB=sin(ϑ).

Substituting and simplifying:

$$(\sigma_\theta - u_w) = (\sigma_x - u_w)cos^2(\theta) + (\sigma_z - u_w)sin^2(\theta) + 2\tau_{zx}\cos(\theta)\sin(\theta) \quad (1.40)$$

$$\tau_\theta = (\sigma_x - u_w)sin^2(\theta) + (\sigma_z - u_w)cos^2(\theta) + \tau_{zx}sin^2(\theta) - \tau_{zx}cos^2(\theta) \quad (1.41)$$

And reminding that $\sin(\alpha)\cos(\alpha)=\sin(2\alpha)$, $\sin^2(\alpha)=(1-\cos(2\alpha))/2$ and $\cos^2(\alpha)=(1+\cos(2\alpha))/2$:

$$(\sigma_\theta - u_w) = \frac{(\sigma_x - u_w)(1 + cos(\theta))}{2} + \frac{(\sigma_z - u_w)(1 - cos(2\theta))}{2} - \tau_{zx}\sin(2\theta) \quad (1.42)$$

$$\tau_\theta = \frac{(\sigma_x - u_w)sin(2\theta)}{2} + \frac{(\sigma_z - u_w)cos(2\theta)}{2} + \tau_{zx}(sin^2(\theta) - cos^2(\theta)) \quad (1.43)$$

Doing some further adjusting:

$$\begin{cases} (\sigma_\theta - u_a) = \dfrac{(\sigma_x + \sigma_z)}{2} + \dfrac{(\sigma_z - \sigma_x)(cos(2\theta))}{2} - \tau_{zx}\sin(2\theta) - u_a \\ \tau_\theta = \dfrac{(\sigma_z - \sigma_x)sin(2\theta)}{2} + \tau_{zx}cos(2\theta) \end{cases} \quad (1.44)$$

Finally, the equation 1.44 represents the state of stress acting on a generic plane oriented by an angle $\vartheta$ with respect to the z axis. It is possible to see that $\sigma_\vartheta$ and $\tau_\vartheta$ both depends from $\vartheta$, thus it is possible to compute the maximum value by placing the derivative equal to zero, is possible to demonstrate that when $\sigma_\vartheta$ is maximum then there is no shear stress, that means that the angle (Equation 1.48) is the angle that gives the principals directions for the acting stresses:

$$\frac{d\left(\frac{(\sigma_x + \sigma_z)}{2} + \frac{(\sigma_z - \sigma_x)(cos(2\theta))}{2} - \tau_{zx}\sin(2\theta) - u_a\right)}{d\theta} = 0 \quad (1.45)$$

Reminding that D[f(g(x))] = f'[g(x)] * g'(x), D[sinx] = cosx and D[cosx] = -sinx:

$$\frac{-2(\sigma_z - \sigma_x)\sin 2\theta}{2} + 2\tau_{zx}\cos 2\theta = 0 \tag{1.46}$$

Adjusting:

$$(\sigma_z - \sigma_x)\sin 2\theta = 2\tau_{zx}\cos 2\theta \tag{1.47}$$

$$\theta = tan^{-1}\left(\frac{2\tau_{xz}}{\sigma_x - \sigma_z}\right) \tag{1.48}$$

The Equation 1.48 has two solutions: one for ϑ and the other one for ϑ +π/2, that corresponds to two planes on which the normal stress once is maximum and the other is minimum.

If the vertical and the horizontal stresses are, like generally happen in to isotropic soils, the principal directions, the shear stress component are null and the equations 1.38 becomes:

$$\begin{cases} (\sigma_\alpha - u_a) = \dfrac{(\sigma_x + \sigma_z)}{2} + \dfrac{(\sigma_z - \sigma_x)(cos(2\alpha))}{2} - u_a \\ \tau_\alpha = \dfrac{(\sigma_z - \sigma_x)sin(2\alpha)}{2} \end{cases} \tag{1.49}$$

The stress state shown in the above Equation (1.49) can be represented by a circle in to a modified Mohr's plane with the addition of a new matric suction ($u_a$-$u_w$) axis, as shown in **Figure 1-12**.

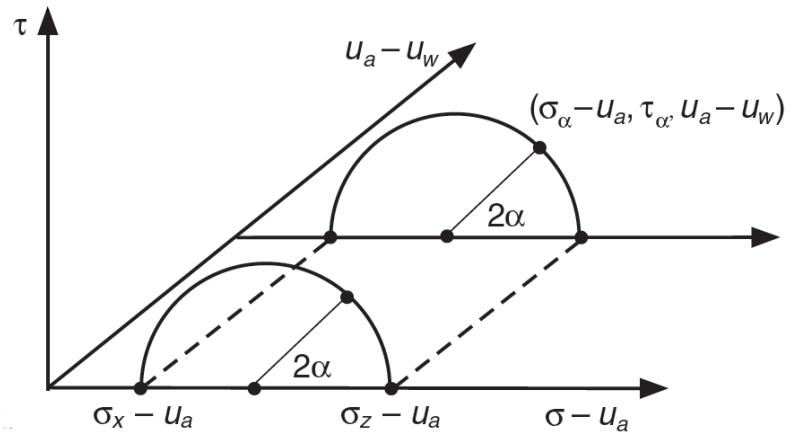


*Figure 1-12; Mohr's circle stress state for unsaturated soils (LU & LIKOS, 2004)*

Experimental observations on the shear strength of unsaturated soils, had been mainly driven in laboratory tests by mean of modified (to control air and water pore pressure) triaxial or direct shear apparatus. The results, of those experiment, highlighted that the shear strength increase with an increment of net normal stress or matric suctions. Those two behaviours are captured by the Extended M-C criterion (FREDLUND, et al., 1978):

$$\tau_f = c' + (\sigma_n - u_a)_f tan\varphi' + (u_a - u_w)_f tan\varphi^b \qquad (1.50)$$

Where: c' is the cohesion for a null matric suction, φ' is the shear strength angle, $\varphi^b$ is an internal friction angle that take in to account the increase of shear strength due to matric suction, all the "f" subscript stays for failure.

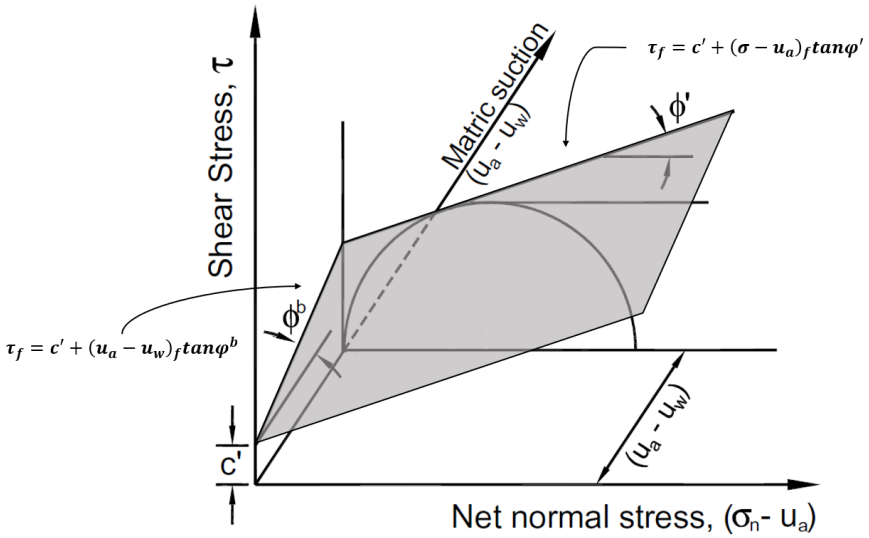


***Figure 1-13**; Extended M-C criterion (VANAPALLI, 2009) modified*

In **Figure 1-13** are clearly shown the experimental trends mentioned above and the independence of φ' from the matric suction. It is also possible to see that for a constant value of the matric suction, the projections of the failure envelopes in to a $\sigma_{net}$-τ plane are parallels straight lines.

The limitations of this approach are that it considers the whole matric suction acting on the soil interparticle and the non-linear dependence of the internal friction angle $\varphi^b$ from the matric suction component (LU & LIKOS, 2004).

Since as shown in the equation (1.18) suction stress is an acting stress that results directly from the partial saturation of the soil, hence is possible to adopt another shear strength parameter: integrate in to the M-C criterion the Bishop's effective stress definition:

$$\sigma' = \sigma_{net} + \chi(u_a - u_w) \qquad (1.51)$$

$$\tau_f = c' + \sigma' tan(\varphi') \tag{1.52}$$

Substituting the 1.51 in to the 1.52 and remembering that $\sigma_{net}$ is equal to the total stress minus the air pore pressure:

$$\tau_f = c' + \chi(u_a - u_w)\, tan(\varphi') + (\sigma_t - u_a)\, tan(\varphi') \tag{1.53}$$

The Equation 1.53 describes the failure obtained criterion and its shear strength surface can be visualized in **Figure 1-14**.

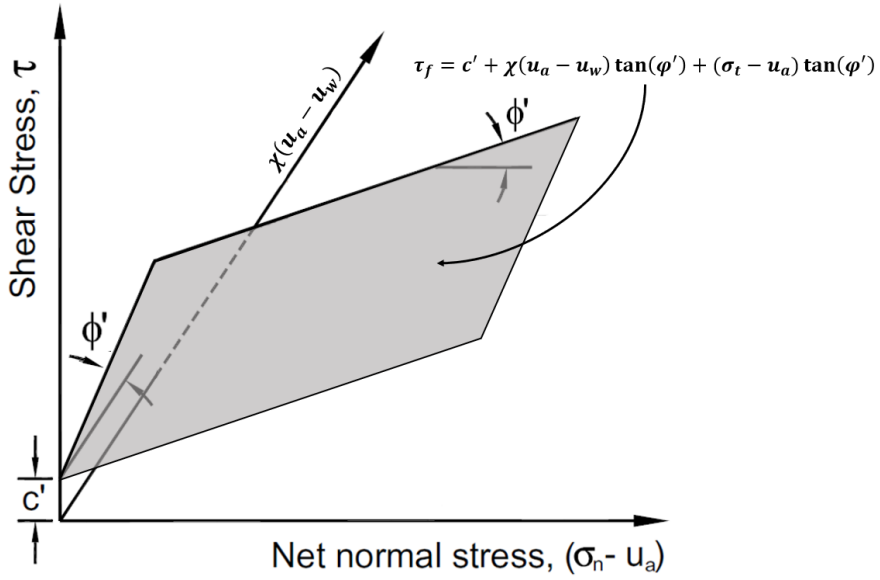


***Figure 1-14**; Representation of the failure surface obtained by using M-C shear strength criterion with the Bishop's effective stress definition*

As for the extended M-C criterion is possible to project the failure surface for a constant value of the shear stress parameter (**Figure 1-15**); the figure highlights an upward translation of the failure envelopes due to a shear stress gain. Since soils generally do not have any tensile strength, a tensile cut-off should be adopted in order to neglect the left side of the figure (negative values of the net normal stresses).

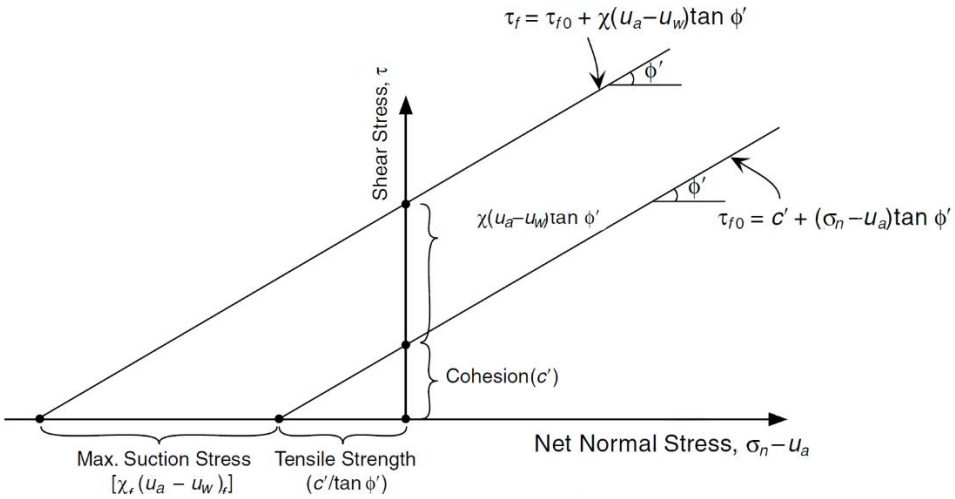


*Figure 1-15 projection of the surface shown in Figure 1-14 in to a shear stress net normal stress plane (LU & LIKOS, 2004) modified*

# Chapter 2 Experimental Determination of SWRC

As introduced in the previous chapter the SWRC is a curve that relates the amount of water with the suction.

For computing the active thrust force acting on the wall, are needed some properties of the soils involved in to the analysis: a sand and a Sion silt. Because, the relation between water content and matric suction is lacking, its experimental characterization is required.

The determination of those curve can be done by using different techniques, that can be distinguished in function of the measured variable. The most common techniques that allow to measure the matric suction are tensiometers, axis translation technique, electrical or thermal conductivity sensors and contact filter paper. While the most common technique that allow to measure the total suction are: non-contact filter paper, humidity control techniques and humidity measurements techniques.

Tensiometers: the operating principle is based on High-Air-Entry (HAE) materials, those are generally ceramic with microscopic pores whose characteristic is, how suggested by their name, to prevent when the ceramic is saturated, the entrance of air bubble within a certain range of air pressures. The value of the pressure is established by the pore size and can reach values of 15 bar. The conventional equipment is more suitable for field applications while for laboratory applications are used High Capacity Tensiometers (HTC) (**Figure 2-1**) but their working principle are the same.

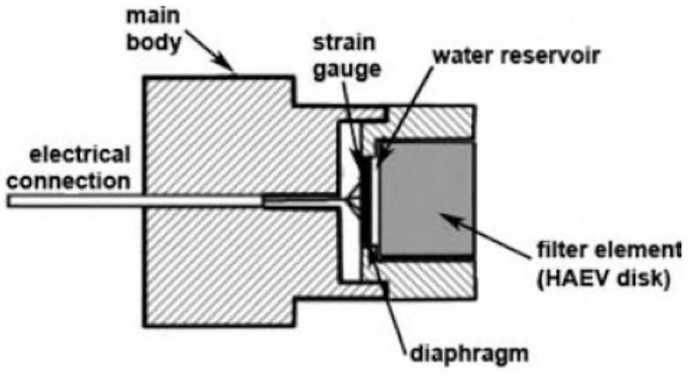


***Figure 2-1**; Example of HCT (TOLL, 2008)*

It is constituted by a hollow cylinder at the base of which is located a ceramic disk in straight contact with the external environment, immediately behind it, there is a small chamber filled with water and placed in continuum contact with the disk and a diaphragm. When the ceramic (that need to be saturated) is exposed to suction, the water contained into it move outward dragging the water contained in the reservoir, since water has a relatively high bulk modulus, the diaphragm deform and with it the strain gauge that convert the deformation in to an electric signal.

Axis translation techniques: operates differently to the tensiometer since the matric suction, instead of being imposed by the environment, is controlled. A saturated soil sample is placed on a saturated HAE ceramic disk so that water continuity is not interrupted. At the bottom of the ceramic is placed a water reservoir connected with a pressure controller. The whole apparatus is placed in to a hermetic cell connected with an air pressure controller. Generally, the water pressure is left as the atmospheric one, while the air pressure is increased, since air cannot flow through the ceramic disk unless it overpasses the ceramic's AEV, the air will displace the water from the sample lowering its water content. There are two types of extraction system the pressure plate (**Figure 2-2**), where more samples can be stored in and the Tempe cell that can host just one sample at time but allowing a continuous measure of the soil mass.

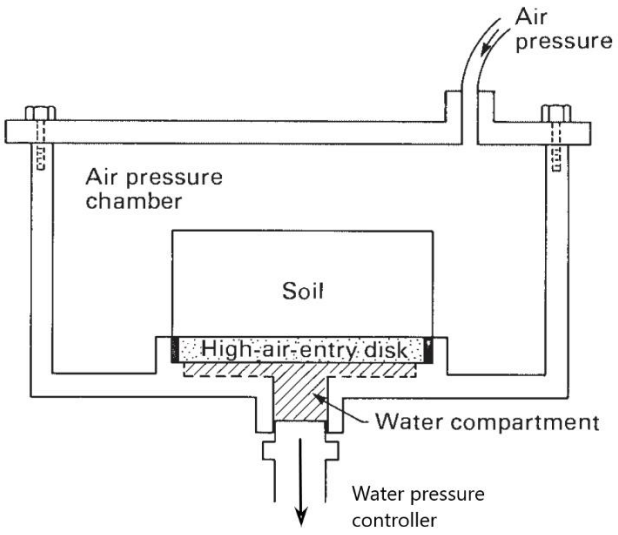


*Figure 2-2; Pressure plate apparatus for axis translation technique (FREDLUND, et al., 1993)*

Electrical and thermal conductivity sensors: they are based on the principle that if a soil sample is placed in to another porous media, if they are in to a sealed space, after a certain time it will reach the equilibrium so that a variation in the suction in the soil affect the water content of the porous media. This variation can be evaluated by a modification of the electrical or thermal conductivity of the porous media.

Filter paper techniques: is based on measuring the variation of the mass of a filter paper due to a moisture change. There are two way to do the test a direct contact one, that allow to measure the suction of the soil, and a non-contact one that measure the total suction of the soil. In the former configuration the filter paper is buried in to the specimen and they are both closed in to a sealed glass jar, so that equilibrium between the filter in direct contact with the menisci of the soil can be reached. In the latter case the filter paper is suspended inside the jar so that the moisture is transferred by the vapour phase.

Humidity measurements techniques: are based on the relation between pore water potential and its vapour pressure. Indeed, if a specimen is placed in to a sealed jar, at equilibrium the vapour pressure inside the jar will be the same of the one inside the soil's pores. By measuring the relative humidity (RH) and knowing the water content, is possible to infer the total soil suction using the kelvin's equation (2.1). The main technique that allow to measure the relative humidity are the thermocouple psychrometers, the chilled-mirror hygrometers and the polymer resistance capacitance sensors.

$$\psi_t = -\frac{RT}{\omega_v v_{w0}} ln(RH) \qquad (2.1)$$

Where: R is the universal gas constant [J/(mol*K)], T is the temperature [K], $v_{w0}$ is the specific volume of water [$m^3$/kg] and $\omega_v$ the molecular mass of water vapor [kg/kmol]

Humidity control techniques: those systems use the same principle of the previous one but instead of controlling the water content, a total suction is imposed in the chamber that contain the specimen and thus to the specimen. Suction is controlled in two ways: using a isopiestic or a two-pressure method, the former achieve vapour pressure equilibrium for solutions in a closed chamber at a constant temperature, the latter by combining the desired proportion a saturated gas with a dry one.

A comparison, based on the capability of the different techniques to cover a certain suction range, is here (**Figure 2-3**) briefly reported.

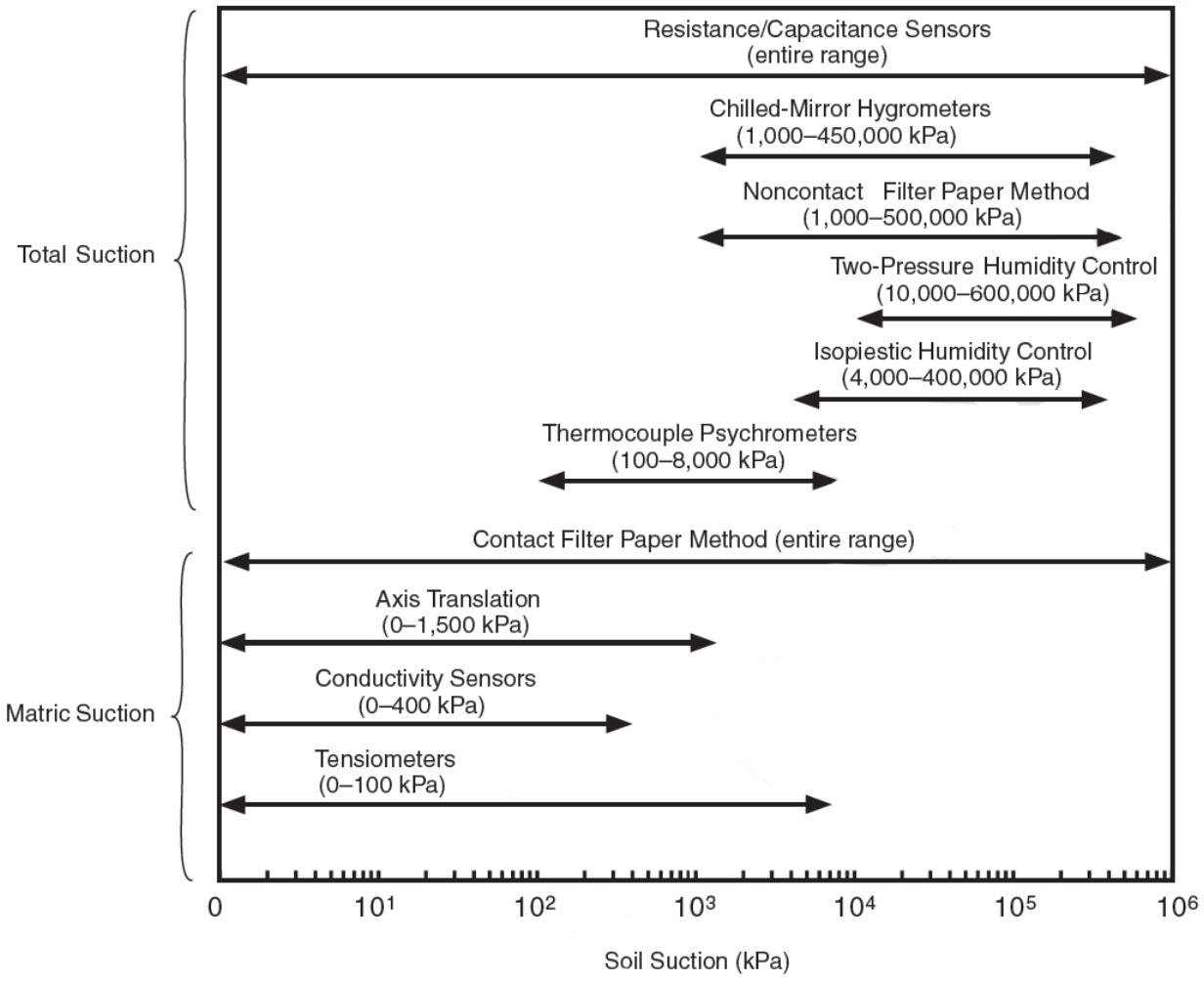


*Figure 2-3; Working range of the different techniques for measuring the soil suction after (LU & LIKOS, 2004).*

By looking at **Figure 2-3**, there are two technique that cover the entire range (contact filter paper and resistance-capacitance sensors), as it is possible to imagine, they are not that precise (LU & LIKOS, 2004) and thus it is better not to use them if high precision is needed. Another parameter is that the range of the tensiometer do not include the more recent HTC that are able to detect suctions of 15 bar (LÓPEZ MARTÍN, 2016) and the experimental UHTC that apparently should be able to detect suctions up to 70 bar (MENDES, 2018). Resuming the matric suction techniques are more advisable for low suction measurements from o to 15 bar, while total suctions technique for higher range.

## 2.1 Materials

The materials involved in the next analysis and thus the ones for which the SWRC is required are the two here described.

The silt used is the one described by (GEISER, 1999) in to his PhD thesis; the material come from the gravel of Billieux in Grone (CH), as a collateral product extracted from the cleaning of the gravel.

The geo-mechanical characterization of the silt was performed on two different sample, that's the reason of the two particle-size distribution curves of **Figure 2-4**, the first one is relative the old material and the second one to ne new one.

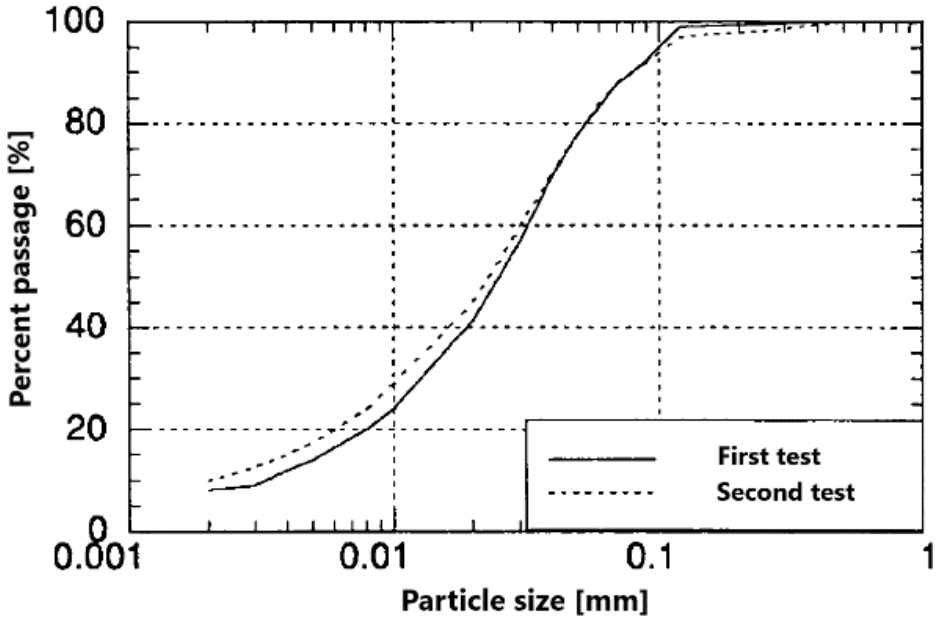


*Figure 2-4; Sion silt particle-size distribution curve (GEISER, 1999).*

Observing the **Figure 2-4**, the soil has a particle size distribution of 8% clay, 72% silt and 20% sand, thus result as a silty loam with sand.

*Table 3; Plastic limit, liquid limit, plastic limit and composition (GEISER, 1999) modified.*

| $W_l$ (%) | $W_p$ (%) | $I_p$ | (%) < 0.002 mm | (%) < 0.02 mm | (%) < 0.06 mm | $\gamma_s$ (kN/m$^3$) |
|---|---|---|---|---|---|---|
| 25.4 | 16.7 | 8.7 | 8 | 41 | 84 | 27.41 |

| | Plagioclase | Quartz | Orthoclase | Calcite | Dolomite | Anhydrite | Phyllosilicates |
|---|---|---|---|---|---|---|---|
| Weight (%) | 37 | 17 | 16 | 6 | 1 | 1 | 22 |

| | Illite | Chlorite | Kaolinite | Smectite |
|---|---|---|---|---|
| Compared to Phyllosilicates (%) | 27 | 60 | - | 13 |

Using the Unified Soil Classification System (USCS) it results a CL-ML as is possible to infer by the data showed in the first row of **Table 3**. In the same table are shown the clay minerals, and the only swelling one is smectite (only the 2% of the total weight of the Sion silt) thus it's a non-swelling material. As shown in the plasticity chart (**Figure 2-5**), the silt is characterized by a low plasticity and a low compressibility.

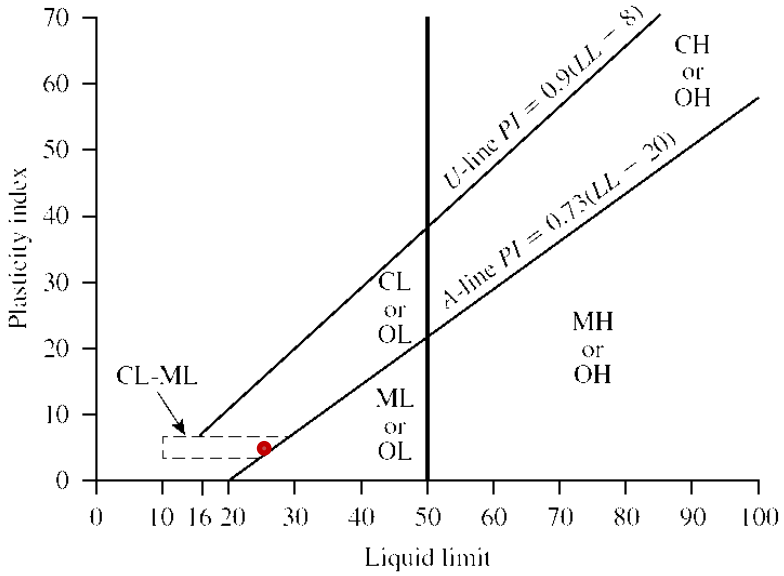


*Figure 2-5; Plasticity chart: position is pointed by the red circle.*

The elastic parameters of the Sion silt have been evaluated by mean of some saturated triaxial test for different confinement values.

The Young's modulus has been evaluated from the axial deformation - deviatoric stress graph, and it has been estimated using the equation shown in **Figure 2-6**, for the tensional state of interest, that is to say 15 kPa, its value is shown in **Table 4**.

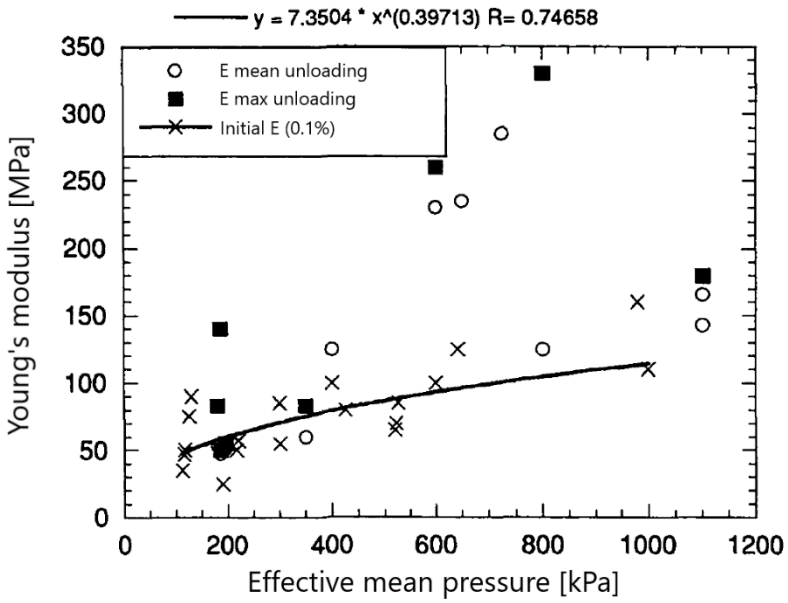


*Figure 2-6; Sion silt Young's modulus evolution with respect the effective mean pressure (GEISER, 1999) .*

The second elastic parameter, the Poisson coefficient ν, it has been evaluated from the unloading curve of a drained test in to an axial-lateral deformation plane.

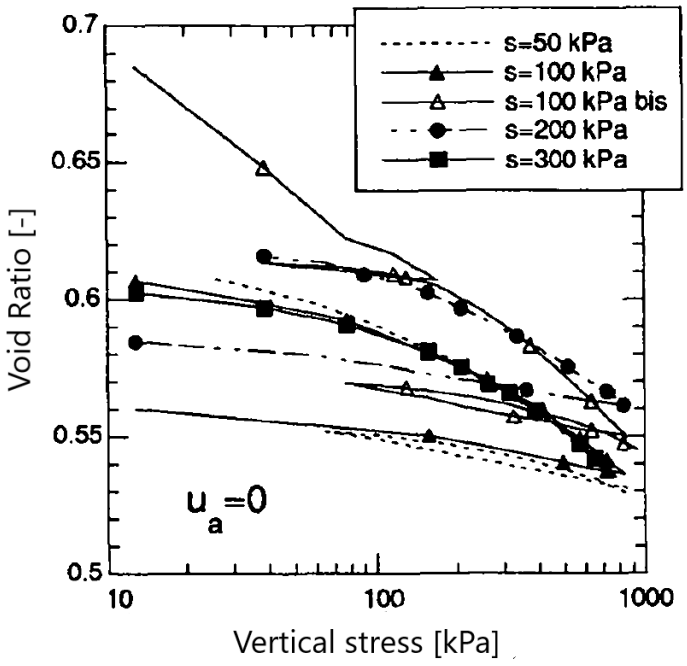


*Figure 2-7; Consolidation test for different value of suction (GEISER, 1999)*

The initial void ratio used for the further analysis is the one taken from a consolidation test done with an osmotic consolidometer (**Figure 2-7**) for different suction values. As there are

no essays for the expected range of suction the used vale is the one that goes closer to the them, that is 50 kPa.

*Table 4; Physical-Hydro-Mechanical parameters of the Sion silt (GEISER, 1999) modified*

| Shear Strength Angle ($\varphi'$) | Intercept Cohesion ($c'$) | Dry Density ($\rho_{dry}$) | Saturated Density ($\rho_{sat}$) | Elastic Modulus ($E$) | Poisson Coefficient ($\nu$) | Initial Void Ratio ($\varepsilon_0$) | Hydraulic Conductivity ($k_s$) |
|---|---|---|---|---|---|---|---|
| 32.0 [Deg] | 5.0 [kPa] | 1700 [kg/m$^3$] | 2460 [kg/m$^3$] | 22000 [kN/m$^2$] | 0.35 [-] | 0.62 [-] | $10^{-7}$ [m/s] |

Regarding the used sand, not all the information where available as for the previous soil, indeed with the exception of the granulometric curve (**Figure 2-8**) all the used parameters are taken either from (TERZIS, 2017) or from literature (TRUTY & OBRZUD, 2011) as a general cohesionless sand.

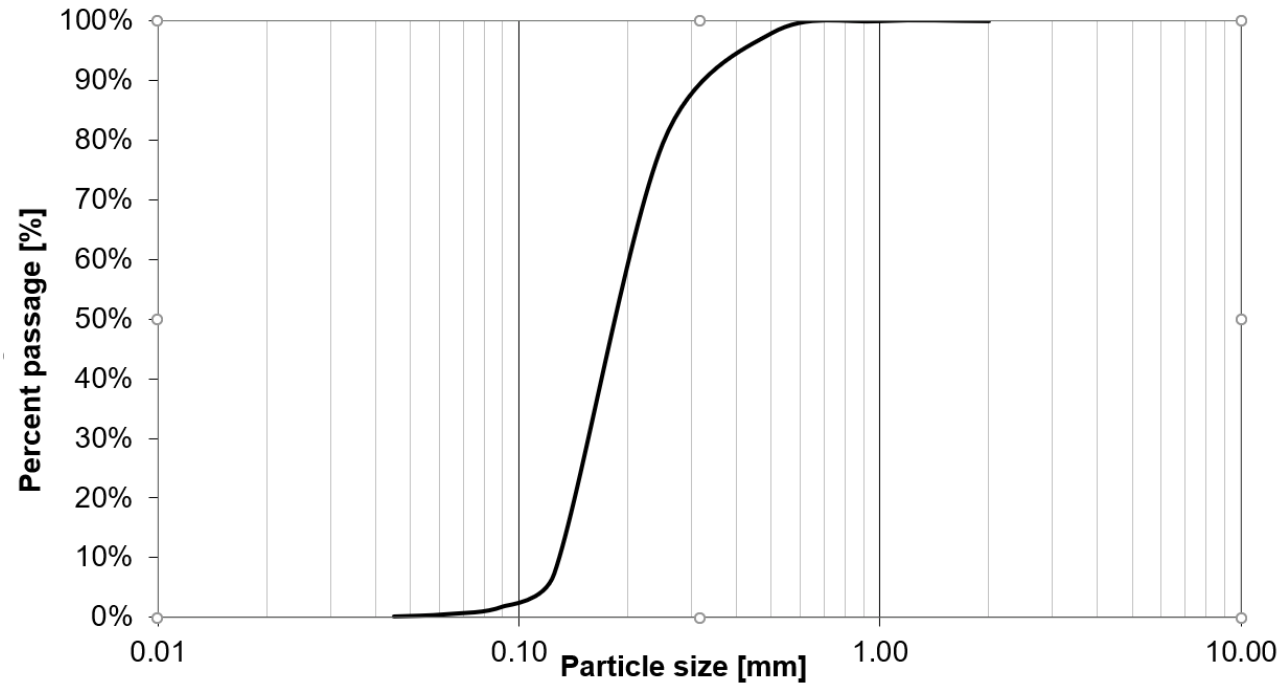


*Figure 2-8; Sand particle-size distribution curve*

By looking at the particle-size distribution curve result that the sand is poorly graded, that is confirmed by the uniformity coefficient reported in **Table 5**. Carry on looking at the same table it is possible to classify the soil following the USCS as a clean sand poorly graded SP. Another observation is that the specific gravity ($G_s$) of the sand is equal to 2.65 that the $G_s$ of the quartz, meaning that with a lot of probability is mainly composed by that mineral.

*Table 5; Physical-Hydro-Mechanical parameters of the Sand*

| $C_c$ | $C_u$ | (%) < 0.075 mm | (%) < 4.75 mm | (%) < 76.2 mm | $\gamma_s$ (kN/m$^3$) |
|---|---|---|---|---|---|
| 0.92 | 1.62 | 0.54 | 100 | 100 | 25.98 |

| Shear Strength Angle (φ') | Intercept Cohesion (c') | Dry Density ($\rho_{dry}$) | Saturated Density ($\rho_{sat}$) | Elastic Modulus (E) | Poisson Coefficient (ν) | Initial Void Ratio ($\varepsilon_0$) | Hydraulic Conductivity ($k_s$) |
|---|---|---|---|---|---|---|---|
| 35.0 [Deg] | 0.0 [kPa] | 1680 [kg/m$^3$] | 2070 [kg/m$^3$] | 20000 [kN/m$^2$] | 0.30 [-] | 0.60 [-] | $10^{-4}$ [m/s] |

Reassuming it's a cohesionless poorly graded clean sand mainly composed by quartz.

## 2.2 Methods

Since sands are generally characterized by low air entry values, that is estimated to be of a few kPa (**Figure 1-7**), one should prefer to adopt a technique such as pressure plate or a Tempe cell. The problem that arise when using those technique is the precision of the pressure controller, in our case the available controller where volumetric pumps with a precision of +/- 1Kpa and since two of those are needed the expected error is the double. To overcome this problem the Buchner-Haines funnel apparatus set up (HAINES, 1930), was thought to be adopted. This technique modified, named hanging water column, relies on the application of suction without using an axis translation and thus by maintaining the air pressure equal to the atmospheric pressure and by imposing an negative water pressure. The working principle of this system and a subsequent modification done by (SHARMA & MOHAMED, 2003) is shown in **Figure 2-9**.

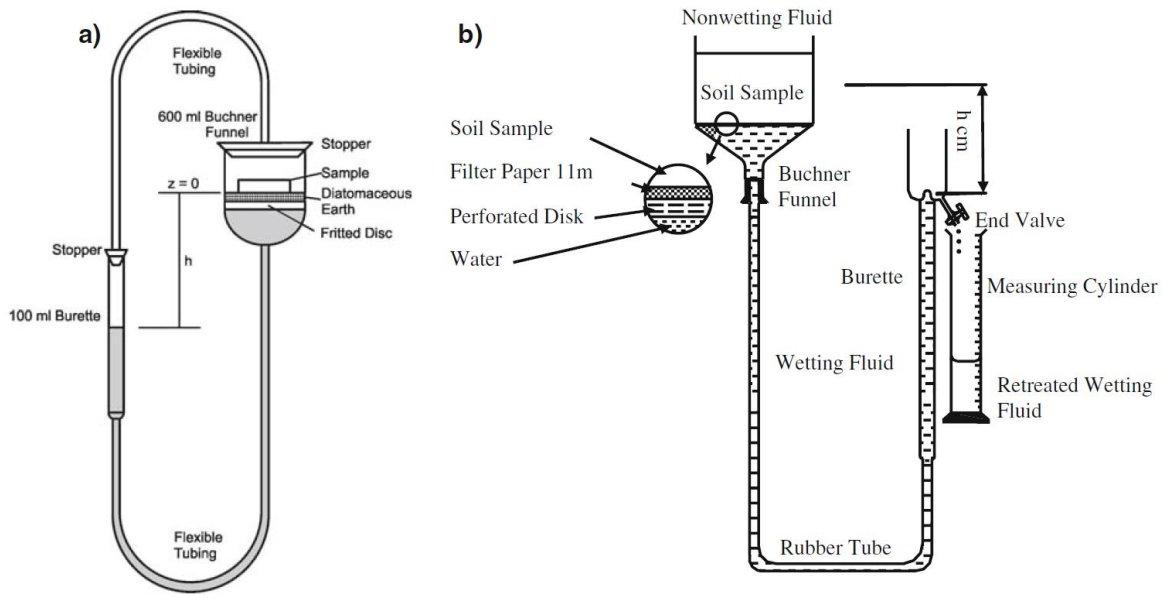


***Figure 2-9;*** *(a) Buchner-Haines funnel apparatus (HAINES, 1930); (b) modified layout of Buchner Funnel (SHARMA & MOHAMED, 2003)*

The disadvantages of the configuration (a) is that if the burette is lowered from the reference position Z=0 by a value of h, the water contained in to the soil specimen will flow in through the flexible tube in order to get to a new equilibrium position. This position is located somewhere in between z=0 and h, hence in order to apply a suction of $\gamma_w$*h is required to remove water since the equilibrium will be reached in the desired position h. The modified layout (b) allow to lower the burette in the desired position and the corresponding suction will be maintained by a valve that allow the outflow of water in to a measuring cylinder that collect the water spilled from the specimen.

In our case the specimens were placed in to a pressure plate conveniently modified (**Figure 2-10**) so that a hanging water column technique could be performed.

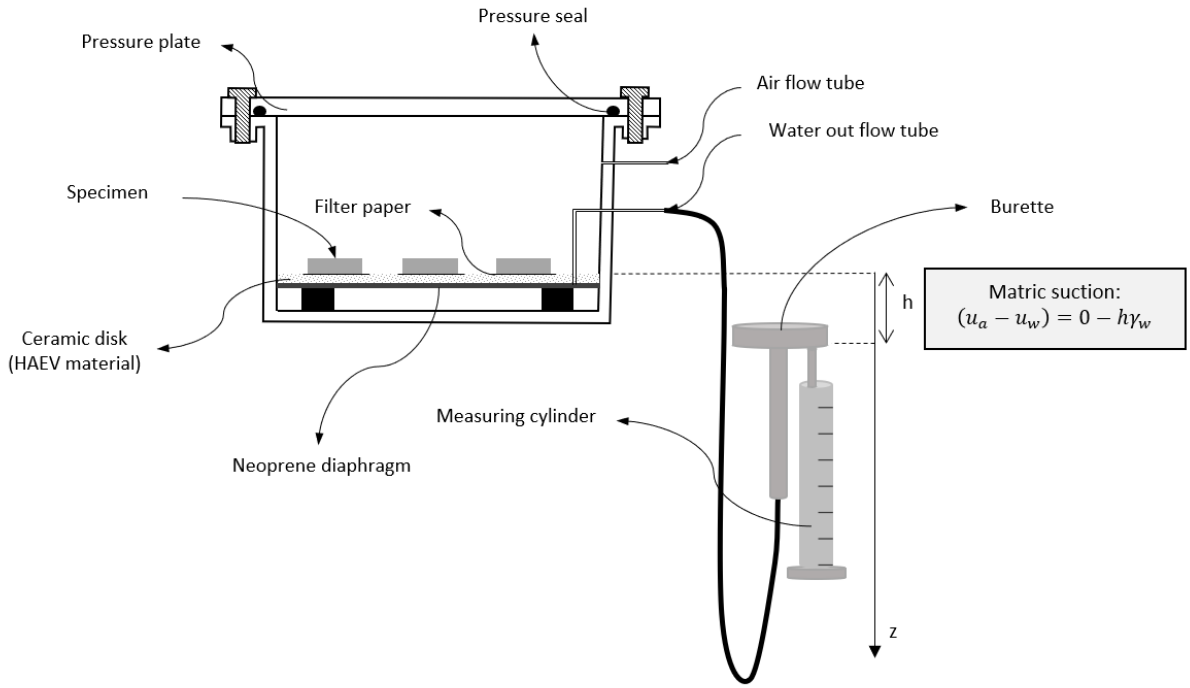


*Figure 2-10; layout of the used apparatus*

In this case the air flow tube was disconnected from the pressure controller so that the pressure inside the cell was equal to the atmospheric one, while the water out flow was connected to a burette by mean of a flexible tube. The burette was linked to a spillway that guarantee to apply always the same suction and that allowed to measure the water flowed out from the soil samples.

With this technique a drying and a wetting test have been performed for the Sion sand. Follow the description of the adopted procedure.

To obtain the soil water retention curve in drying condition 21 soil sample had been prepared as follow:

21 cylindrical shell had been used characterized by a height of 14 mm and a dimeter of 36 mm, at whose basal perimeter a filter paper was attached with a glue. Afterwards the cylinder shell had been filled with the sand and compacted with the purpose to reach the maximum compaction ($e_{min}$). To get the minimum void ratio sand was wetted in order to obtain a 10% of water content and then was manually added in to the cylinder shell and compacted layer by layer with a standard weight. This quite long operation has been performed for all the specimen.

All the specimens (**Figure 2-11**) had been labelled and next saturated leaving them for 7 days in to a closed box with water till a half of the sample height. Subsequently the samples were taken and placed in to the pressure plate (**Figure 2-11**) whose ceramic disk (characterised by

an AEV of 5 MPa) had been previously saturated, otherwise wouldn't be possible to guarantee the fluid continuity and thus to apply suction.

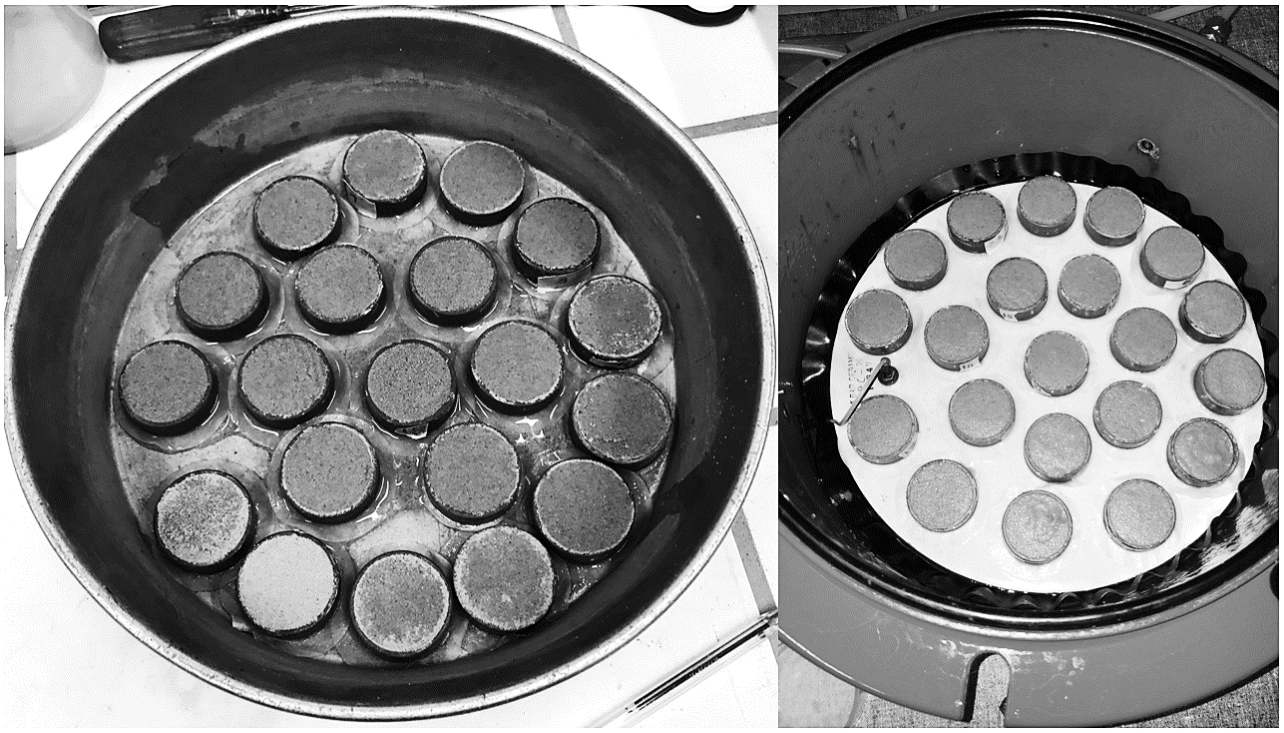

*Figure 2-11; Sand specimens: on the left the box used to saturate them; on the right the saturated specimen in the pressure plate before starting the test.*

The lid of the plate was closed and nine different loads of suction had been applied by lowering the burette (**Figure 2-12**) of 5, 10, 20, 30, 40, 50, 60, 70 and 100 centimetres to the reference height that corresponded with the ceramic disk.

For each step of suction the water flowed in to the measuring cylinder (**Figure 2-12**) was recorded and when no more water flowed out, equalization was considered to be reached and thus three sample were taken.


*Figure 2-12; Used apparatus (a) pressure plate with burette and graduated cylinder; (b) a detail of the graduated cylinder and the burette; (c) detail of the graduated cylinder.*

Six crucibles previously cleaned and marked where weighted; the three samples were divided in two, placed in the crucible and weighted. With this procedure was possible to evaluate the total weight of a portion of the soil sample. The sample where subsequently placed in to an oven at the temperature 105°C for 48 hours and then weighted again so the total dry volume of a portion of a sample was available. By difference of the aforesaid quantities the weight of the water was computed, thus the water content (w) is computed as the ratio of the mass of water ($m_w$) and the mass of the dry soil ($m_s$). The degree of saturation $S_r$ is calculated as a function of the water content by using the Equation 2.2

$$S_r = \frac{w\, G_s}{e} \tag{2.2}$$

Where: w is the water content and $G_s$ the specific gravity of soil solids.

This operation includes the assumption that there is no volume change in the specimen during the essay as the used value of the void ratio is the minimum one that is e=0.62.

To pass from the saturation ratio to the volumetric water content is necessary to multiply the saturation ratio with the porosity (n) where the relationship between porosity and void ratio Equation 2.3:

$$n = \frac{e}{1+e} \tag{2.3}$$

Regarding the wetting 18 samples were prepared, as for the drying, saturated and subsequently placed in to the pressure plate. In this case, closed the lid, the burette was lowered from the position zero of 100 cm, equalization was waited and then raised of 20, 40, 80 100 centimetres. For each step water was added in the burette till the water level stabilized in to the burette at the required height, this was a long process therefore, to avoid evaporation from the top of the burette, a plastic tube had been linked to the air flow tube of the pressure plate to the top of the burette. Since there was no more outflow from the sample the graduated cylinder was useless and hence removed. The computation of the saturation ratio was done in the same way used for the drying test.

In addiction the residual point is computed by mean of the Kelvin's equation (2.1) leaving three sample in to a standardized environment inside the laboratory at a temperature of 21.5°C and with a relative humidity RH=66 %, knowing the molecular mass of the water (18.016 kg/kmol), the universal gas constant (R=8.314 J/(mol*K)) and specific volume of water at 21.5°C ($1.00212*10^{-3}$ kg/m$^3$).

All the data have been treated by removing the extreme values and standard deviation was computed.

## 2.3 Results

The drying test started on the 09-04-18 and finished on the 04-05-18, while the wetting started on the 18-05-18 and finished on the 29-08-18. Thus, while the former had been quite fast (it was performed in one month) the second had been way longer since it lasted for more than three months. That it is due to the extra equalization time due to the manual water supplement. Indeed, to reach the desired value of suction during the wetting phase was necessary to rise the burette to the height required to guarantee the suction, subsequently water was added. After a certain amount of time the water level decrease to reach a new equilibrium point, lower to the demanded, then water was added again, till after a certain number of times the equalization occur where desired.

*Table 6; Matric suction and Saturation ratio derived from the hanging water column test on Sion sand*

| Drying | | | |
|---|---|---|---|
| ***Matric Suction [kPa]*** | ***Saturation Ratio Sr [-]*** | ***Volumetric Water Content ϑ [-]*** | ***Standard Deviation [-]*** |
| 0 | 1 | 0.394 | 0 |
| 0.5 | 1.030 | 0.394 | 0.015 |
| 1 | 0.996 | 0.381 | 0.008 |
| 2 | 1.007 | 0.386 | 0.011 |
| 3 | 0.984 | 0.377 | 0.022 |
| 4 | 0.793 | 0.303 | 0.018 |
| 5 | 0.699 | 0.268 | 0.041 |
| 6 | 0.296 | 0.109 | 0.011 |
| 7 | 0.226 | 0.084 | 0.002 |
| 10 | 0.163 | 0.060 | 0.009 |
| 56447 | 0.005 | 0.002 | 0.000 |
| **Wetting** | | | |
| ***Matric Suction [kPa]*** | ***Saturation Ratio Sr [-]*** | ***Volumetric Water Content ϑ [-]*** | ***Standard deviation [-]*** |
| 10 | 0.108 | 0.002 | 0.018 |
| 8 | 0.100 | 0.038 | 0.018 |
| 6 | 0.142 | 0.055 | 0.003 |
| 4 | 0.242 | 0.092 | 0.070 |
| 2 | 0.510 | 0.195 | 0.084 |
| 0 | 0.881 | 0.337 | 0.017 |

Here in **Table 6** the results of the test drying and wetting tests are reported, the results are quite satisfactory since, with the exception of some point, have a quite low standard deviation. Indeed, the error related to the three weighting of each sample has an average value of the 7%. As shown in **Figure 2-13** the average time required for the equalization is around 2 days and this time was shorter for low level of suction and longer for the higher level of suction. Indeed, going on with the drying less specimen where placed in the pressure plate and thus was more complicated to detect the equalization to the point where not enough water flowed in to the graduated cylinder. Therefore, the equalization of the last two step (7 and 10 kPa) had been detected when water started to evaporate from the burette. Regarding the point relative to the residual condition, is the one listed at the end of the drying point in **Table 7**.

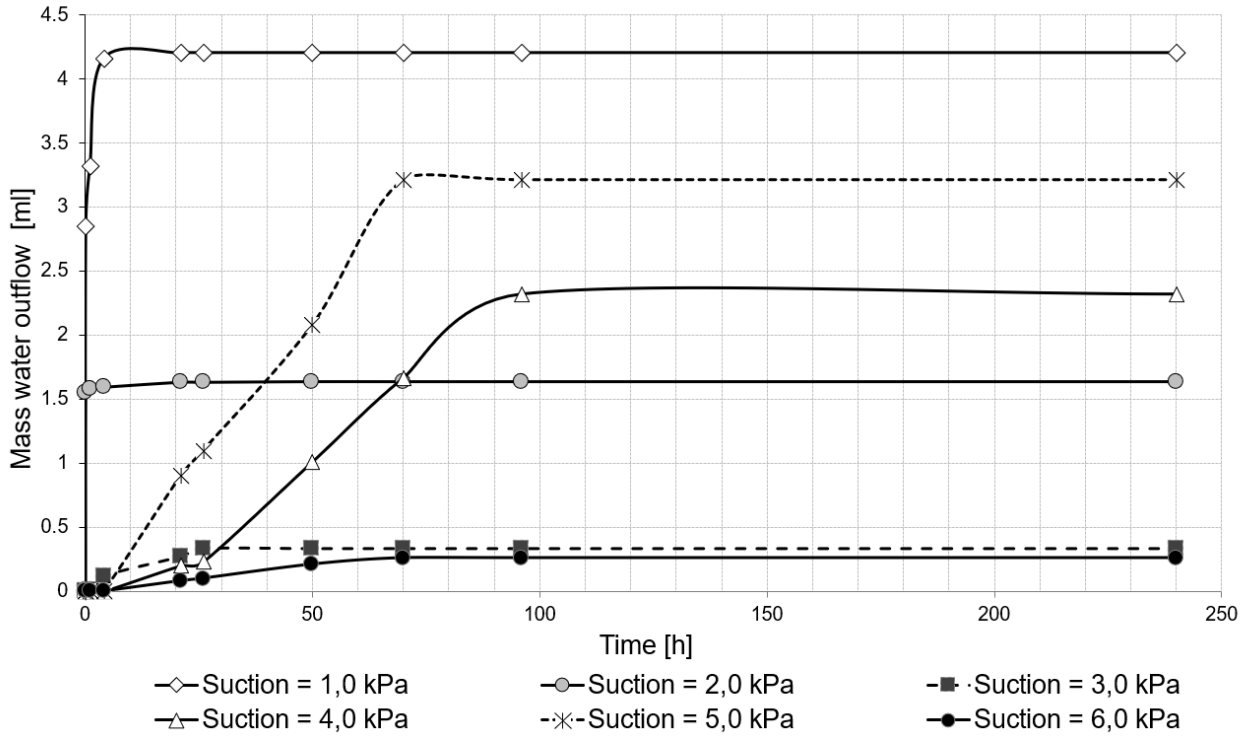


*Figure 2-13; Equalization curve for the wetting steps*

The data of **Table 6** have been subsequently fitted in order to obtain the parameters of the exponential and Van Ghenucten models. That are described in the end of the paragraph 1.3 by the Equation 1.32 and 1.33.

The data have been fitted by using a non-linear least squares solver script on the Software *Matlab* that allow to find the coefficient x that solve the problem:

$$\min_x \|F(x, xdata) - ydata\|_2^2 = \min_x \sum_i (F(x, xdata_i) - ydata_i)^2 \qquad (2.4)$$

Two different sets of parameters (**Table 7**) have been computed for the wetting and drying since, due to the hysteresis effect, the two curves are not the same.

*Table 7; Estimated fitting parameters for the exponential and Van Genuchten SWRC models*

| | ***Drying Van Genuchten*** | ***Wetting Van Genuchten*** |
|---|---|---|
| *beta [1/m]* | 0.2256 | 0.7991 |
| *m [-]* | 0.4355 | 0.2252 |
| *n [-]* | 7.2632 | 5.04 |
| | ***Drying Exponential*** | ***Wetting Exponential*** |
| *beta [1/m]* | 0.1292 | 0.3053 |

By mean of the value of **Table 7** had been possible to pass from a discretized SWRC to a continuum model. Those curves (**Figure 2-14**) will be used in the next chapter to evaluate the action on the retaining wall.

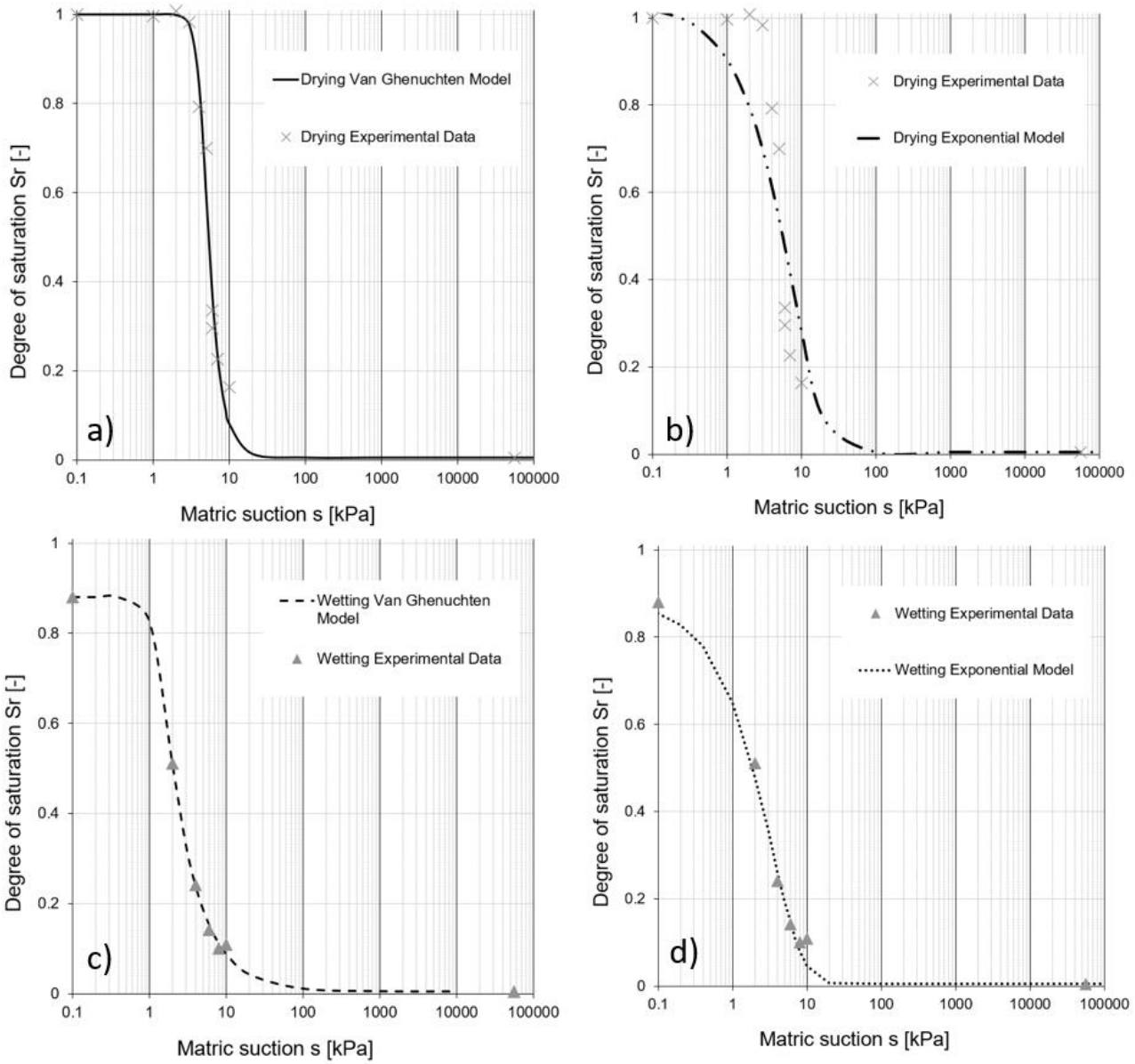


*Figure 2-14; Sion sand SWRC: (a) Van Genuchten model drying; (b) Exponential model drying; (c) Van Ghenuchten model wetting; (c) Exponential model wetting.*

Is clear that the Van Ghenuchten model fit much better the data since the exponential model is not able to represent the knee done by the air entry value. Likewise, is confirmed the hysteresis phenomena that is pretty clear in this case. Unfortunately, in the wetting phase some more point for low value of suction should had taken to better understand how the saturation would evolve. By drawing the tangents to the curve in the transient zone and to the boundary effect zone is possible to evaluate the AEV that is assessed to be at 3.8 kPa.

## 2.4 Conclusion

The adopted method is a good solution to determine the SWRC for a LAEV soil such a sand, the good control of the suction allow to have good precision in the determination of the AEV. Indeed, for the wetting phase the time required for the experiment is reasonable as it allow to obtain the curve in one month. The main incertitude arises with regard the wetting phase since, the role of the neoprene membrane below the ceramic disk is not so clear, by the way, as matter of principle, it should not affect the results. Nevertheless, the wetting is really long mainly, and this is due to the log time required for the equalization.

Neglecting the issues linked to the wetting or drying phase, the main incertitude that emerged from the method are linked with the sample preparation. Indeed, wasn't possible to check the void ratio of the sample and the homogeneity between them can be guaranteed only by the precision of the operator.

It is clear that the technique is suitable just for little range of pressure since for each 10 kPa of suction applied is necessary to lower the burette of one meter, thus there is the practical problem of applying high value of suction. Indeed, there is the physical constrain that in order to avoid metastable condition it is not possible to apply suction heads higher than 10 meters.

Concluding the technique allow to have a good control of the pressure but some improvement can be done with regard the specimen preparation and the wetting procedure.

# Chapter 3 Actions on retaining structures

In this chapter the main principles allowing for the computation of lateral earth actions are firstly introduced and discussed. In particularly, both dry and saturated conditions of the soil are considered following Rankine's theory of active pressure and the Coulomb's methods (paragraph 3.1). Then, in the following paragraph (paragraph 3.2) an uncoupled Hydro-mechanical approach is illustrated presenting the Lateral Earth Pressure (LEP) and Limit Equilibrium Method (LEM) analytical solutions for hydraulic steady state analysis. In the end, in the last paragraph (paragraph 3.3), analytical solution for transient analysis are shown.

## 3.1 Classic theories

The evaluation of the thrust exerted by a soil against a retaining wall is a classical problem of the geotechnical engineering, that can be handled by mean of two historical theories properly modified in sight of the effective stress theory: Rankine's and the Coulomb's theory.

The Rankine's theory moves from the fundamental concept of earth pressure at rest.

Let's consider a generic spot at a generic depth z (Figure 3-1), in to a cohesive-less dry soil characterized by a unit weight ($\gamma_{dry}$), constant with the depth and bounded above and below by a horizontal flat surface. For symmetry reasons the geostatic tensional state is axial-symmetric. At the considered spot, in a state of static equilibrium, the vertical stress ($\sigma'_{v0}$) is determined by the translation equilibrium in the vertical direction, and its value is $\sigma'_{v0}= z*\gamma_{dry}$, while the horizontal stress is the same in all the directions but is not statically determined and is equal to: $\sigma'_{h0}= K_0\sigma'_{v0}$.

Where: $K_0$ is named at-rest earth pressure coefficient and can be experimentally evaluated or by mean of empirical relationship such as the Jacky one (JAKY, 1944). Since it has a value lower than the unit, the vertical stress corresponds to the principal main stress $\sigma'_1$ while the horizontal stress corresponds to the principal minor stress $\sigma'_3$. Let's assume the Mohr Coulomb failure criterion, the geostatic stress state in the generic spot is represented in the MC plane of Figure 3-1.

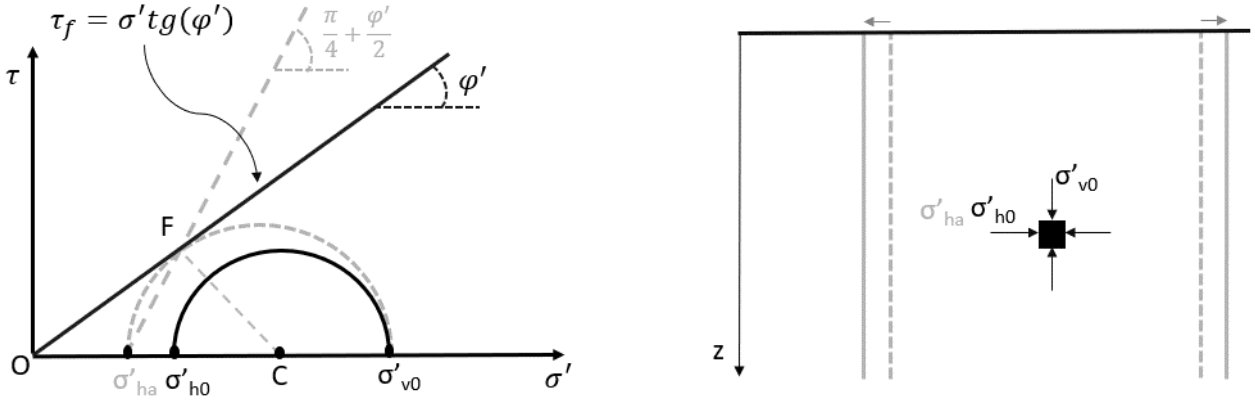


*Figure 3-1; At-rest state of stress in the generic point (black) and active conditions (grey).*

Supposing to insert on the left and right side of the generic spot two idealized frictionless vertical walls, at the generic depth z on both the walls, the exerted effective stress is $\sigma'_{h0} = K_0\sigma'_{v0}$. If the two walls are gradually displaced outwards, the symmetry conditions persist, and so vertical and horizontal stress are still the principals. The vertical stress won't change while the horizontal one decrease. Thus, the Mohr circle change as show in Figure 3-1: the principal main stress stays constant while the minimum principal stress decrease from the initial value $\sigma'_{h0}$ to the minimum compatible with the equilibrium. This limit value of stress named active earth pressure $\sigma'_{ha}$ corresponds to the minor principal stress of the Mohr's circle tangent to the failure envelop. The radius of the active stress state circle described, is equal to:

$$R = \frac{1}{2}(\sigma'_{v0} - \sigma'_{ha}) \tag{3.1}$$

Ad its distance from the origin:

$$OC = \frac{1}{2}(\sigma'_{v0} + \sigma'_{ha}) \tag{3.2}$$

Considering the right triangle OCF:

$$R = FC = OC sin\varphi' \tag{3.3}$$

$$\frac{1}{2}(\sigma'_{v0} - \sigma'_{ha}) = \frac{1}{2}(\sigma'_{v0} + \sigma'_{ha}) sin\varphi' \tag{3.4}$$

$$\sigma'_{ha}(1 + sin\varphi') = \sigma'_{v0}(1 - sin\varphi') \tag{3.5}$$

$$\sigma'_{ha} = \frac{(1 - sin\varphi')}{(1 + sin\varphi')}\sigma'_{v0} = tan^2\left(\frac{\pi}{4} - \frac{\varphi'}{2}\right)\sigma'_{v0} \tag{3.6}$$

Finally, the ratio:

$$K_a = \frac{(1 - sin\varphi')}{(1 + sin\varphi')} = tan^2\left(\frac{\pi}{4} - \frac{\varphi'}{2}\right) \tag{3.7}$$

Is named coefficient of Rankine's active earth pressure. This show that the failure planes make an angle of +/-(45+1/2φ') degrees with respect the direction of the major principal plane (horizontal).

The horizontal thrust ($P_a$) acting on each inner side of the two walls, from z=0 to z=H can be computed as the integral of the effective stress distributions:

$$P_a = \int_0^H \sigma'_{ha}\, dz = \int_0^H K_a * (z\gamma_{dry})\, dz = \frac{1}{2}\gamma_{dry}H^2K_a \tag{3.8}$$

Analogously it is possible to rewrite the Equation 3.6 by considering the soil fully saturated:

$$\sigma'_{ha} = K_a\sigma'_{v0} = K_a z\gamma' \tag{3.9}$$

In terms of total stress:

$$\sigma_{ha} = \sigma'_{ha} + u_w = K_a z\gamma' + z\gamma_w \tag{3.10}$$

In this case the horizontal thrust ($P_a$) acting on each inner side of the two walls, from z=0 to z=h can be computed as the integral of the total stress distributions:

$$P_a = \int_0^H \sigma_{ha}\, dz = \int_0^H (K_a z\gamma' + z\gamma_w)\, dz = \frac{1}{2}\gamma' H^2 K_a + \frac{1}{2}\gamma_w H^2 \tag{3.11}$$

If the soil has some cohesion is possible to repeat the same reasoning but, the MC failure criterion will change and by referring at **Figure 3-2**.

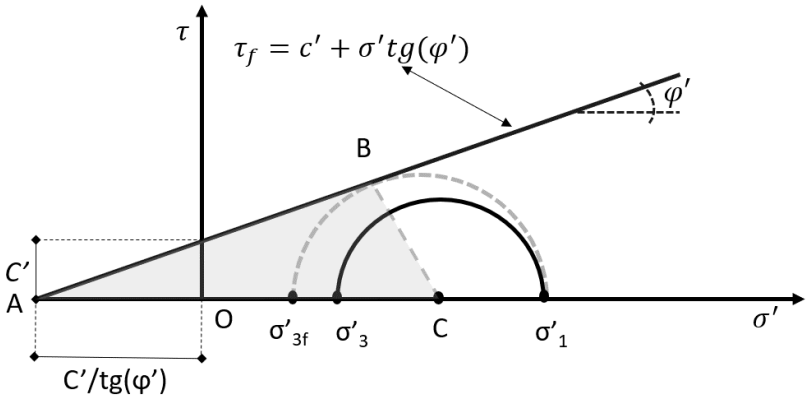


***Figure 3-2;*** *Rankine's active state of stress*

Let's consider the right triangle ABC:

$$R = BC = ACsin\varphi' = \left(\frac{c'}{\tan(\varphi')} + \frac{\sigma'_1 + \sigma'_{3f}}{2}\right) sin\varphi' \tag{3.12}$$

But also:

$$R = \frac{\sigma'_1 - \sigma'_{3f}}{2} \tag{3.13}$$

Thus:

$$\frac{\sigma'_1 - \sigma'_{3f}}{2} = \left(\frac{c'}{\tan(\varphi')} + \frac{\sigma'_1 + \sigma'_{3f}}{2}\right) sin\varphi' \tag{3.14}$$

Rearranging:

$$\sigma'_1(1 - sin\varphi') - \sigma'_{3f}(1 + sin\varphi') = \frac{2c'}{tg\varphi'} sen\varphi' \tag{3.15}$$

Expliciting $\sigma'_{3f}$:

$$\sigma'_{3f} = \frac{\sigma'_1(1 - sin\varphi')}{(1 + sin\varphi')} - \frac{\frac{2c'}{tg\varphi'} sen\varphi'}{(1 + sin\varphi')} \tag{3.16}$$

Recalling the relation:

$$\frac{(1 - sin\varphi')}{(1 + sin\varphi')} = tan^2\left(\frac{\pi}{4} - \frac{\varphi'}{2}\right) \tag{3.17}$$

And:

$$\frac{cos\varphi'}{(1+sin\varphi')} = tan\left(\frac{\pi}{4} - \frac{\varphi'}{2}\right) \tag{3.18}$$

We get:

$$\sigma'_{3f} = tan^2\left(\frac{\pi}{4} - \frac{\varphi'}{2}\right)\sigma'_1 - 2c'tan\left(\frac{\pi}{4} - \frac{\varphi'}{2}\right) \tag{3.19}$$

And substituting the 3.7 in to the 3.19:

$$\sigma'_{3f} = K_a\sigma'_1 - 2c'\sqrt{K_a} \tag{3.20}$$

And as before, there is an axial symmetric stress state and vertical and horizontal stress are considered to be the principals one, thus the 3.20 can be rewritten as:

$$\sigma'_{ha} = K_a\sigma'_v - 2c'\sqrt{K_a} \tag{3.21}$$

That is the Rankine's active pressure, in this case the horizontal stress correspond to the minor principal stress, while the vertical one correspond to the main principal stress. Here it is important to remark that soils do not have traction strength, thus the above equation is valid only for depth bigger than the one where $\sigma'_{ha} = 0$. As for the previous case (cohesionless soil) is possible to evaluate the thrust on the walls either for dry soil or saturated. In dry conditions:

$$P_a = \int_0^H \sigma_{ha}\, dz = \frac{1}{2}\gamma_{dry}H^2K_a - 2c'\sqrt{K_a} \tag{3.22}$$

For saturated conditions:

$$P_a = \int_0^H \sigma_{ha}\, dz = \frac{1}{2}\gamma' H^2K_a + \frac{1}{2}\gamma_w H^2 - 2c'\sqrt{K_a} \tag{3.23}$$

The presented solution can be extended to a generalized case for Rankine active pressure for a frictionless sub vertical wall with an inclined backfill fore this solution please refer to (CHU, 1991).

Long before Rankine the problem of the thrust on a retaining structure was presented by the French engineer Coulomb, by mean of a method based on the equilibrium of the acting forces.

Let's consider a wall of height H that support a granular dry soil and let's do the following further assumption: frictionless vertical wall, horizontal backfill, MC shear stress and flat failure surface.

If the wall is moved to the left, for Coulomb the failure happen with the detachment of the wedge ABC (**Figure 3-3**).

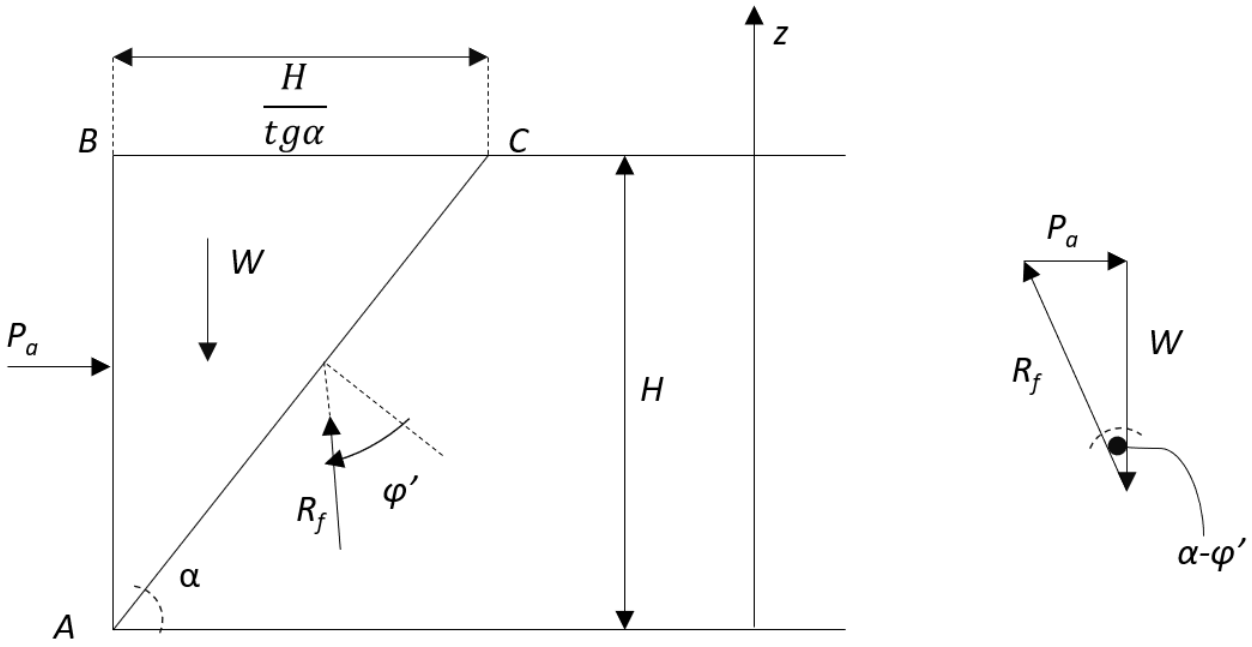


***Figure 3-3;*** *Trial failure wedge and force polygon for dry cohesionless Coulomb case.*

For limit equilibrium condition the forces that act on the wedge are: the weight of the soil that act in the vertical direction ($W=1/2\gamma_{dry}H^2\cot\alpha$), the resultant of the shear and normal forces on the surface of failure $R_f$ (inclined of an angle φ' to the normal at the failure's surface and with a tangential component pointing upward) and the active force that act horizontally due to the assumption of frictionless wall.

For the law of sines equilibrium:

$$\frac{P_a}{sin(\alpha-\varphi')}=\frac{W*tan(\alpha-\varphi')}{cos(\frac{\pi}{2}-\alpha+\varphi')} \tag{3.24}$$

$$P_a=\frac{1}{2}\gamma_{dry}H^2cot\alpha*tan(\alpha-\varphi') \tag{3.25}$$

That is a function of alpha, thus to evaluate the condition of the active limit equilibrium the maximum of the function 3.12 need to be computed by imposing its partial derivative equal to zero.

$$\frac{dP_a}{d\alpha}=\frac{1}{2}\gamma_{dry}H^2\frac{d}{d\alpha}[cot\alpha*tan(\alpha-\varphi')\ ]=0 \tag{3.26}$$

$$cot\alpha \frac{1}{cos^2(\alpha - \varphi')} - tan(\alpha - \varphi') \frac{1}{sen^2\alpha} = 0 \quad (3.27)$$

$$\frac{cos\alpha}{sin\alpha} \frac{1}{cos^2(\alpha - \varphi')} - \frac{sin(\alpha - \varphi')}{cos(\alpha - \varphi')} \frac{1}{sin^2\alpha} = 0 \quad (3.28)$$

$$\frac{cos\alpha sin\alpha - sin(\alpha - \varphi')cos(\alpha - \varphi')}{cos^2(\alpha - \varphi')sin^2\alpha} = 0 \quad (3.29)$$

$$-\sin[2(\alpha - \varphi')]] + sin2\alpha = 0 \quad (3.30)$$

$$\alpha = \frac{\pi}{4} + \frac{\varphi'}{2} \quad (3.31)$$

Finally substituting the 3.31 in to the 3.25:

$$P_a = \frac{1}{2}\gamma_{dry}H^2 tan^2\left(\frac{\pi}{4} - \frac{\varphi'}{2}\right) \quad (3.32)$$

And substituting the 3.7 in to the 3.32:

$$P_a = \frac{1}{2}\gamma_{dry}H^2 K_a \quad (3.33)$$

That is the same solution obtained with Rankine.

Now let's derive the Coulomb solutions by maintaining the same hypothesis of the previous case with the exception that the soil is considered saturated. By referring to the **Figure 3-4** is possible to find the active thrust $P_a$ by solving the polygon of forces.

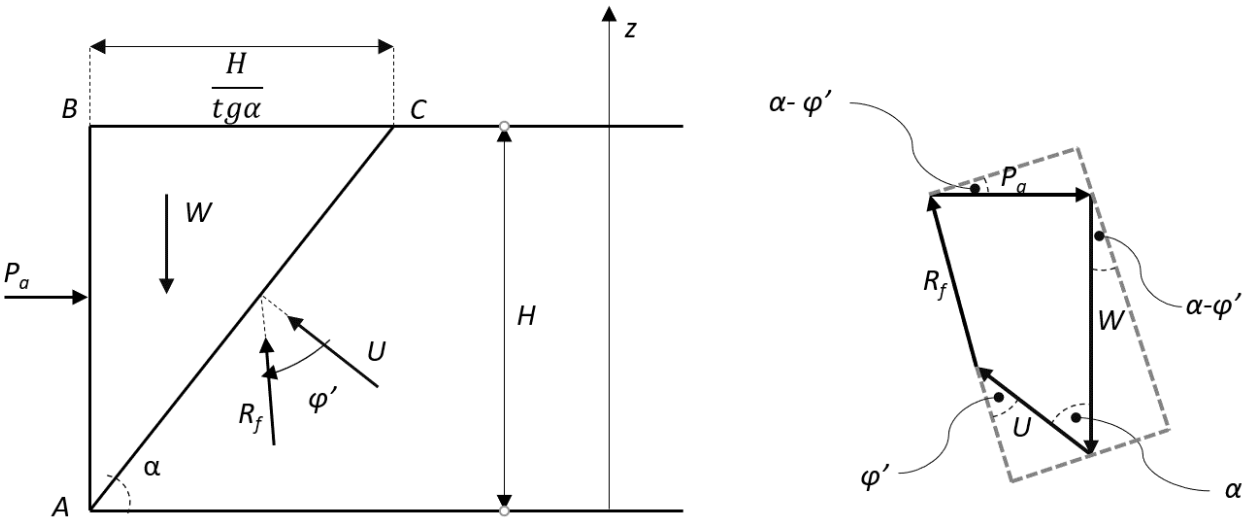


***Figure 3-4****; Trial failure wedge and force polygon for saturated cohesionless Coulomb case.*

Is possible to resolve the polygon quite easily by doing the equilibrium in the direction perpendicular to the resulting force $R_f$:

$$P_a \cos(\alpha - \varphi') = U sin(\varphi') + W sin(\alpha - \varphi') \tag{3.34}$$

That is:

$$P_a = \frac{U sin(\varphi') + W sin(\alpha - \varphi')}{cos(\alpha - \varphi')} \tag{3.35}$$

Where: U is the water thrust acting along the surface of failure AC and W the saturated weight of the soil.

Thus:

$$U = \frac{H^2 \gamma_w}{2 sin\alpha} \tag{3.36}$$

While:

$$W = \frac{H^2 \gamma_{sat}}{2 tan\alpha} \tag{3.37}$$

As for the dry case to find the value of alpha that maximise the active thrust, by computing the total derivative with respect to α and imposing that is equal to zero. The result is the same obtained for the previous case, that is:

$$\alpha = \frac{\pi}{4} + \frac{\varphi'}{2} \tag{3.31}$$

And placing the 3.32, 3.37 and 3.36 in to the 3.35 and rearranging we get:

$$P_a = \frac{1}{2}\gamma_{sat} H^2 tan^2\left(\frac{\pi}{4} - \frac{\varphi'}{2}\right) + \frac{1}{2}\gamma_w H^2 \frac{sin\varphi'}{sin^2\left(\frac{\pi}{4} + \frac{\varphi'}{2}\right)} \tag{3.38}$$

Remembering:

$$K_a = \frac{(1 - sin\varphi')}{(1 + sin\varphi')} = tan^2\left(\frac{\pi}{4} - \frac{\varphi'}{2}\right) \tag{3.7}$$

Substituting the 3.7 into 3.38 and rearranging we get the Equation 3.39 that it is exactly the same solution obtained with the Rankine's method for a cohesionless saturated soil.

$$P_{a=}\frac{1}{2}\gamma_{sat} H^2 K_a + \frac{1}{2}\gamma_w H^2 (1 - K_a) \tag{3.39}$$

Is possible to extend the Coulomb solutions in other to account more variables such as: inclined backfill and wall, soil-wall friction, cohesion and also earthquake forces (DAS & SOBHAN, 2013).

## 3.2 Actions of unsaturated soils – steady state analysis

Here two uncoupled hydro mechanical solutions for computing active thrust on retaining structures, are presented for steady vertical fluid flow. Saying uncoupled means that firstly is solved the hydraulic problem that is later used for solving the mechanical problem.

As shown in the paragraph 1.1 the vertical distribution of the matric suctions is widely variable in natural soils, nevertheless the main hydrologic properties that control the process are soil water retaining curve and the hydraulic conductivity. In case of no a flow condition the suction profile assume the linear behaviour of a hydrostatic distribution and the water content is the one given by the SWRC with a minimum value close to the upward

boundary (surface) and the maximum possible at the GWT. If from the mentioned no flow condition, water starts to infiltrate, as happen during a rain event, the water content increase and consequently the matric suction decrease.

The profile for a given vertical downward fluid flux can be given by imposing a null matric suction at the water table, as follow (LU & LIKOS, 2004): let's write the Equation 1.22 in the only vertical direction:

$$q = k\left(\frac{dh_m + 1}{dz}\right) \tag{3.40}$$

And by substituting the hydraulic conductibility Gardner's exponential model (Equation 1.34):

$$q = k_s * e^{\beta h_m}\left(\frac{dh_m + 1}{dz}\right) \tag{3.41}$$

Integrating and imposing the above-mentioned BC (BEAR, 2013):

$$h_m = \frac{1}{\beta} ln\left[\left(1 + \frac{q}{k_s}\right) e^{-\beta(z-h_0)} - \frac{q}{k_s}\right] \tag{3.42}$$

That gives the matric head for a given flux knowing the parameters β and $K_s$ (cf. § 1.1). It can be also be written in terms of matric suction:

$$s = \frac{1}{\alpha} ln\left[\left(1 + \frac{q}{k_s}\right) e^{-\alpha(z-h_0)} - \frac{q}{k_s}\right] \tag{3.43}$$

In the paragraph 1.2 the Bishop effective stress definition had been introduced and thus also the effective stress parameter χ, that can be written as the effective saturation described, for instance by the Van Genuchten model:

$$\Theta = \left[\frac{1}{1 + (\beta h_m)^n}\right]^m \tag{1.32}$$

That in terms of matric pressure became:

$$\Theta = \left[\frac{1}{1 + (\alpha s)^n}\right]^m \tag{3.44}$$

Since the stress state induced by suction is written as the product of the effective stress parameter and the matric suction, we get:

$$\Theta s = \frac{1}{\alpha} ln\left[\left(1 + \frac{q}{k_s}\right) e^{-\alpha(z-h_0)} - \frac{q}{k_s}\right]\left[\frac{1}{1 + (\alpha s)^n}\right]^m \tag{3.45}$$

and by substituting the 3.41 in to 3.43:

$$\Theta s = \frac{ln\left[\left(1+\frac{q}{k_s}\right)e^{-\alpha(z-h_0)}-\frac{q}{k_s}\right]}{\alpha\left[1+\left(\alpha s=\frac{1}{\alpha}ln\left[\left(1+\frac{q}{k_s}\right)e^{-\alpha(z-h_0)}-\frac{q}{k_s}\right]\right)^n\right]^m} \tag{3.46}$$

That is the vertical profile of the suction stress for a steady water flux and represent the analytical solution, of the steady hydraulic model used in to the mechanical solution.

Regarding the mechanical behaviour is possible to infer stress distributions for an unsaturated soil at rest. This can be done by mean of the Hooke's stress-strain constitutive law (LU & LIKOS, 2004):

$$\varepsilon_x = \frac{\sigma'_x}{E} - \frac{\upsilon}{E}\left(\sigma'_y + \sigma'_z\right) \tag{3.47}$$

$$\varepsilon_y = \frac{\sigma'_y}{E} - \frac{\upsilon}{E}\left(\sigma'_x + \sigma'_z\right) \tag{3.48}$$

$$\varepsilon_z = \frac{\sigma'_z}{E} - \frac{\upsilon}{E}\left(\sigma'_y + \sigma'_x\right) \tag{3.49}$$

Where: $\varepsilon_x$, $\varepsilon_y$ and $\varepsilon_z$ are the principal strain components along the cartesian axis, E is the Young's modulus and ν the Poisson's ratio. By substituting the Bishop's effective stress definition (Equation 1.37) in to the 3.47, 3.48 and 3.49:

$$\varepsilon_x = \frac{\sigma_x - u_a + \chi s}{E} - \frac{\upsilon}{E}\left(\sigma_y + \sigma_z - 2u_a - 2\chi s\right) \tag{3.50}$$

$$\varepsilon_y = \frac{\sigma_y - u_a + \chi s}{E} - \frac{\upsilon}{E}\left(\sigma_y + \sigma_z - 2u_a - 2\chi s\right) \tag{3.51}$$

$$\varepsilon_z = \frac{\sigma_z - u_a + \chi s}{E} - \frac{\upsilon}{E}\left(\sigma_x + \sigma_y - 2u_a - 2\chi s\right) \tag{3.52}$$

If we do the assumption that $\sigma_x=\sigma_y=\sigma_h$ and $\sigma_z=\sigma_v$, the above relations become:

$$\varepsilon_h = \frac{\sigma_h - u_a + \chi s}{E} - \frac{v}{E}(\sigma_h + \sigma_v - 2u_a - 2\chi s) \tag{3.53}$$

$$\varepsilon_v = \frac{\sigma_v - u_a + \chi s}{E} - \frac{v}{E}(2\sigma_h - 2u_a - 2\chi s) \tag{3.54}$$

By considering the stress null and comparing:

$$\frac{\sigma_h - u_a}{\sigma_v - u_a} = \frac{v}{1-v} - \frac{1-2v}{1-v}\frac{\chi s}{\sigma_v - u_a} = K_0 \tag{3.55}$$

That is the coefficient of earth pressure at rest.

Following the same line of reasoning, adopted in the previous paragraph for Rankine's active pressure coefficient, is possible to derive the lateral earth pressure (LEP) solutions for the unsaturated case.

Lets' consider a horizontal layer of an unsaturated cohesive soil, the horizontal tensional state can be described by mean of the coefficient of earth pressure at rest (Equation 3.51). If we do the mental experiment of placing two vertical frictionless walls on both the sides of a generical element and we displace those wall outwards, the minimum principal stress will gradually decrease while the main one remains constant.

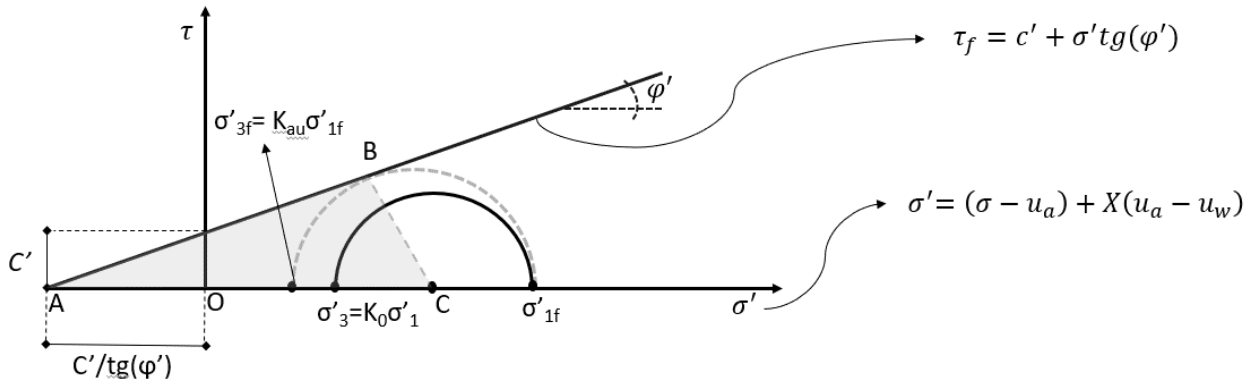


*Figure 3-5; MC failure criterion for unsaturated soil; active earth pressure stress state*

To the value of the minor principal stress at failure can be inferred by the geometry showed of **Figure 3-5**:

$$R = BC = ACsin\varphi' = \left(\frac{c'}{\tan(\varphi')} + \frac{\sigma'_1 + \sigma'_{3f}}{2}\right) sin\varphi' \tag{3.56}$$

$$R = \frac{\sigma'_1 - \sigma'_{3f}}{2} \tag{3.57}$$

$$\frac{\sigma'_1 - \sigma'_{3f}}{2} = \left(\frac{c'}{\tan(\varphi')} + \frac{\sigma'_1 + \sigma'_{3f}}{2}\right) sin\varphi' \tag{3.58}$$

Rearranging:

$$\sigma'_1(1 - sin\varphi') - \sigma'_{3f}(1 + sin\varphi') = \frac{2c'}{tg\varphi'} sen\varphi' \tag{3.59}$$

$$\sigma'_{3f} = \frac{\sigma'_1(1 - sin\varphi')}{(1 + sin\varphi')} - 2c' \frac{cos\varphi'}{(1 + sin\varphi')} \tag{3.60}$$

Recalling:

$$K_a = \frac{(1 - sin\varphi')}{(1 + sin\varphi')} = tan^2\left(\frac{\pi}{4} - \frac{\varphi'}{2}\right) \tag{3.7}$$

$$\sigma'_{3f} = \sigma'_1 K_a - 2c'\sqrt{K_a} \tag{3.61}$$

Placing the principal stress equal to the horizontal and vertical stress and substituting the Bishop's stress definition in to the previous 3.61:

$$\sigma_{hf} - u_a + \Theta s = (\sigma_{vf} - u_a + \Theta s)K_a - 2c'\sqrt{K_a} \tag{3.62}$$

Finally, rearranging the 3.62, we get the lateral earth pressure for the unsaturated case as:

$$(\sigma_{hf} - u_a) = (\sigma_{vf} - u_a)K_a - 2c'\sqrt{K_a} - \Theta s(1 - K_a) \quad (3.63)$$

Where: $(\sigma_{hf} - u_a)$ is the net horizontal stress, $(\sigma_{vf} - u_a)K_a$ is the earth pressure due to the soil weight, $2c'sqrt(K_a)$ is the mobilized cohesion and $\Theta s(1- K_a)$ is the contribute of the suction stress.

Doing the ratio of the two net stress term is possible to write the coefficient of unsaturated active earth pressure $K_{au}$ as:

$$\frac{(\sigma_{hf} - u_a)}{(\sigma_{vf} - u_a)} = K_a - \frac{2c'\sqrt{K_a}}{(\sigma_{vf} - u_a)} - \frac{\Theta s}{(\sigma_{vf} - u_a)} = K_{au} \quad (3.64)$$

In the figure below are shown the contributes of each term considering the suction profile model introduced at the beginning of the paragraph.

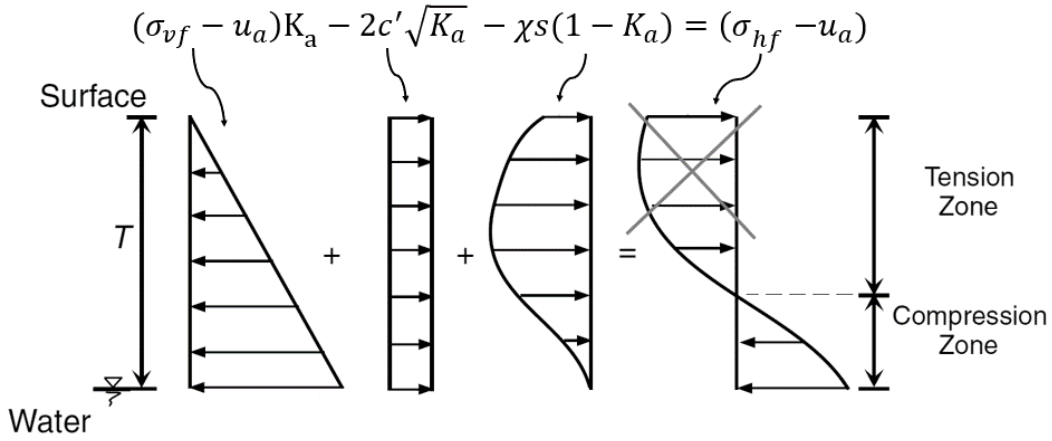


*Figure 3-6; Representation of the horizontal active net stress components (LU & LIKOS, 2004) modified.*

The presence of suction, as shown in **Figure 3-6**, always induces, in to unsaturated soils, a tension close to the ground surface. The existence of those tension stress, coupled with the null tensile strength of soils is the cause of the tension cracks, a phenomenon, clear also at the macroscopic scale. Indeed, is possible to observe in to silty or clayey soils exposed to evaporation such as dry puddles, where is common to see repetitive textures of fissures, precisely due to this phenomenon.

In this case the total active thrust exerted on a retaining structure by unsaturated soil exposed to a certain water flux q. Can be assessed, if the position of the water table is known, as the integral of the positive horizontal net stress given by the Equation 3.63.

An alternative approach, for computing the thrust on retaining structures, is to consider the limit equilibrium of a soil's wedge as for the Coulomb's method. Here is presented an

analytical solution with the limit equilibrium method (LEM) to evaluate the active thrust in to unsaturated soils.

As for the Coulomb's method presented in the previous paragraph let's consider a vertical frictionless retaining wall, a horizontal backfill and a plane surface of failure, with the exception that in this case a cohesive unsaturated soil is considered.

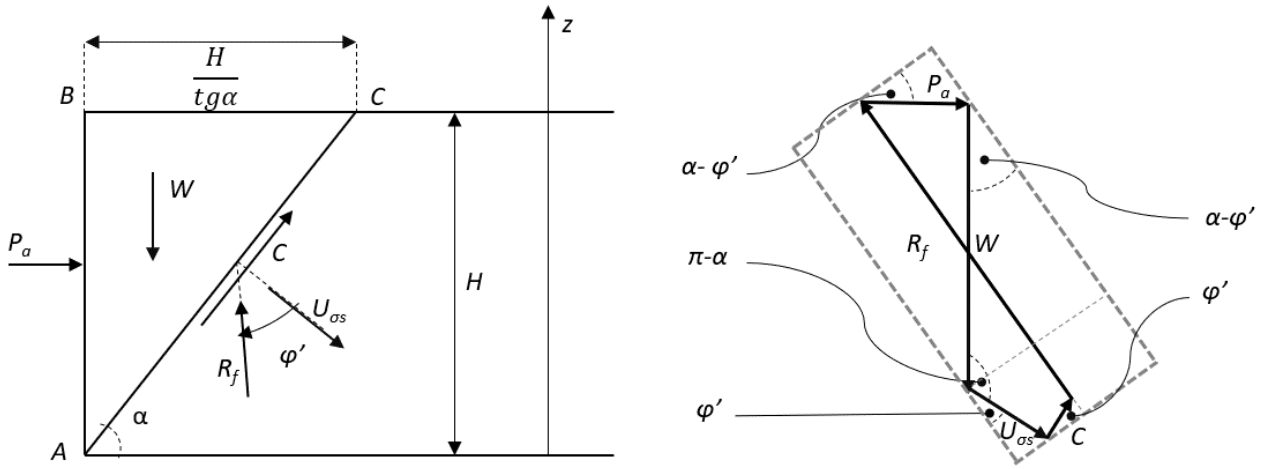


*Figure 3-7; LEM for an unsaturated cohesive soil; wedge and equilibrium polygon.*

With reference to the **Figure 3-7**, let's suppose to gradually move leftward the ideal wall, at limit equilibrium condition there is the formation of the wedge ABC. At incipient failure the acting forces are the one represented in the above figure and thus is possible to resolve the polygon of forces by solving the equation of equilibrium in the direction perpendicular to the resultant force $R_f$:

$$P_a\, cos(\alpha - \varphi') = U_{\sigma s} sin(\varphi') + W sin(\alpha - \varphi') + C cos(\varphi') \tag{3.65}$$

That is:

$$P_a = \frac{U_{\sigma s} sin(\varphi') + W sin(\alpha - \varphi') + C cos(\varphi')}{cos(\alpha - \varphi')} \tag{3.66}$$

Where C is the cohesive force acting along the failure surface AC, given by the intercept cohesion c' times the length of AC:

$$C = \frac{H * c'}{sin\alpha} \tag{3.67}$$

And $U_{\sigma s}$ is the suction stress force acting along the failure surface AC (**Figure 3-8**), given as the integral of the projection on the surface AC, of the vertical suction stress profile (Equation 3.46):

$$U_{\sigma s} = \frac{1}{sin\alpha} \int_0^H \Theta s \, \mathrm{dz} \tag{3.68}$$

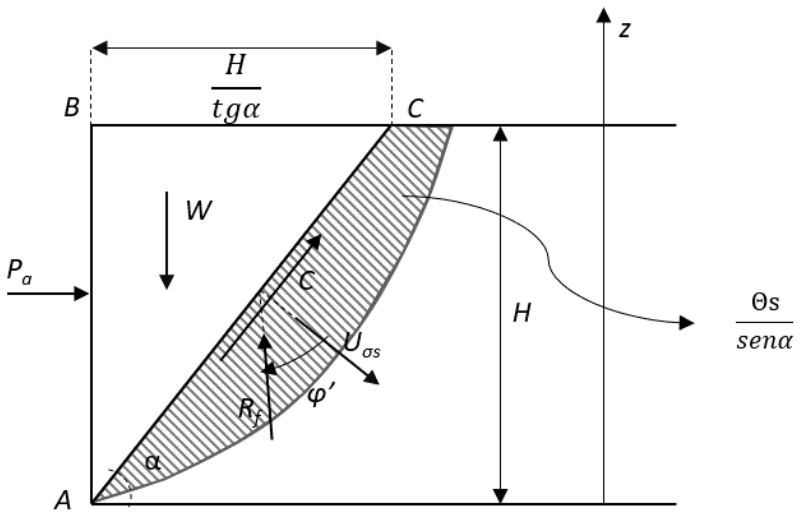


*Figure 3-8; Suction stress acting on the failure surface AC*

Finally, is possible to compute the total derivative of the Equation 3.66 with respect the angle of failure α to find the maximum value of thrust and hence the solution.

A more general case that allow to account also for soil-wall friction, soil-wall adhesive force and inclination of the wall is given by (SAHOO & GANESH, 2017), with the differential equation of the equilibrium solution.

## 3.3 Actions of unsaturated soils – transient analysis

In this paragraph a one-dimensional analytical transient solution of Richard's Equation (Eq. 1.30; cf. § 1.2), it is presented. This solution is afterward implemented in to the LEM and LEP mechanical solution (cf. § 3.2), allowing to perform uncoupled hydro mechanical analysis with transient flow in to unsaturated soils.

$$C(h_m)\frac{\partial h_m}{\partial t} = div[k(h_m)\nabla h_t] \tag{1.30}$$

To approach a problem concerning the solution of a non-linear partial differential equation it is possible to choose between a numerical resolution and an analytical solution. The

former case consists in the choice of a numerical technique (such as finite difference method or finite element method), the discretization of the equation and the writing of a code that solve the problem. The latter option does not require such a computational effort and might be preferred insight of a better handling of the process and a lighter computational demand (KEVORIKAN, 1993).

For the Richard's equation (1.30) there are no general analytical solution, but some specific solution might be available. In the current issue, (YUAN & LU, 2005) give a solution to transient flow for homogenous soils and time dependent surface fluxes under the following initial condition (steady state matric head profile):

$$h_m(z,0) = h_{m,0}(z) \tag{3.69}$$

And boundary conditions (matric head at the lower boundary and time dependent flux at ground surface):

$$\begin{gathered} h_m(0,t) = h_{m,1} \\ \left[k(h_m)\left(\frac{\partial h_m}{\partial z} + 1\right)\right]_{z=L} = -q_1(t) \end{gathered} \tag{3.70}$$

Using the exponential hydraulic conductivity and volumetric water content models proposed in the paragraph 1.2:

$$\theta = e^{\beta h_m} \tag{1.33}$$

$$k = k_s * e^{\beta h_m} \tag{1.34}$$

Is possible to linearize the Equation 1.30 by mean of the Kirchhoff transformation:

$$\Phi(z,t) = \int_{-\infty}^{h_m} k(h_m)dh = \frac{k(h_m)}{\alpha} = \frac{k_s}{\alpha} e^{\beta h_m} \tag{3.71}$$

And:

$$\frac{\partial^2 \Phi}{\partial z^2} + \beta \frac{\partial \Phi}{\partial z} = \frac{1}{D}\frac{\partial \Phi}{\partial t} \tag{3.72}$$

The new initial condition is:

$$\Phi(z,0) = \frac{k_s}{\beta} e^{\beta h_{m,0}(z)} \tag{3.73}$$

And the boundary conditions became:

$$\begin{gathered} \Phi(0,t) = \frac{k_s}{\beta} e^{\beta h_{m,1}} \\ \left[\frac{\partial \Phi}{\partial z} + \beta\Phi\right]_{z=L} = -q_1(t) \end{gathered} \tag{3.74}$$

Resolving by mean of Laplace transformation:

$$\begin{aligned} \Phi(z,t) = \Phi_s(z) \\ + 8Dexp\left[\frac{\beta(L-z)}{2}\right] \sum_{n=1}^{\infty} \frac{\left(\lambda_n^2 + \frac{\beta^2}{4}\right) sin(\lambda_n L)\, sin(\lambda_n z)}{2\beta + \beta^2 L + 4L\lambda_n^2} \int_0^t [q_0 \\ - q_1(\tau)] exp\left[-D\left(\lambda_n^2 + \frac{\beta^2}{4}\right)(t-\tau)\right] d\tau \end{aligned} \tag{3.75}$$

Being $\Phi_s(z)$ the initial condition:

$$\Phi_s(z) = \frac{k_s exp\left[\beta(h_{m,1} - z)\right]}{\beta} + \frac{q_0}{\beta}[exp(-\beta z) - 1] \tag{3.76}$$

Where: $\lambda_n$ is the nth positive root of the equation $\sin(\lambda L)+(2\lambda/\beta)\cos(\lambda L)=0$.

In order to adopt the solution given by the Equation 3.75 in to the LEM and LEP mechanical solutions, is convenient to explicit in the Equation 3.71 the matric head:

$$h_m(z,t) = \frac{1}{\beta} ln \frac{\beta\Phi(z,t)}{k_s} \tag{3.77}$$

Remembering that we placed the effective stress parameter equal to the normalized volumetric water content and that this last one can be written by mean of the Equation 1.33, substituting we obtain:

$$\chi(z,t) = \Theta(z,t) = \frac{\theta(z,t) - \theta_{res}}{\theta_{sat} - \theta_{res}} = \frac{e^{\beta h_m(z,t)} - \theta_{res}}{\theta_{sat} - \theta_{res}} \tag{3.78}$$

And remembering that is possible to pass from matric head to matric suction by the following relation:

$$s = g\rho_w h_m \tag{3.79}$$

We get:

$$s(z,t) = g\rho_w \frac{1}{\beta} ln \frac{\beta}{k_s} \Phi(z,t) \tag{3.80}$$

Thus, the suction stress, now time dependent can be substituted in to the LEP solution:

$$\sigma_{h,net}(z,t) = (\sigma_{vf} - u_a)K_a - 2c'\sqrt{K_a} - \Theta(z,t)s(z,t)(1 - K_a) \tag{3.81}$$

And in to the LEM solution:

$$P_a(t) = \frac{\frac{1}{sin\alpha}\int_0^H \Theta(z,t)s(z,t)dz\, sin(\varphi') + Wsin(\alpha - \varphi') + \frac{H * c'}{sin\alpha}\, cos(\varphi')}{cos(\alpha - \varphi')} \tag{3.82}$$

The so obtained Equations 3.57 and 3.58 are the transient analytical solutions that allow to compute the trust exerted by an unsaturated soil on to retaining structures.

# Chapter 4 The adopted methodology in the framework of current standards

In this chapter, after a review of the European and Italian standards a method to investigate the retaining walls performances during rainfalls events is illustrated. This is done by mean of coupled hydromechanical analysis and by taking in to account, effective infiltration and the critical precipitation. Effective infiltrations, how described by the Horton model, are taken in to account to allow higher infiltrations in to the soil; Indeed, critical precipitation are evaluated by mean of a statistical inference.

Nowadays, the guideline and the regulations to which refer, for the design of a structure are: the *Norme Tecniche per le Costruzioni, NTC* (D.M. 17 gennaio 2018) in Italy and the Eurocodes in Europe. In this case, the standards for retaining structures are contained in the chapter 4.5 of the NTC and in the chapter 9 of the (EN 1997-1). In both cases pore water pressures (PWP) are mentioned only in the paragraph containing the design values of actions or the basis of geotechnical design (BOND, 2013).

Within this regard, the Italian standards (NTC 2018) states: "*Nei muri di sostegno, il terreno di riempimento a tergo del muro deve […] avere granulometria tale da consentire un drenaggio efficace nel tempo [..] e deve essere progettato in modo da risultare efficace in tutto il volume significativo a tergo del muro.* [D.M. 17 gennaio 2018 § 6.5.1]". It means that the material used for the back fill need to have an adequate particle size, that should allow a proper drainage over the time and in the needed volume.

And goes on*: "*[..]*Devono essere valutati gli effetti derivanti da parziale perdita di efficacia di dispositivi particolari quali sistemi di drenaggio superficiali e profondi […]. Deve essere predisposto un dettagliato piano di controllo e monitoraggio nei casi in cui la loro perdita di efficacia configuri scenari di rischio.* [D.M. 17 gennaio 2018 § 6.5.1]". Meaning that, a decrease of the drainage's performances should be considered. Indeed, a detailed maintenance plan need to be provided if a loss of efficiency is a risk factor.

After it is written: "[..] *devono essere valutati gli spostamenti del terreno a tergo dell'opera e verificata la loro compatibilità con le condizioni di sicurezza e funzionalità delle costruzioni*

*preesistenti. Inoltre […] a seguito della adozione di sistemi di drenaggio si determini una modifica delle pressioni interstiziali nel sottosuolo se ne devono valutare gli effetti, anche in termini di stabilità e funzionalità delle costruzioni preesistenti*. [D.M. 17 gennaio 2018 § 6.5.1]". It says that, displacement of the ground should be accounted, and that operative condition and safety of the pre-existing structures must be guaranteed also by considering the effect of drainage system on the pore water pressure variation.

And finishes saying: "*Il livello della superficie libera dell'acqua deve essere scelto sulla base di misure e sulla possibile evoluzione del regime delle pressioni interstiziali anche legati a eventi di carattere eccezionale e a possibili malfunzionamenti dei sistemi di drenaggio. In assenza di particolari sistemi di drenaggio, nelle verifiche allo stato limite ultimo, si deve sempre ipotizzare che la superficie libera della falda non sia inferiore a quella del livello di sommità dei terreni con bassa permeabilità (k < 10-6 m/s).* [D.M. 17 gennaio 2018 § 6.5.2.2]". It's stated that, the GWT level must be chose as a result of, investigations and a possible change in the PWP, caused by exceptional event or by a malfunction of the drainage system. If no drainage system is planned, the position of the GWT must be placed above low permeability soils layer ($k_s$ < 10-6 m/s).

Summarizing: the position of the GWT should be chosen as a result of proper investigations that must account for PWP changes or should be placed on the top of low permeability soils ($k_s$ < 10-6 m/s). If a drainage system is designed, it should guarantee an efficient drainage over time and a possible change of their performances should be accounted. If the loss of the efficiency represents a risk, a maintenance programme is required. Finally, the influence of a PWP change, on the stability and the operability of structures, must be taken in to account. All need to consider the effect of any exceptional events.

For what concerns the Eurocode 7, it states: "When dealing with ground-water pressures for limit states with severe consequences [..], design values shall represent the most unfavourable values that could occur during the design lifetime of the structure. For limit states with less severe consequences [..], design values shall be the most unfavourable values which could occur in normal circumstances. [EN 1997-1 § 2.4.6.1 (6)]".

But then: "Design values of ground-water pressures may be derived either by applying partial factors to characteristic water pressures or by applying a safety margin to the characteristic water level […]. [EN 1997-1 § 2.4.6.1 (8)]".

After: "The following features, which may affect the water pressures should be considered: the level of the free water surface or the ground-water table; the favourable or unfavourable effects of drainage, both natural and artificial, taking account of its future maintenance; the

supply of water by rain, flood, burst water mains or other means; changes of water pressures due to the growth or removal of vegetation. [EN 1997-1 § 2.4.6.1 (9)]".

And finally: "Unless the adequacy of the drainage system can be demonstrated and its maintenance ensured, the design ground-water table should be taken as the maximum possible level, which may be the ground surface. [EN 1997-1 § 2.4.6.1 (11)]".

Similarly to what is stated in the Italian standard, the GWT is required to be placed at the maximum level unless a proper drainage system is demonstrated. It is also said that, should be taken in to account the features that can affect the PWP (such as rain, vegetation etc.).

Thus, both the standards identify two different cases: one with a reliable design of a drainage system and another one, without a reliable design of a drainage system (BOND, 2013) and (AVERSA, 2011). In the former case the GWT can be placed below the head of the wall, while in the latter, must be taken at the head of the wall. Furthermore, extraordinary rainfall events should be considered, loss of efficiency of the drainage system should be accounted and maintenance intervention need to be planned.

In light of the requirements of the European and Italian standards (NTC 2018 and Eurocode 7) an approach to evaluate performances of a retaining walls during rainfalls events is illustrated (**Figure 4-1**).

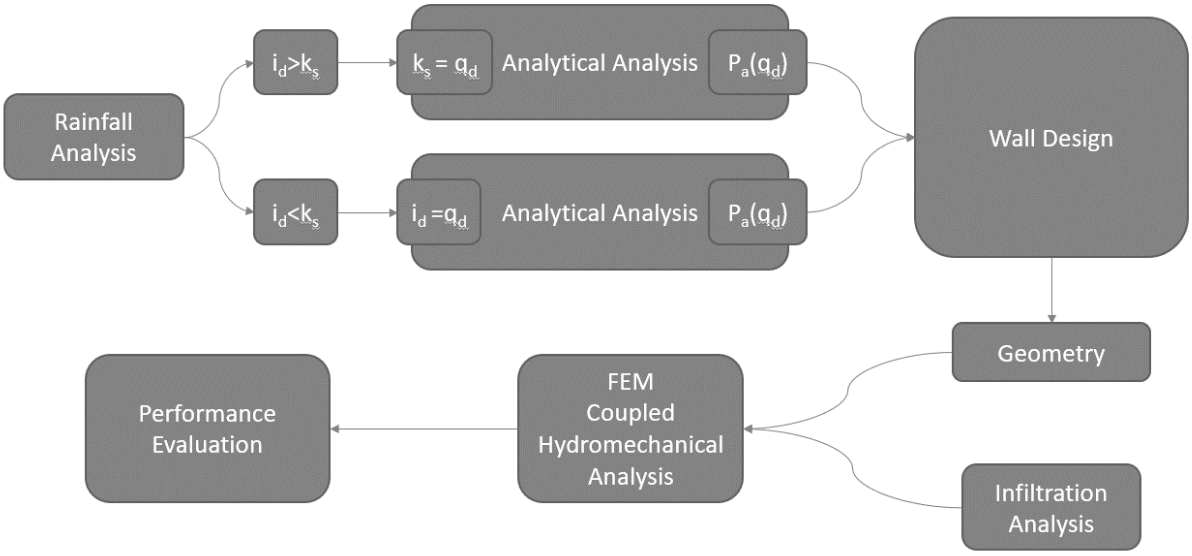


*Figure 4-1; Adopted approach for the evaluation of the wall performances*

Here is assumed that, the position of the GWT and the hydromechanical parameter of the involved materials, have already been identified into a previous field campaign and by lab test.

The first step necessary to perform all the consecutive analysis is the determination of a critical rainfall intensity ($i_c$) related to a certain critical duration ($t_c$). This latter should be chosen as the most critical one; generally, as shown in the chapter five, the most critical rainfall event, for those kinds of structures are the long one.

This can be done by a statistical inference on the available data, which should be as much as possible representative of the area of interest. Such a process allows to estimate a statistical population starting from the statistical sample, and thus subsequently, to extrapolate the data corresponding to the desired odds. The most common distributions used to fit raining data are: the two parameters distributions Gumbel and Log-normal and the three parameters Generalized Extreme Value (GEV). The choice between those functions need to be done, one on the basis of the quality and the length of the dataset available (CHOW, et al., 1988). Thus, estimated the parameters for the given duration, is possible to assess the rainfall intensity correspondent to a certain return period, that generally for civil structures, is of a hundred years.

Once the rainfall intensity is known this value should be compared to the saturated hydraulic conductivity ($k_s$) of the soil. If $i_c > k_s$, then a flux ($q_d$) equal to the saturated hydraulic conductivity of the soil should be used in the next analytical analysis. If $i_c < k_s$, then a flux ($q_d$) equal to the rainfall intensity is used in the next analytical analysis. This choice is due to the physical constrain of the Equation 3.26.

In this step uncoupled hydromechanical analytical analysis are performed with the method illustrated in the previous paragraph (cf. § 3.3): LEM and LEP solution for transitory and steady state. Here is computed the active thrust ($P_a(q_d)$) exerted on the retaining wall, for the previously chosen flux. One should for conservatism reasons, choose the active thrust computed by mean of the steady solutions. This value is then used to design the wall and to do the Ultimate Limit State check for overturning, sliding and bearing capacity. Moreover, the highest value of the critical rainfall intensity, previously identified should be used to design also the drainage system.

Since, the effective infiltration of a soil is bigger than its saturated hydraulic conductivity (MAIONE, 1999), is better to analyse the time infiltration capacity trend f(t). That can be done by mean of the Horton's model (Equation 4.1). This model has been chosen since, as the LEM and LEP transitory solution, derive from a solution of the Richard's equation.

$$\frac{df(t)}{dt} = -\frac{f(t) - f_c}{k} \tag{4.1}$$

Where: f(t) is the infiltration capacity trend; $f_c$ is the value of f(t) for $t \rightarrow \infty$ and is considered to be equal to $k_s$ [mm/h]; k is the decay rapidity of f(t) [min-1];

Integrating the 4.1:

$$f(t) = f_c + (f_0 - f_c)e^{-t/k} \tag{4.2}$$

Where: $f_0$ is the value of f(t) at t=0 [mm/h]; $i_d(t)$ rain fall intensity obtained from the rainfall analysis [mm/h].

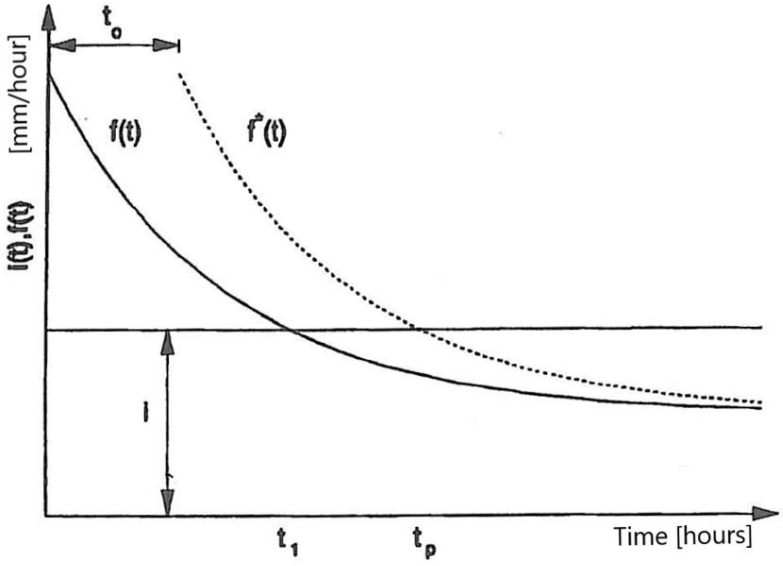


*Figure 4-2; Effective rainfall capacity and pounding time (MAIONE, 1999)*

The f(t) curve (**Figure 4-2**) describe the effective infiltration trend only if $i_d(t)>f(t)$ for each instant, if this inequality is not respected, the effective infiltration speed f*(t) is higher. f*(t) is equal to f(t), but translated of a $t_0$ time step, so that at the time $t_p$ (pounding time), the volume infiltrated since the beginning of the rain event is equal to the maximum that can infiltrate, and the rain fall intensity coincide with the effective rain fall capacity f*(t).

The pounding time can be computed as:

$$t_p = \frac{1}{i_c k} * \left[ (f_0 - i_c) - \left( f_c log\left( \frac{i_c - f_c}{f_0 - f_c} \right) \right) \right] \tag{4.3}$$

Now is possible to individuate two cases:

- If $t_p>t_c$ then the effective infiltration in the soil ($f_e$), during the given critical rainfall event $i_c$, used in the next analysis, is equal to:

$$f_e = i_c \tag{4.4}$$

- if $t_p<t_c$ then the effective infiltration in the soil ($f_e$), during the given rainfall event $i_c$, used in the next analysis, is equal to:

$$\begin{cases} f_e = i_c; & for\ t < t_p \\ f_e = f^*(t); & for\ t < t_p \end{cases} \tag{4.5}$$

Now all the information necessary to improve a Finite Element Model are available. Indeed, the geometry of the retaining structure has been identified in the design step, the critical rainfall event, has been chosen in the precipitation analysis step and the capacity of the soil to adsorb a certain amount of water, has been evaluated in the infiltration analysis step.

Thus, by mean of a FEM that can perform coupled hydromechanical analysis, is possible to evaluate the global stability of a retaining structure and the displacements induced by an extreme rainfall event.

# Chapter 5 The case study

It is hypothesized that, a recent derivation of Rhone, a big river that cross the whole region of Valais in Swiss, Left on its old path a three meters high bank. In Sion (**Figure 5-1**), a city located by the Rhone, a the three-meter cliff formed after the collapse of one of the old levee (**Figure 5-2**). The citizen worried about the stability of the cliff asked the major to intervene.

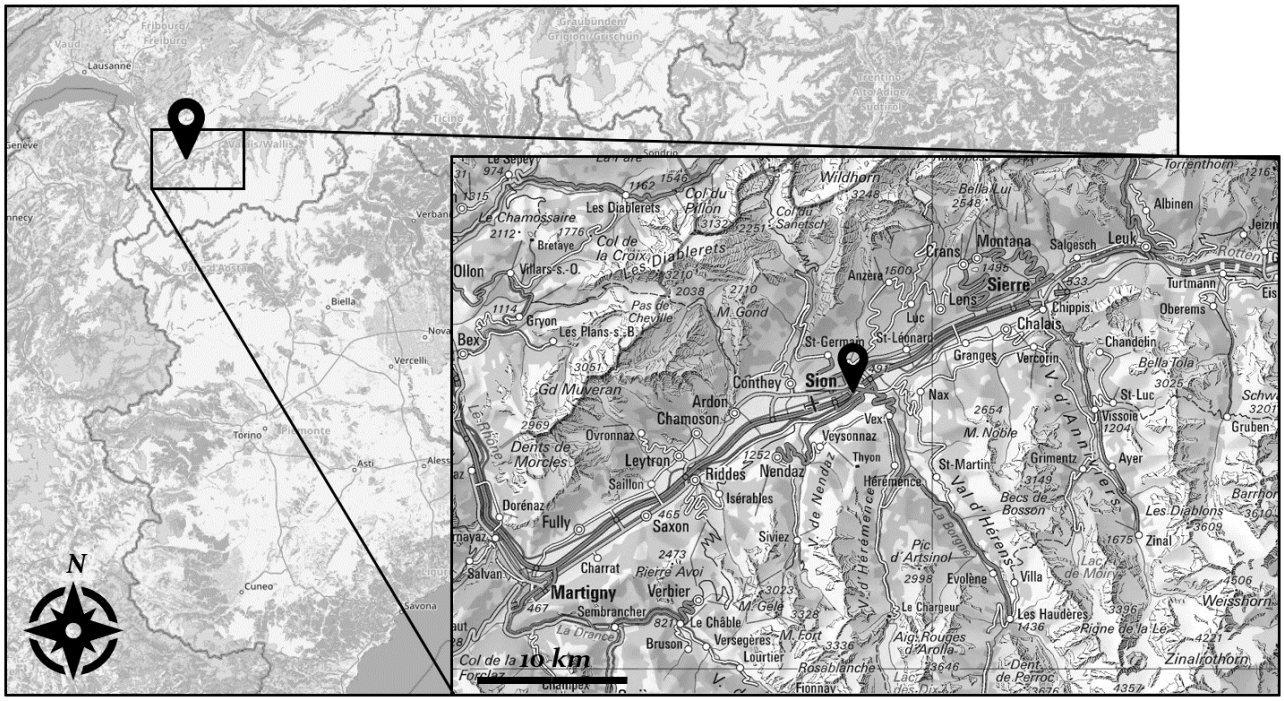


*Figure 5-1; Position of the Retaining wall: Sion (CH)*

The geometry of the problem is the one illustrated in **Figure 5-2**, where the above mentioned three meters cliff is considered to link two horizontal ground surfaces. The soil of the ground is, as previously mentioned, a silt and thus have been decided to consider it as the Sion silt previously characterised in the Chapter 2.

Since no data are available with regard the position of the ground water table, have been decided to consider a horizontal GWT to be in one of the most unfavourable position, that is coincident with the toe of the three meters high bank.

In the area are present a lot of open pit, used for the extraction of sand and gravel, thus have been decided to use the sand coming from one of those quarries. It is supposed that the used sand is the one previously characterised in the Chapter 2.

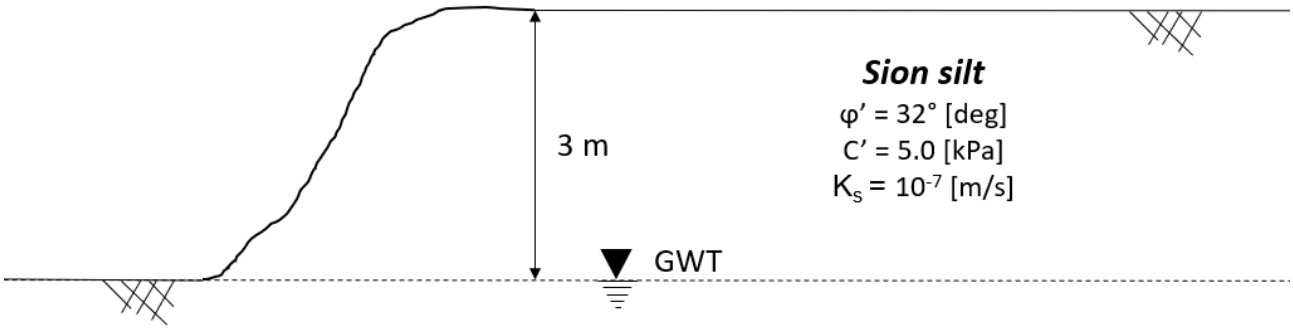


*Figure 5-2; Silt cliff*

### 5.1.1 Hydrological analysis

Here the rainfall analysis is done. In order to show the different effects that a short and intense event and a long event, can cause to a retaining structure, here one hour and five days, times are chosen as critical duration. The cumulated precipitation over one hour are available for the meteorological station of Sion, while the cumulated precipitation over five days, are available for the meteorological station of Sierre (CH). The former town is placed at an elevation of 482 m.a.s.l while the latter at 536 m.a.s.l. and their distance is about 15

km, thus the data coming from the neighbour station, can be used without committing big errors. The extreme values analysis from the two stations are shown in **Figure 5-3**:

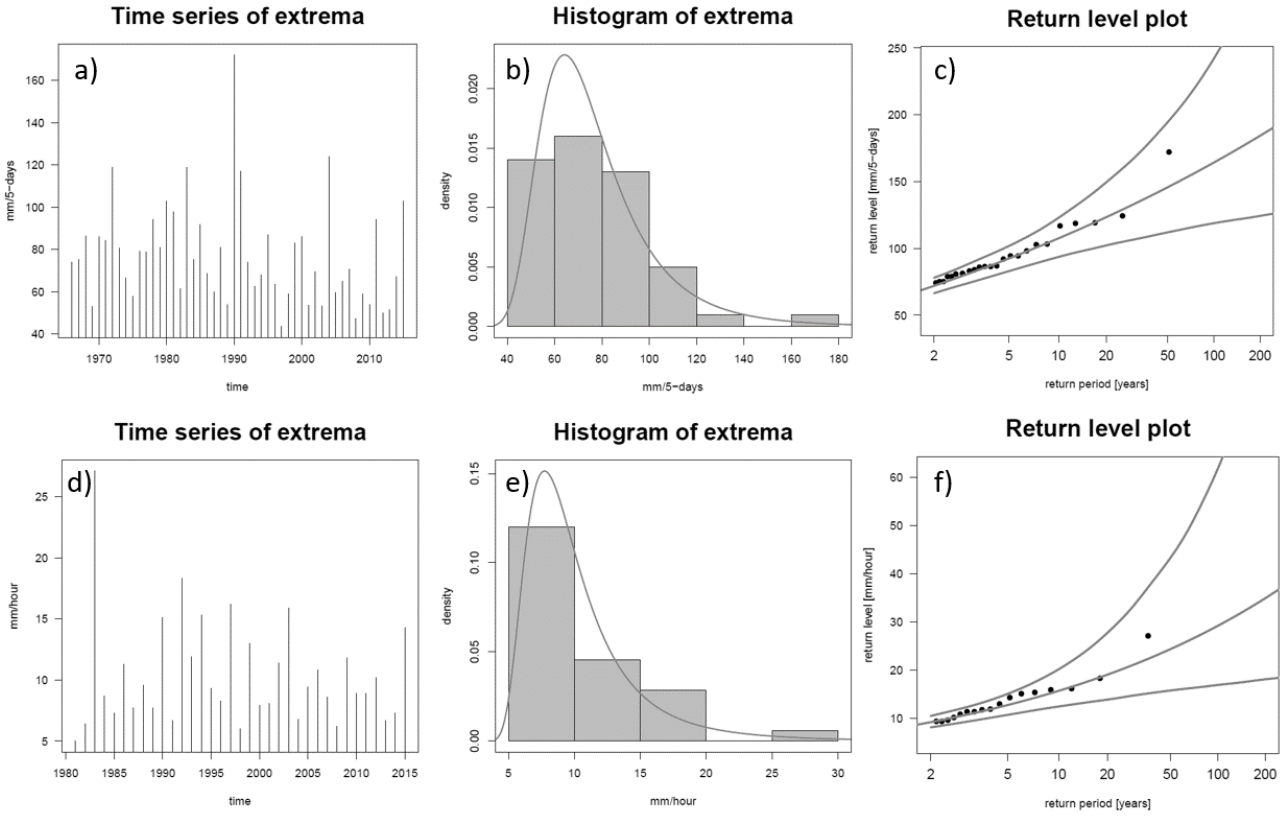


***Figure 5-3;*** *Extreme value analysis for five-days data (a-b-c) for one-hour data (d-e-f): in the graph (b-c) the grey line in the histogram of extrema is the fitted GEV density distribution; in the graph (c-f) the upper and lower line return level 95% confidence intervals (MeteoSwiss, 2016).*

In the **Table 8** are listed the intensities values for the corresponding period of return and the 95% confidence interval. The inferred data spans from the 1966 to the 2105, that are 49 and thus they are just enough for the use of a generalize extreme value distribution.

***Table 8****; Table of return levels for a selection of return periods.*

| | 1-hour precipitation | | | 5-day precipitation | | |
|---|---|---|---|---|---|---|
| **Return Period [years]** | **Return Value [mm/hour]** | **Confidence Interval 95% [mm/hour]** | | **Return Value [mm/5-days]** | **Confidence Interval 95% [mm/5-days]** | |
| 2.33 | 9.8 | 8.6 | 11.2 | 75.6 | 69.6 | 82.1 |
| 5 | 12.8 | 10.7 | 15.1 | 92.5 | 83 | 101.8 |
| 10 | 15.7 | 12.5 | 20.2 | 107.6 | 93.7 | 123 |
| 20 | 19.1 | 13.9 | 27.7 | 123.4 | 102.3 | 149.3 |
| 30 | 21.3 | 14.8 | 34 | 133.1 | 106.7 | 167.4 |
| 50 | 24.4 | 15.8 | 43.5 | 145.8 | 111.9 | 194.7 |
| 100 | 29.2 | 16.9 | 62 | 164.3 | 118.8 | 242.2 |

As said in the previous paragraph, for civil engineering structures is generally used a return value of a hundred years, thus the correspondent critical intensities are 29.2 mm/h for the one-hour event and 164.3 mm/5-days that are 1.36 mm/h for the 5-day rain event.

Remembering that, the value of the Sion silt saturated hydraulic conductibility is $k_s=10^{-7}$ m/s that is $k_s=0.36$ mm/h, being $I_c > k_s$ for both the critical intensities, the design flux used for the analytical solutions is $q_d = k_s = 0.36$ mm/h.

### 5.1.2 Preliminary uncoupled hydromechanical analysis

Let's recall here (**Figure 5-4**) the material proprieties presented in chapter 2.2 and the geometry of reference:

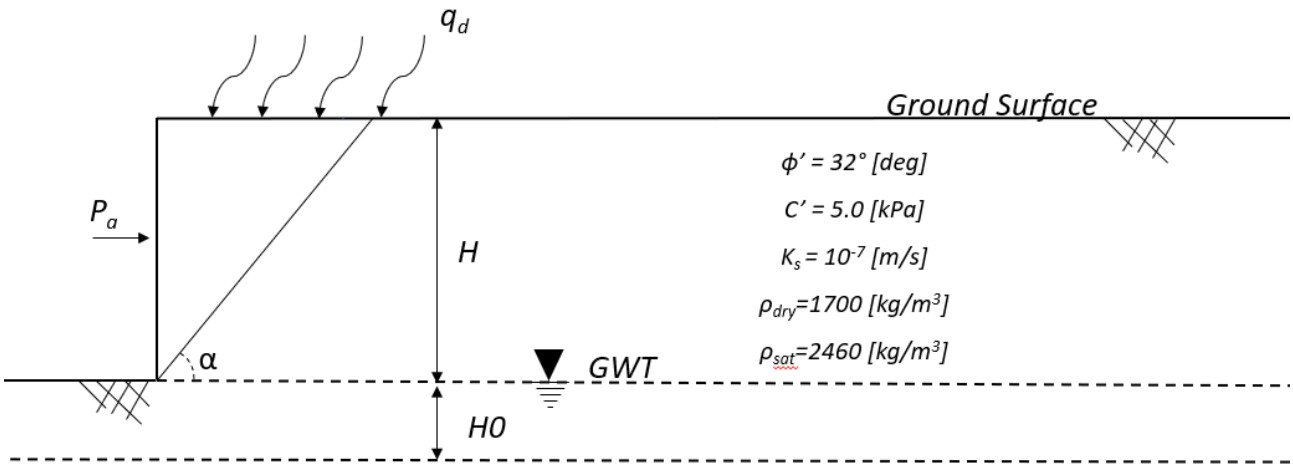


***Figure 5-4**; General case and Sion silt proprieties*

The LEM and LEP solution for transient and steady state presented in the Paragraphs 3.3 and 3.2, have been implemented on the Software *Matlab,* that allowed to carry on the uncoupled hydromechanical analysis, reported in the following pages.

Before showing the results obtained by considering the soil unsaturated, let's see the results that should give the normal approach, rather by considering the soil fully saturated or completely dry.

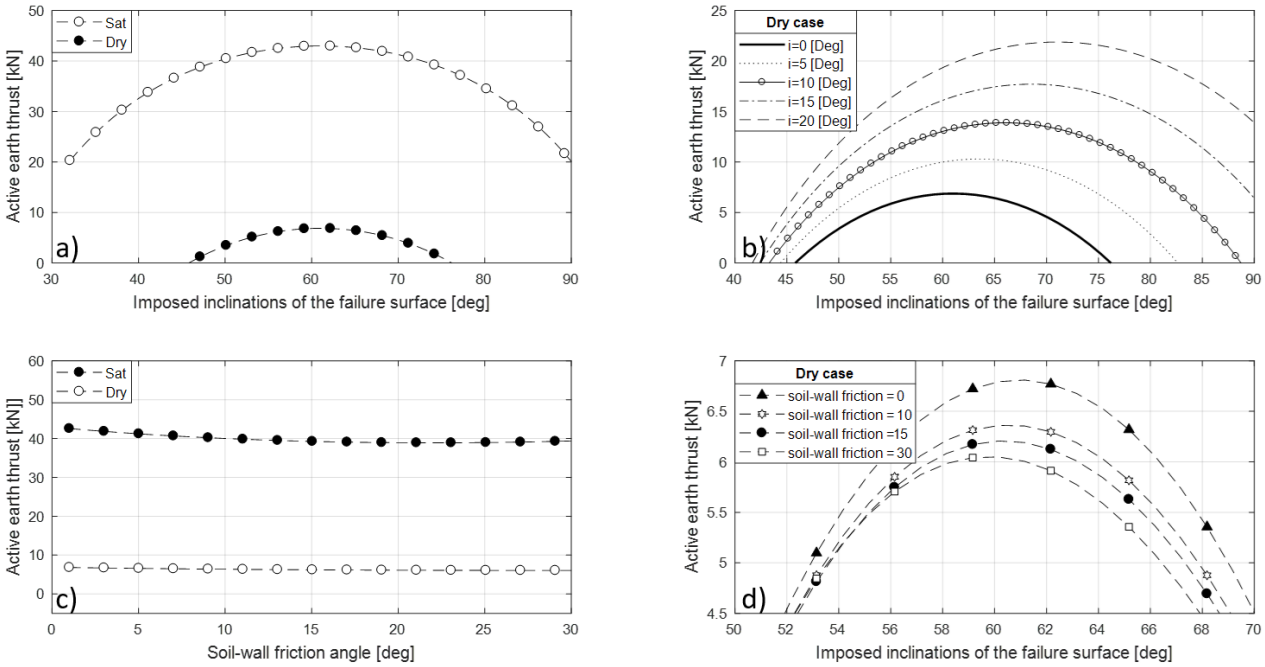


*Figure 5-5; Coulomb's solutions: a) active earth thrust for dry and saturated case[δ=0 i=0]; b) dry case for different walls inclination[δ=0]; c) dry and saturated case for different soil wall friction angle [i=0]; d)dry case for different friction angle [i=0].*

The difference in considering the soil totally dry or saturated how is relevant (**Figure 5-5**), the former case give a thrust of 6.87 kN while the latter 42.97 kN that is a force more than six time bigger, the angle (α) on which happen the failure is of 61.2 degrees. Furthermore, the **Figure 5-5**-b-c-d shows as expected, a decrease of the thrust with an increase of the soil-wall friction angle while it rise with the wall inclination, this last is explained since inclining the wall, an additional vertical component of the soils weight, start to act on the wall.

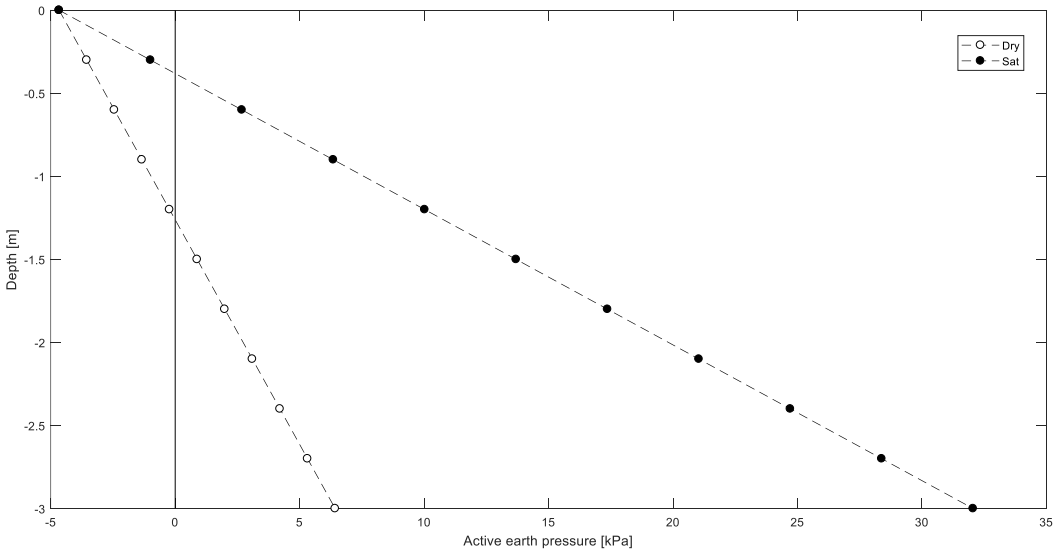


*Figure 5-6; Rankine's solutions: active earth pressure for saturated and dry conditions*

In **Figure 5-6** are shown the Rankine's solutions, it's clear that the negative pressures in left side of the graph are not accounted in the computation of the force that for this method is $P_a$=43.92 [kN] for the saturated case and $P_a$=9.76 [kN] for the dry case. The differet solution between the two method, Rankine and Coulomb, is due to the presence of cohesion. Indeed, in the Coulomb's model the cohesion is acting all along the failure surface, while in the Rankine's one the negative pressure, due to cohesion, are not accounted. The more correct solution is the Rankine's one, since soils are not able to support tensile stress. By the way should be possible to take in to account this effect also in the coulomb model by considering tensions crack.

Now is time to see the effect of the unsaturated conditions. Since here uncoupled hydromechanical analysis are performed, lets firstly look at the results given by the hydraulic solutions. Here are shown the solutions for different values of fluxes but let's remember that for the design purpose the one that is used is $q_d=k_s$. Furthermore, the given solution unless is clearly specified are for $H_0$=0 that means that the GWT is considered to be at the foot of the wall.

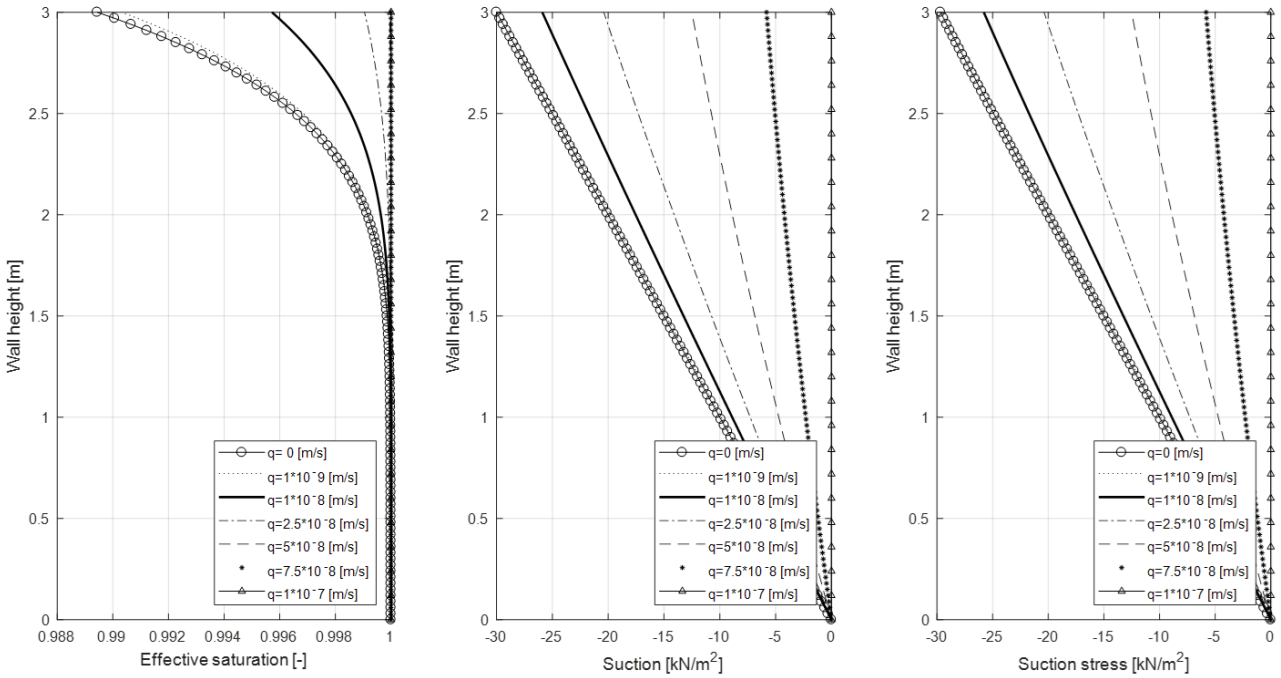


*Figure 5-7; Steady state solutions of the hydraulic model for different fluxes*

The **Figure 5-7** shows how, the effective saturation, suction and suction stress, changes with different fluxes that span from zero to $K_s$. The low value of the saturation is caused by the proximity of the GWT, that means that the soil is quasi saturated. Suction and suction stress rises with an increase of the flow, while their absolute value decreases till zero. This means that an infiltration equal to the value saturated hydraulic conductivity nullify all the suction and consequently the suction stress. The shape of suction stress would have been more

pronounced if the GWT would have been deeper, indeed in this case the effective saturation would have been closer to zero increasing its effect.

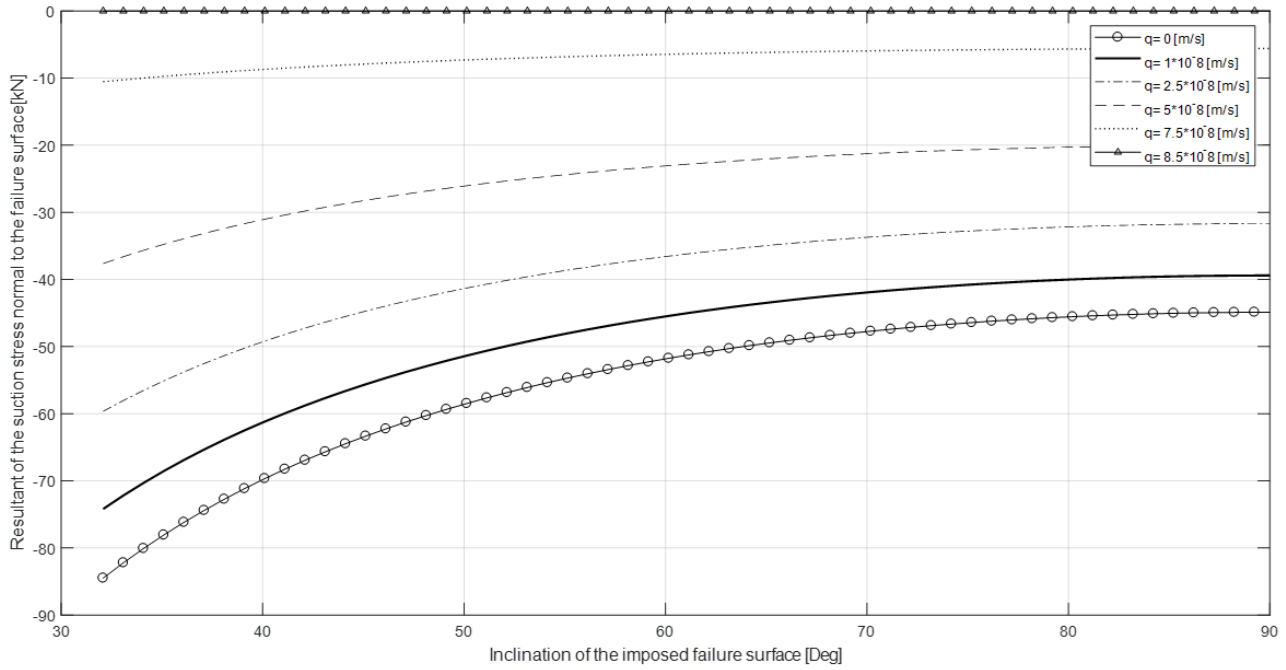


***Figure 5-8;*** *LEM steady state component of suction stress force acting along the failure surface.*

In **Figure 5-8** is show the LEM steady state component of suction stress force ($U_{\sigma s}$) acting along the failure surface. This force changes with the inclination of the failure surface, and the one that maximise the solution is for alpha = 61° deg. The contribute given by the suction span from 0 to 50 kN (zero for $q=k_s$ and 50 for a null flux).It is important to remark that this component do not act horizontally, but at ninety degrees with respect to the failure surface.

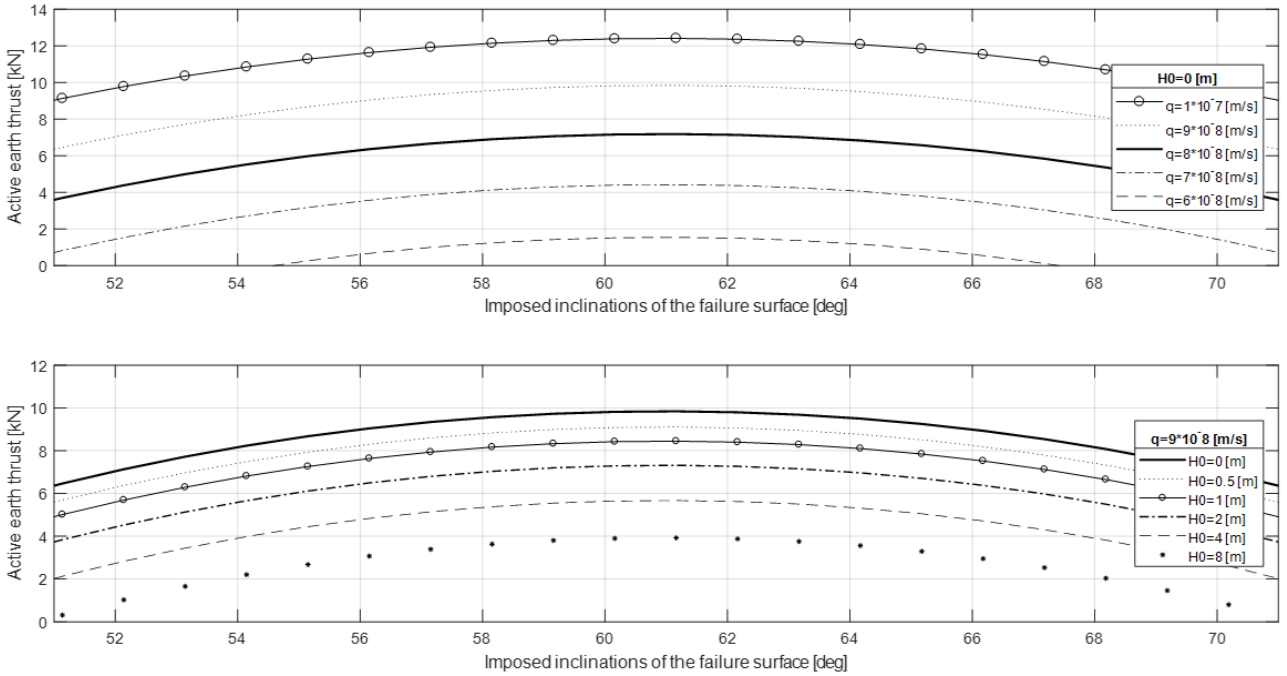


***Figure 5-****9; LEM steady state solutions: above the flux is changed while below the is changed the GWT depth.*

The active earth thrust computed with the LEM steady state solution is $P_a$ = 12.40 kN, (value obtained for $H_0$=0 and $q_d$=$k_s$). This is a small force especially if compared with the one of the saturated case, that is more than four times bigger. By observing **Figure 5-**9, the role of the position of the GWT became clear: for a given flux (close to the value of the hydraulic conductivity in the example), 10 meters drop of the water level erase the thrust. Furthermore, a decrease in the flux reduce the active force till zero. Actually, for a null flux the solution gives a negative force, that would mean that the wall is somehow pushed forward the soil by suction. Obviously, a negative solution is not physically correct, since soils do not have any tensile strength. The reason of this it is of the same principle given for the Coulomb solution, that is the suctions is acting all along the failure plane and thus all the area close to the ground surface undergoes to tension forces, that should be considered null.

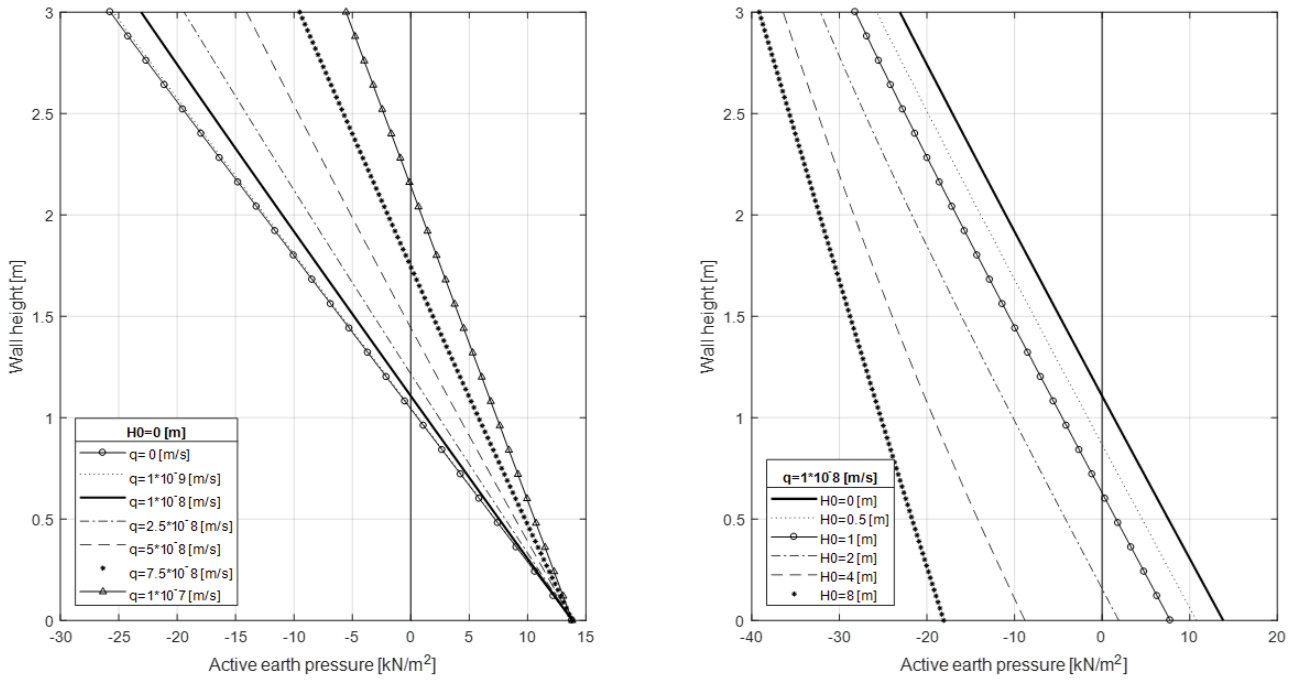


***Figure 5-10;*** *LEP steady state solutions: on the left is changed the flux, on the right the position of the GWT.*

The active earth thrust computed by mean of the LEP steady solutions is $P_a$ = 14.79 kN, (value obtained for $H_0$=0 and $q_d$=$k_s$). The**Figure 5-10** show the results obtained by decreasing the flux and by lowering the water table, in the former case the stresses decreases and as well for the latter case. Is important to keep remarking that the value of the active earth thrust is equal to the integral of the positive stresses as already specified.

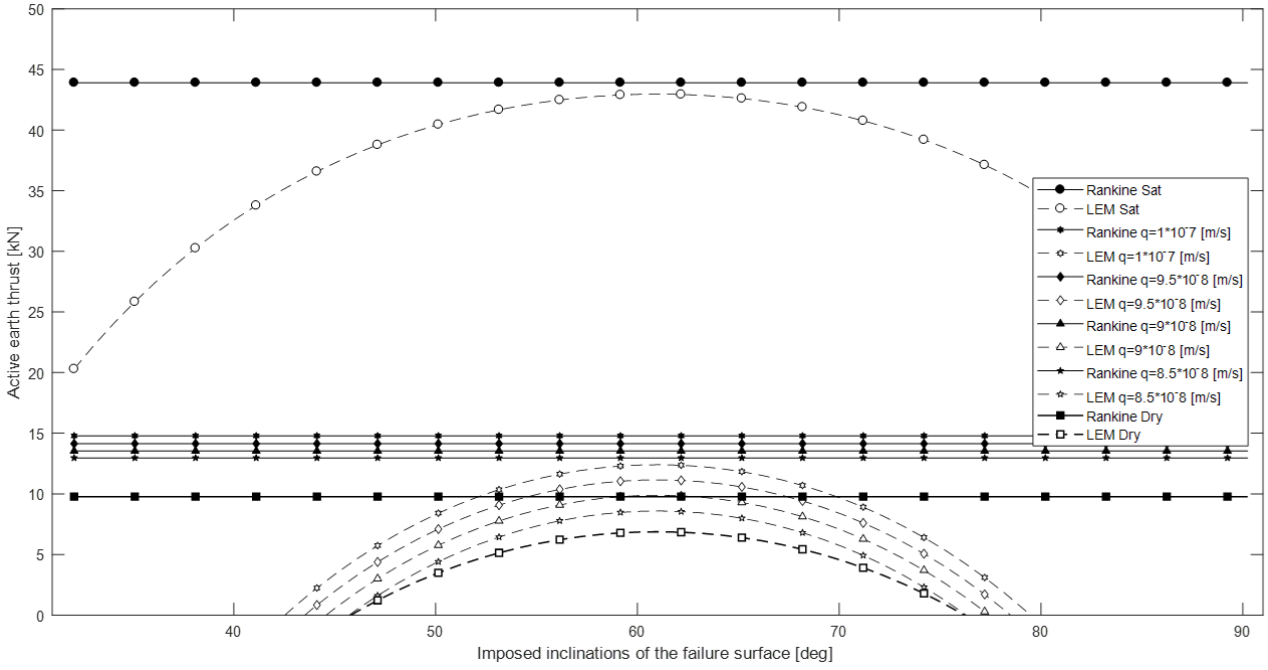


***Figure 5-11****; LEM and LEP steady state solutions compared with Rankine and Coulomb*

Summarizing, as shown in **Figure 5-11**, the LEP solutions give more reliable solutions as it allow to neglect the tensions that develop nearby the ground surface. This phenomenon is not taken in to account by the LEM solutions and thus cohesion and suction acts whit a further stabilization of the wedge. In spite of this, both analyses give similar trend and the results given for $q_d=k_s$ are far away from the one obtained in saturated condition. So, recognizing unsaturated conditions in place of saturated ones, means for this case, to deal with thrust that can be 4 time smaller. Moreover, is important to state the more conservativity of the LEP solution with respect the LEM one.

Here, the results obtained by mean of the LEM and LEP transitory analysis are illustrated. Let's firstly see the hydraulic solutions.

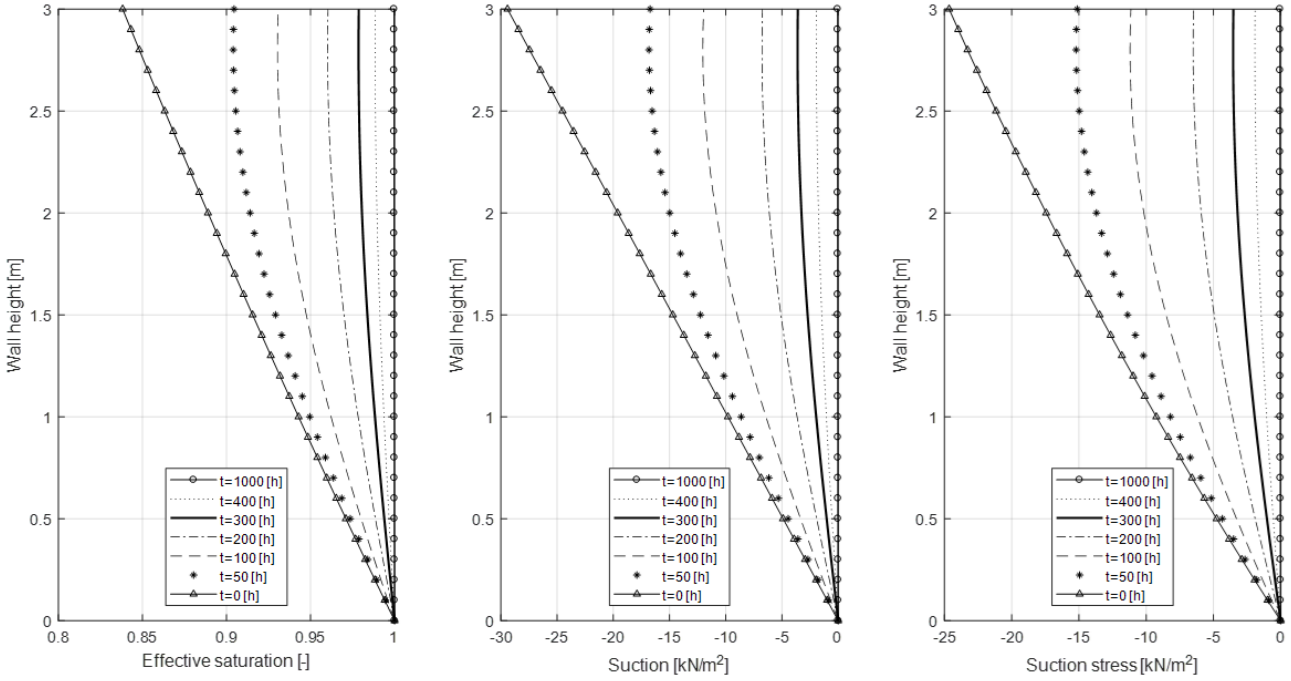


***Figure 5-12**; Hydraulic transient solutions: behaviour of effective stress (left), suction (middle) and suction stress (right).*

The solutions showed in **Figure 5-12** are obtained with an initial condition of no flow, that in the graphs is represented by t=0 straight line, and a flux on the ground surface $q_1=k_s$ and the GWT at the bottom of the wall (z=0). The first thing that stands out is the different shape of those graph with respect the steady one (**Figure 5-7**) that's due to the different model adopted for the SWRC (cf. § 3.3 and 2.2) indeed the steady state solution use a Van Ghenuchten model (Equation 1.32) for the soil water retention curve while an exponential one (Equation 1.33) is used for the transient. These solutions show a fast decrease of the absolute value, of suction and suction stress in the first hundred hours and afterwards, slowly move towards the steady state, that is reached after thousand hours. The same behaviour is traced by the effective saturation.

These results obtained from the hydraulic model are here used to obtain the LEP and LEM mechanical solutions:

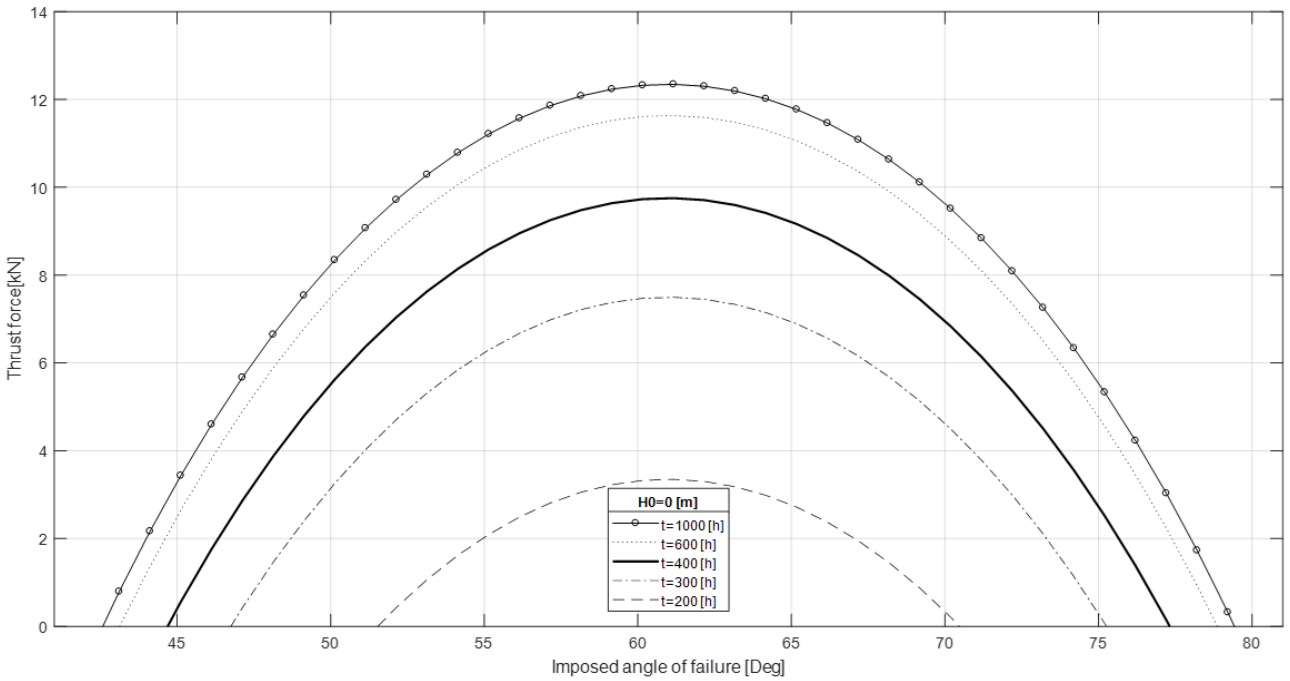


*Figure 5-13; LEM transient solutions, for a flux $q_d=k_s$*

The LEM transient solutions, give positive value of thrust after 200 hours of an imposed flux at the surface, equal to the saturated hydraulic conductivity of the soil, then it slowly increases till all the suction became null. With this flux at the upper boundary, are necessary 42 days to nullify all the suctions behind the wall. After that time, stationary conditions are reached, that gives the constant thrust of $P_a$ = 12.40 kN.

Let's suppose that during the rainfall analysis, was computed, as example, a critical duration of 200 hours and if the precipitation intensity, was lower than $k_s$, in that case, would have been possible in principle, to use an active earth thrust of approximately 4kN for the next design step.

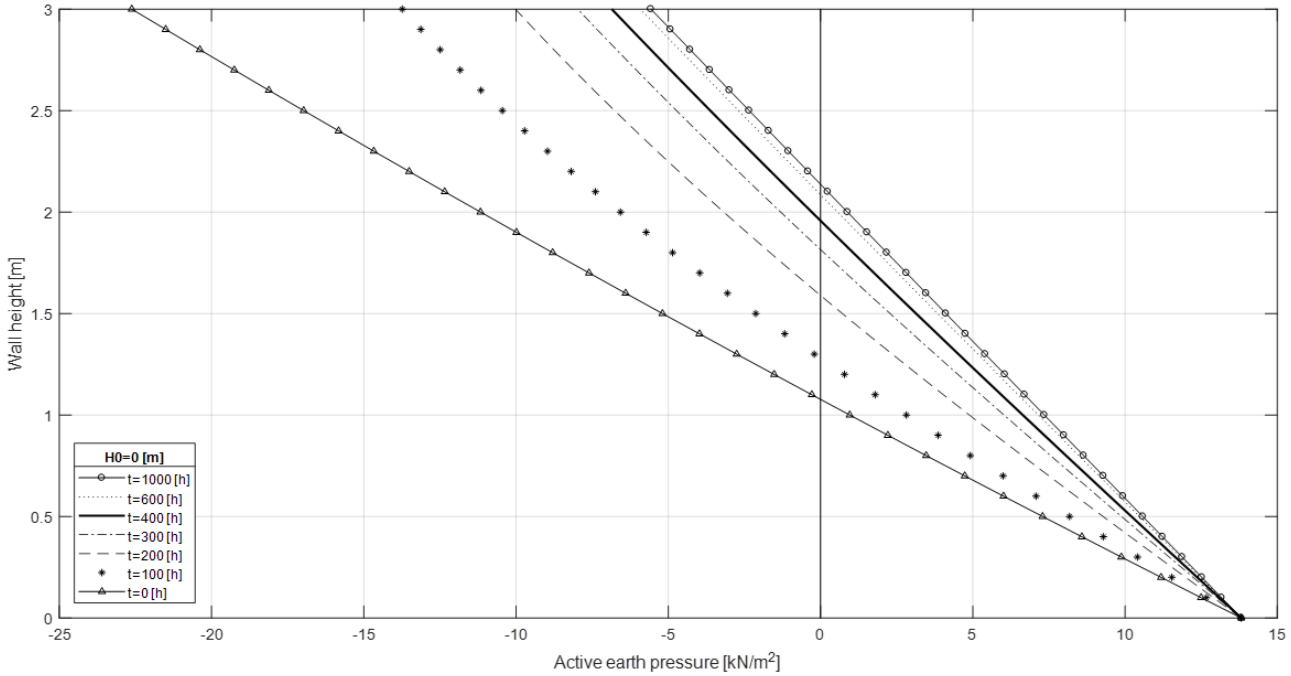


***Figure 5-14**; LEM transient solutions, for a flux $q_d=k_s$.*

The active earth thrust computed by mean of the LEP transient solutions, for a flux at the upper boundary equal to the saturated hydraulic conductibility after 45 days is $P_a$ = 14.79 kN. This time is representative of a stationary condition, where water suctions became null and thus do not contribute anymore to reduce the active earth pressure. The negative stress shown in **Figure 5-14** for at t=1000 hours are the effects given by the cohesion, and not from the suction such at that time it's null. As already stated, the value of the thrust does not account for the negative stress in the right side of the graph.

Also, in this case let's suppose that during the rainfall analysis, was computed, as example, a critical duration of 200 hours and a that the precipitation intensity was lower than $k_s$. In this case would have been possible, in principle, to use an active earth thrust of approximately 7 kN for the next design step.

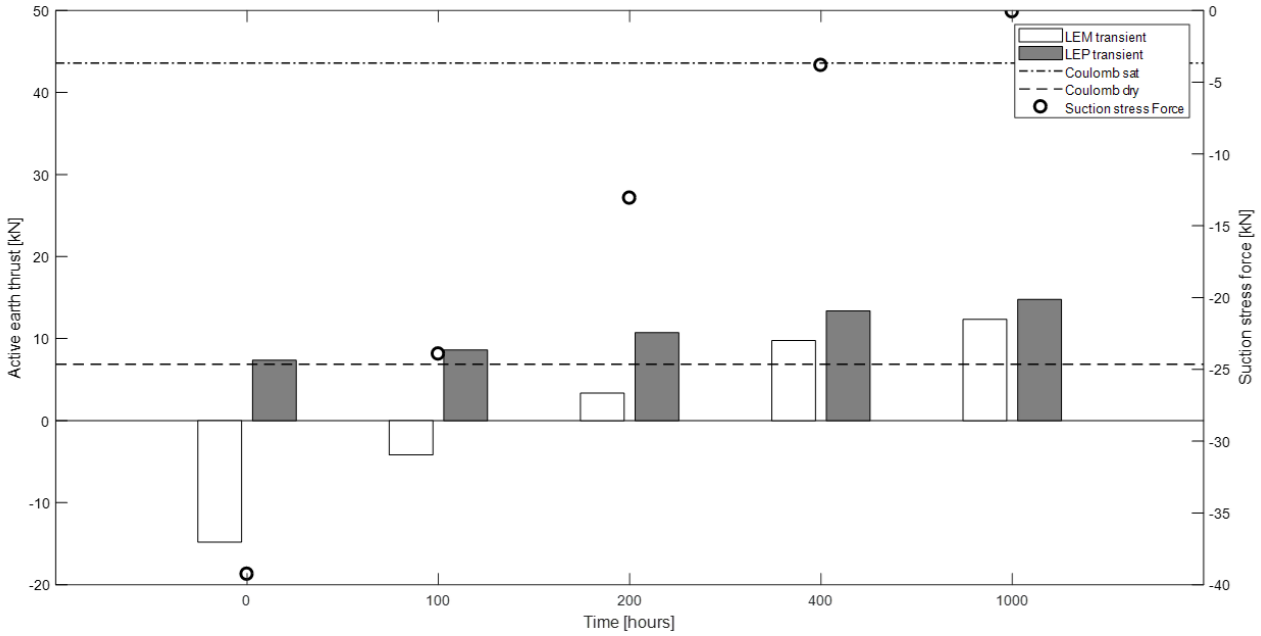


*Figure 5-15;Comparison between LEM and LEP transient solutions, obtained for a flux $q_d=k_s$*

Here (**Figure 5-15**), is clear the difference between the two solutions: the LEM ones gives tensile forces for high levels of the absolute value of the suctions stress force ($U_{\sigma s}$), that is for the beginning of the infiltration t < 150h. Instead since with the LEP solution is possible to neglect the tensile stress the results more, that are more correct, gives always positive values of thrusts. In figure also the suction stress force $U_{\sigma s}$ are shown, it is clear that for a hydrostatic distribution (t=0) its value is really high and that with the flow time it goes towards zero.

The effect of the suction has a really high impact on the LEM solutions that thus are considered not reliable at this stage. The implementation of the tension crack in the model is a necessary step that will allow to take in to account also more complicated geometry.

In light of those aspects and in order to remain in safety conditions, is used for the next design step a value of the active earth thrust equal to the one obtained by mean of the LEP steady solutions, that moreover, is coincident with the one obtained by the LEP transient solutions, when stationary conditions are reached: $P_a$ = 14.79 kN.

By mean of this value an initial geometry for the retaining wall is evaluated. This in order to be as much as possible similar the geometry of the adopted solution, it is decided to be a concrete gravity wall.

### 5.1.3 The design of the retaining wall

*Ultimate Limit State (ULS) verifications for retaining walls, according to the Eurocode 7, can be performed by mean of one of the tree design approaches listed in*

**Table 9**. In Europe, the different countries, have adopted the ones shown in **Figure 5-16** (BOND, 2013).


***Figure 5-16**; Adopted design approach for retaining walls after (HARRIS & BOND, 2006)*

As shown in the figure above, in Italy the adopted approaches are the A1-1, A1-2 and A2 and both must be verified (AVERSA, 2011).

With regard the drainage system, it is designed in order to allow an outflow through a set of sub horizontal pipe, without the development of any positive water pressure. The material used for the backfill is the sand presented in the Chapter 2.2. Geosynthetics membrane should be used to prevent silts particle to flow inside the backfill, but those elements wouldn't be possible to be implemented in the Finite Element Model. The backfill is designed with an inclination of 70° degrees; The number of sub horizontal drain has been choice to

allow an outflow, equal to the most critical intensity of the rain (that is the one of the short event $i_d$=29.2mm/h), times the unitary ground surface of the backfill.

*Table 9; Summary of the design approaches (underlined > 1)*

| Design Approach: | DA1-1 | DA1-2 | DA2 | DA3-1 | DA3-2 |
|---|---|---|---|---|---|
| Partial Factors Applied to: | Actions | Material Properties | Actions and Resistances | Structural Actions and Resistance | Structural Actions and Resistance |
| Partial Factors Sets: | A1+M1+R1 | A2+M2+R1 | A1+M1+R2 | A1+M2+R3 | A2+M2+R3 |

The obtained final geometry (**Figure 5-17**) is the one able to satisfy all the presented design approaches. the factors of safety obtained for each design approach are summarized in **Table 10**:

*Table 10; Safety factors for the different design approach.*

| Design Approach: | DA1-1 | DA1-2 | DA2 | DA3-1 | DA3-2 |
|---|---|---|---|---|---|
| **Overturning FS:** | 4.43 | 5.3 | 4.43 | 4.43 | 5.3 |
| **Sliding FS:** | 1.93 | 1.97 | 1.93 | 1.55 | 1.97 |
| **Bearing Capacity FS:** | 6.4 | 6.5 | 4.57 | 3.1 | 6.92 |

Considering the speed of the water to be equal to the saturated hydraulic conductibility and having chosen a nominal dimeter for the PVC pipe of 170 mm, results that five of those pipes are needed for unitary length of the wall, thus has been chosen a quincunx distribution (**Figure 5-17**).

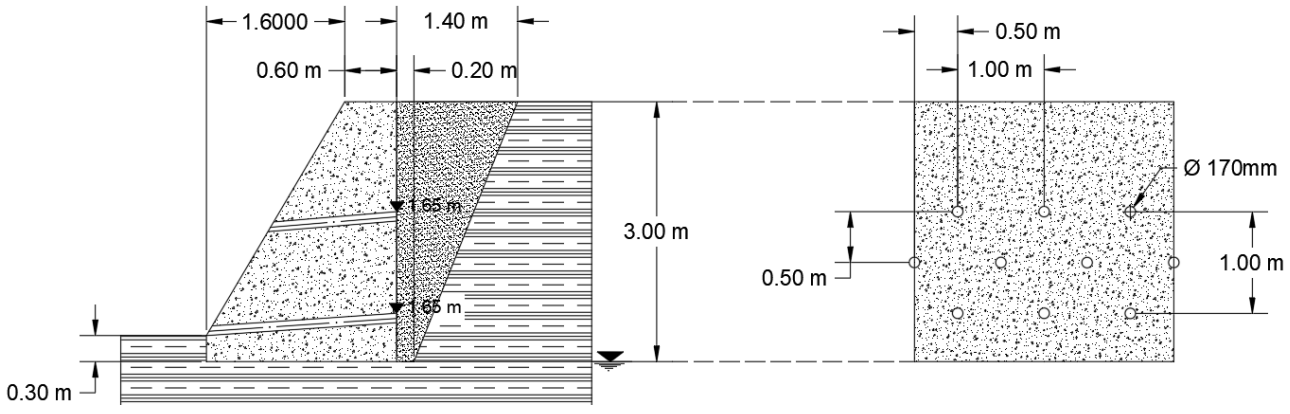


*Figure 5-17; Wall design: lateral view (left), frontal view (right)*

Now that the geometry is defined, the last step necessary to build the Fine Element Model is the infiltration analysis. The missing parameters of the Horton's model, $f_0$ and k, have been taken from literature. The soil we dealt with, the Sion silt, can be considered a "soil with slow infiltration rates when thoroughly wetted" so belonging to the C category of soils of the SCS classification, for this category is possible to consider $f_0$=125 mm/h and k=2 $h^{-1}$ (MAIONE, 1999). Substituting those values, $f_0$=125 mm/h, k=2 $h^{-1}$, $f_c=k_s$= 0.36 mm/h and considering the log rainfall event (120h) $i_c$=1.36 mm/h, in to the Equation 4.3 we get a pounding time $t_p$=46.1 h. While for the intense rain event $i_c$=29.2 mm/h (1 hour) we get a pounding time $t_p$=1.65 h. So following the thinking line of the Paragraph 4.1 we get that the effective infiltration ($f_e$) for the critical rain event of five day is described by the Equation 4.5 since $t_p<t_c$, while in the case of the critical rain event of one hour the effective infiltration ($f_e$) is described by the Equation 4.4 and thus is placed equal to the correspondent critical rainfall intensity $i_c$ since $t_p>t_c$.

Now are available all the information for performing the coupled hydromechanical analysis that are described in the following chapter.

# Chapter 6 Numerical analysis of a retaining wall in unsaturated soils

Here after a briefly explanation of the equation adopted by the Software *Zsoil*, to perform coupled hydromechanical analysis, the geometry, the meshing and the boundary condition adopted in the Finite Element Model, are described. Subsequently, the results obtained are reported for different six scenarios (three cases: operative, clogged drain and no drainage system; two critical rainfall events: one-hour one $i_c$=29.2 mm/h and a long one 5-day $i_c$=1.36 mm/h).

## 6.1 Hydromechanical Coupling

In the previous chapters (cf. § 3.3 and § 4.2) uncoupled hydromechanical analysis have been performed, it means that (at least in our case), before is solved the hydraulic problem and its results are used to solve the mechanical problem. While hydromechanical analysis are performed by solving simultaneously the hydraulic and the mechanical problem and their solutions have a reciprocal effect. The equations adopted by the Software *Zsoil* for solving coupled hydromechanical problems are:

The overall equilibrium:

$$\sigma_{ij,j} + f_i = 0 \tag{6.1}$$

Where: $\sigma_{ij}$ is the total stress with the Bishop's definition with null pore air pressure ($u_a$=0) and $f_i$ the solid body forces:

$$\sigma_{ij} = \sigma'_{ij} + \chi p \delta_{ij} \tag{6.2}$$

And:

$$f_i = \left(\gamma_{dry} + \chi n \gamma_w\right) b_i \tag{6.3}$$

Where: s is the suction, χ the effective stress parameter, $v^F_{kk}$ the divergence of fluid velocities, p the pore water pressure (remark here tensions are positive) and n the porosity.

And the fluid flow continuity equation:

$$\chi \varepsilon_{kk} + v^{F}_{k,k} - D\frac{dp}{dt} = 0 \tag{6.4}$$

Where: $\varepsilon_{kk}$ is the volumetric strain rate in the soil skeleton and D the storage coefficient (cf. § 1.2)

Here the effective stress parameter χ is placed equal to the saturation ratio ($S_r$) that is modelled by a one parameter model (**Figure 6-1**):

$$S_r = \begin{cases} S_{r,res} + \dfrac{1 - S_{r,res}}{[1 + (\beta h_m)^2]^{0.5}} & for\ p > 0 \\ 1 & for\ p \leq 0 \end{cases} \tag{6.5}$$

Where: β is the Van Gehnuchten parameter related to the AEV and $S_{r,res}$ the residual saturation ratio.

The flow is modelled by the Darcy's equation where the hydraulic conductivity $k_{ij}$ is equal to:

$$k_{ij} = ks_{ij}\frac{1}{[1 + (\beta h_m)^2]^{3/2}} \tag{6.6}$$

Where: $Ks_{ij}$ is the saturated hydraulic conductivity and the second term (the ratio) is the relative permeability (**Figure 6-1**).

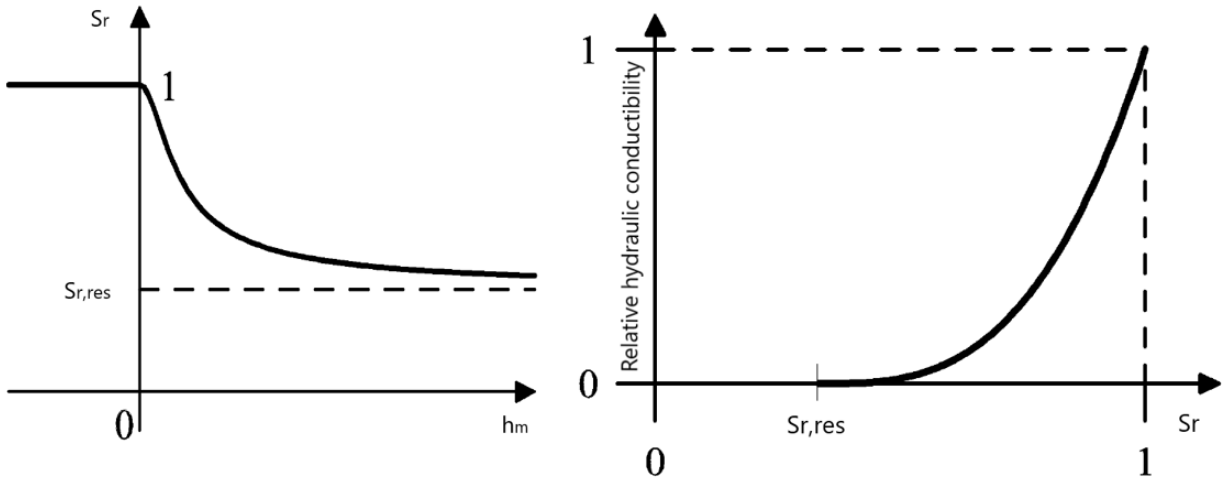


*Figure 6-1; Behaviour of the one parameter SWRC model and the relative hydraulic conductibility (COMMEND, et al., 2016),*

Coupled hydromechanical can be run in the *Zsoil* Software in the Deformation+Flow mode by mean of the time dependent driver's Consolidation. The driver allows to consider the induced effects of the pore water pressure and the relatives strain, due to applied loads or pressure boundary conditions, over time (COMMEND, et al., 2016).

## 6.2 FEM analysis

As previously mentioned, the coupled hydromechanical analysis have been performed by mean of Finite Element Model on the Software *Zsoil*. For all the following analysis has been used the free student version whose limitation is the number of nodes: 4000 for 2D problems and 8000 for 3D ones. In this case a 2D geometry have been used. It's clear that such limitation has a direct impact on the model resolution, but nevertheless by a good mesh refinement has been possible to avoid boundaries' effects and to have a worth detail of the investigated area.

After several trial versions, abandoned due to problems of convergence or resolution here is presented the final model adopted for running all the analysis.

The overall geometry (**Figure 6-2**) used is 60x30 m box, inside it is contained the region of study, where an higher detail is required 12x8 m box and finally in this area is contained the wall who's geometry have been already introduced (**Figure 5-17**).

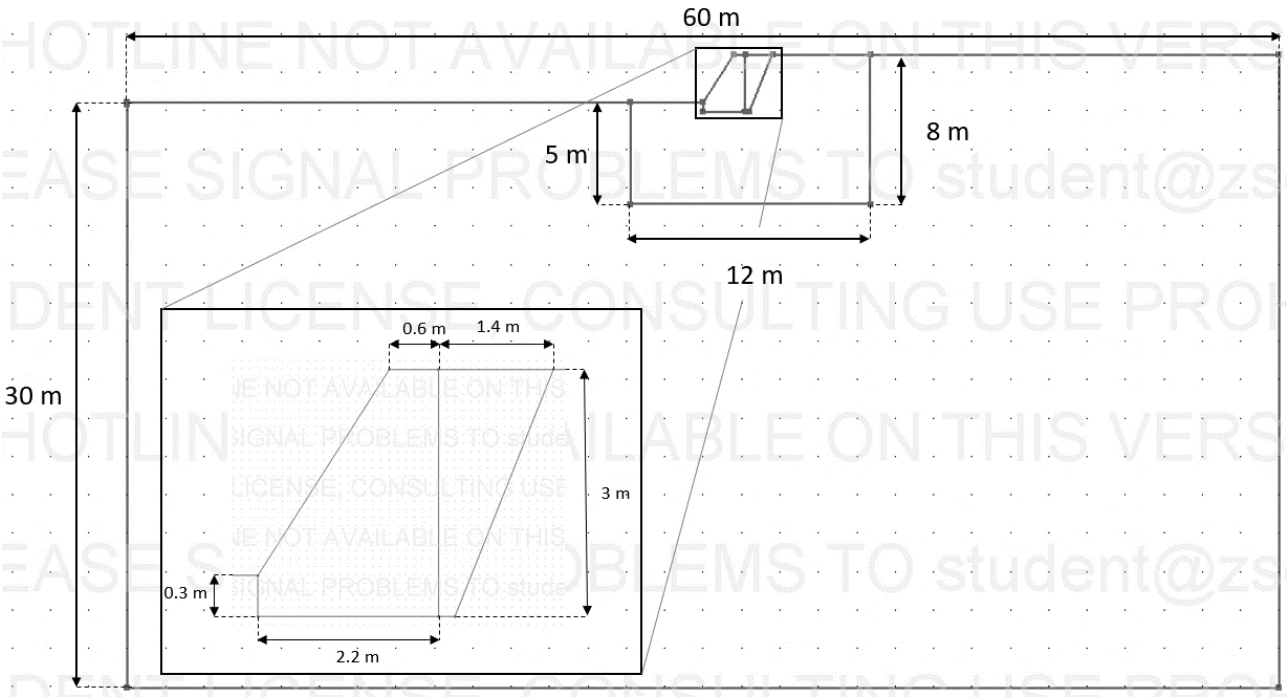


*Figure 6-2; Global geometry of the FEM*

The overall box has been built up with an unstructured quadrilateral mesh (**Figure 6-3**) characterized by a 2m side, while the region of study has a mesh refinement of 0.2m side. Those choice have been done to allow a good resolution in the region of study, and in order to reduce at minimum the boundary effects. The total number of nodes is 2761 and the continuum 2D elements are 2592.

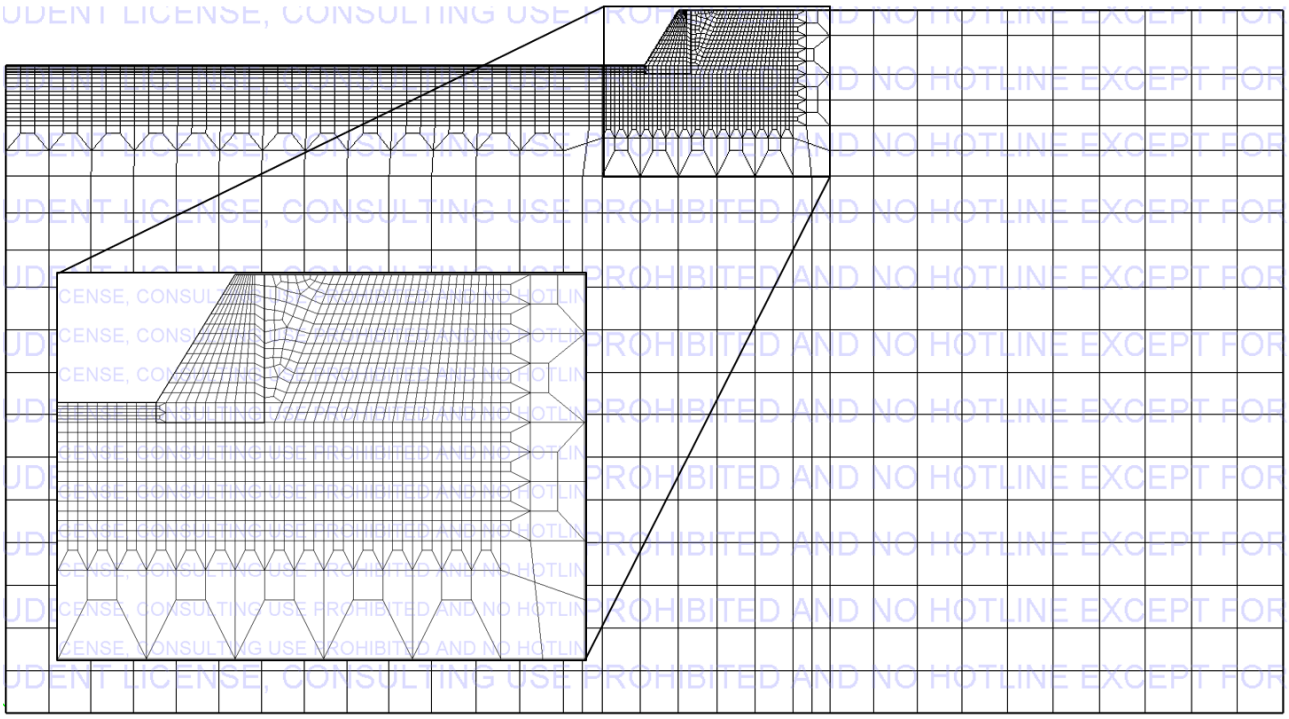

*Figure 6-3; FEM global mesh and mesh refinement.*

The boundary conditions are described referring to the **Figure 6-4**, the solid boundary conditions are placed on the edges DE, EF and FG; a total head of zero (position of the point C) have been imposed at the side of the box DE and GF, meaning that an horizontal GWT is placed at the base of the wall. On the surface AD and GH is placed a water flux $i_d$; seepage elements are used to simulate the drain on the back of the wall (AB), they are characterized by two faces, the external has zero pressure by default and for the internal the pressures are automatically computed on the inner layer (COMMEND, et al., 2016). Contact elements are used to simulate the soil-wall friction (δ), that has been placed as 2/3ϕ'. The used materials are the one presented in the Chapter 2.1, that are the Sion silt and the sand as backfill, their material formulation is Mohr-Coulomb, while the material formulation of the wall is Concrete plastic damage and have been left the default values.

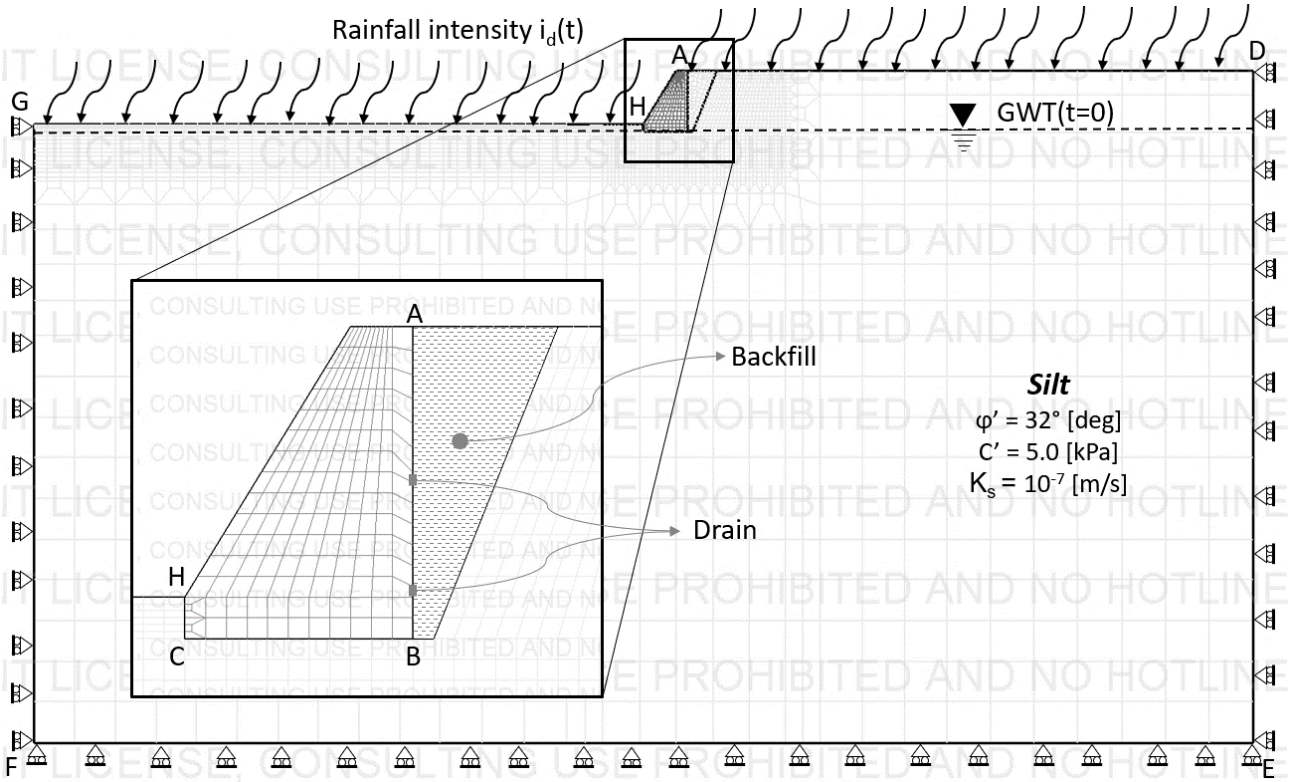


*Figure 6-4; FEM boundary conditions*

The analysis have been done for small displacements and three different load functions have been used. Two for simulating the different rainfalls events ($i_c$=29.2 mm/h and $i_c$=1.36 mm/h) by mean of a constant hyetograph, and one to allow an infiltration equal to the effective infiltration ($f_e$). Indeed when $i_c$ is bigger than $k_s$ the difference between the two value cannot infiltrate in the model, to dirve the operation allowing an infiltration equal to the effective one (cf. § 4.2), the soil permeability has been changed and placed by mean of a load function to be equal to the effective infiltration ($k_{ij}=f_e$).

Using the model here above described are hypotized three scenario for both the rainfall event: one is the operative scenario, that is the one provided by the whole drainage sistem, and thus sandy backfill and subhorizontal drain; the second one is charachterized by the wall without the backfill and the drain, thus is composed by the only wall layng against the silt) ; the third one that is like the first but with clogged drain (the clogged drain have been simulated by removing the seepage elements). Those scenarios are simulated for each the rainfall event and thus for the five day event characterized by a constant hyetograph of 1.36 [mm/h] and for the one hour event characterized by a constant hyetograph of 29.2 [mm/h].

The first driver used to start the analysis is the Initial state, that apply gravity strating from half of its value and increasing it by step of g/10 till it reach the final value. Subsequently is used the stability driver tg(phi)-c, that apply a reduction of the soils strength parameters tan(ϕ') and c', till is not anymore able converge. This driver allow to asses the global stability

of the problem, and give back a Factor of Safety (FS). Is important to remark that those solutions came from a diverged step. Finally, the time dependent driver consolidation is used to perform the hydromechanical analysis as described in the previous pharagraph.

The above-mentioned drivers have been used susequently, with the exception of the initial state used only initialize the problem. The same sequence of drivers have been used for the six cases mentioned above. The details of the drivers sequence and their increment are shown in the **Figure 6-5**. The total time of the whole analysis is of 1000 hours.

| Driver | Type | Ini. load factor | | Fin. load factor | | Increment | | Multiplier |
|---|---|---|---|---|---|---|---|---|
| Initial State | | 0.5 | | 1 | | 0.1 | | |
| Stability | tg(phi)-c | 1 | | 5 | | 0.05 | | |
| Time Depend | Consolidation | 0 | [h] | 0.25 | [h] | 0.05 | [h] | 1 |
| Stability | tg(phi)-c | 1 | | 5 | | 0.05 | | |
| Time Depend | Consolidation | 0.25 | [h] | 0.5 | [h] | 0.05 | [h] | 1 |
| Stability | tg(phi)-c | 1 | | 5 | | 0.05 | | |
| Time Depend | Consolidation | 0.5 | [h] | 0.75 | [h] | 0.05 | [h] | 1 |
| Stability | tg(phi)-c | 1 | | 5 | | 0.05 | | |
| Time Depend | Consolidation | 0.75 | [h] | 1 | [h] | 0.05 | [h] | 1 |
| Stability | tg(phi)-c | 1 | | 5 | | 0.05 | | |
| Time Depend | Consolidation | 1 | [h] | 24 | [h] | 1 | [h] | 1 |
| Stability | tg(phi)-c | 1 | | 5 | | 0.05 | | |
| Time Depend | Consolidation | 24 | [h] | 48 | [h] | 1 | [h] | 1 |
| Stability | tg(phi)-c | 1 | | 5 | | 0.05 | | |
| Time Depend | Consolidation | 48 | [h] | 72 | [h] | 1 | [h] | 1 |
| Stability | tg(phi)-c | 1 | | 5 | | 0.05 | | |
| Time Depend | Consolidation | 72 | [h] | 96 | [h] | 1 | [h] | 1 |
| Stability | tg(phi)-c | 1 | | 5 | | 0.05 | | |
| Time Depend | Consolidation | 96 | [h] | 120 | [h] | 1 | [h] | 1 |
| Stability | tg(phi)-c | 1 | | 5 | | 0.05 | | |

| Driver | Type | Ini. load factor | | Fin. load factor | | Increment | | Multiplier |
|---|---|---|---|---|---|---|---|---|
| Stability | tg(phi)-c | 1 | | 5 | | 0.05 | | |
| Time Depend | Consolidation | 120 | [h] | 500 | [h] | 10 | [h] | 1 |
| Stability | tg(phi)-c | 1 | | 5 | | 0.05 | | |
| Time Depend | Consolidation | 500 | [h] | 1000 | [h] | 10 | [h] | 1 |
| Stability | tg(phi)-c | 1 | | 5 | | 0.05 | | |
| Time Depend | Consolidation | 1000 | [h] | 10000 | [h] | 100 | [h] | 1 |
| Stability | tg(phi)-c | 1 | | 5 | | 0.05 | | |

*Figure 6-5; Drivers sequence used*

## 6.3 Results

Once the analysis described, are finished is possible visualize the results in the post processor, where nodal, element, sectional or maps results can be displayed. To have a better control of the data, those have been exported in to a *".csv"* format and after a first tidy up have been imported on the Software *Matlab* for further elaborations. Here the results of the six scenarios are reported in the following order: firstly, the one-hour rain event and subsequently the 5-day ones are reported. In both cases are initially shown the results for the operative case, subsequently the case with no drainage system and finally the case with clogged drain.

For each case the following information's are reported: the Pore Water Pressure PWP and the Saturation ratio $S_r$, evaluated in the section immediately behind the wall, coincident with the segment AB in **Figure 6-4**; the time evolution of the horizontal displacement at the head of the wall (point A in **Figure 6-4**); the time evolution of the thrust force (integral of the total horizontal stress acting in the section AB) and finally the safety factor.

Follows the results for the operative scenario with the one-hour intense rainfall event.

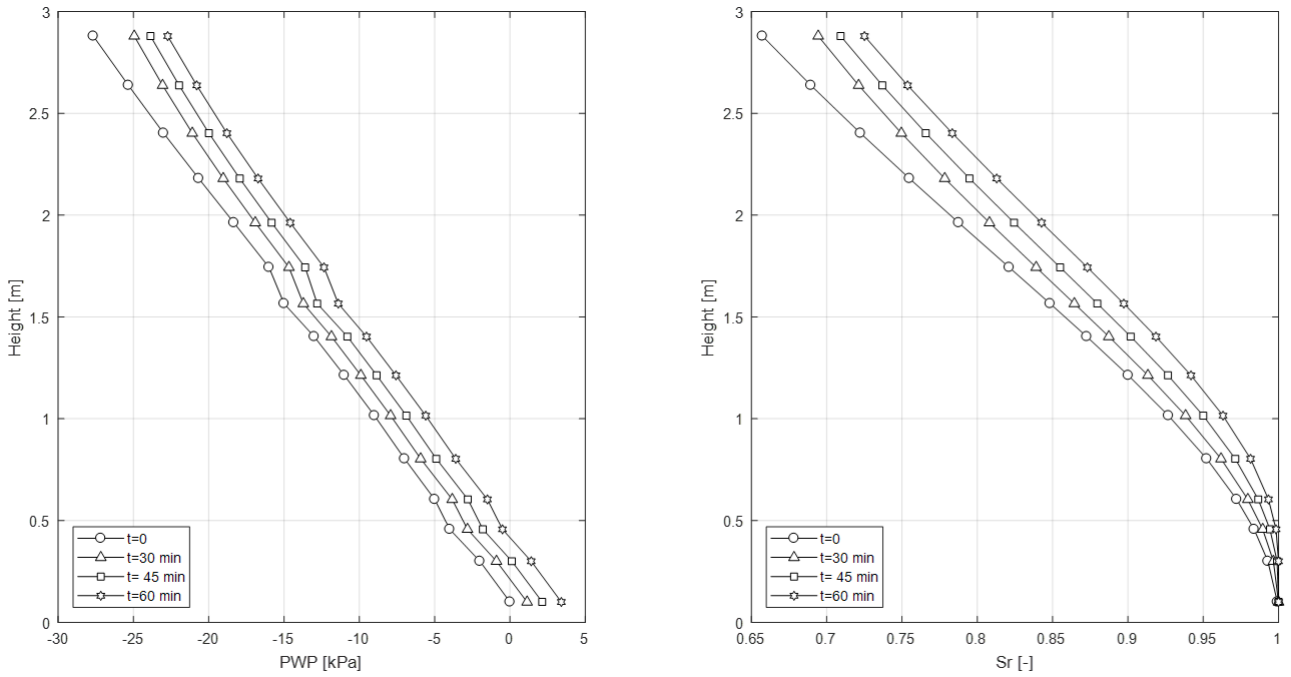


***Figure 6-6;*** *Pore water pressure and saturation ratio for intense rainfall of one hour (operative case)*

In **Figure 6-6** the value of the suction remained high indeed it's value at the top of the wall decreased only of a few kPa. This can be explained by looking at the saturation ratio that as the PWP didn't change much. This can be explained considering the saturated hydraulic conductibility of the sand that is 360 mm/h, much bigger than the flux coming from the rain event that is of 29.2 mm/h, so is not possible for the sand to saturate. By looking at these values we won't expect, a big decrease of the factor of safety for this case, since suction still have a big component.

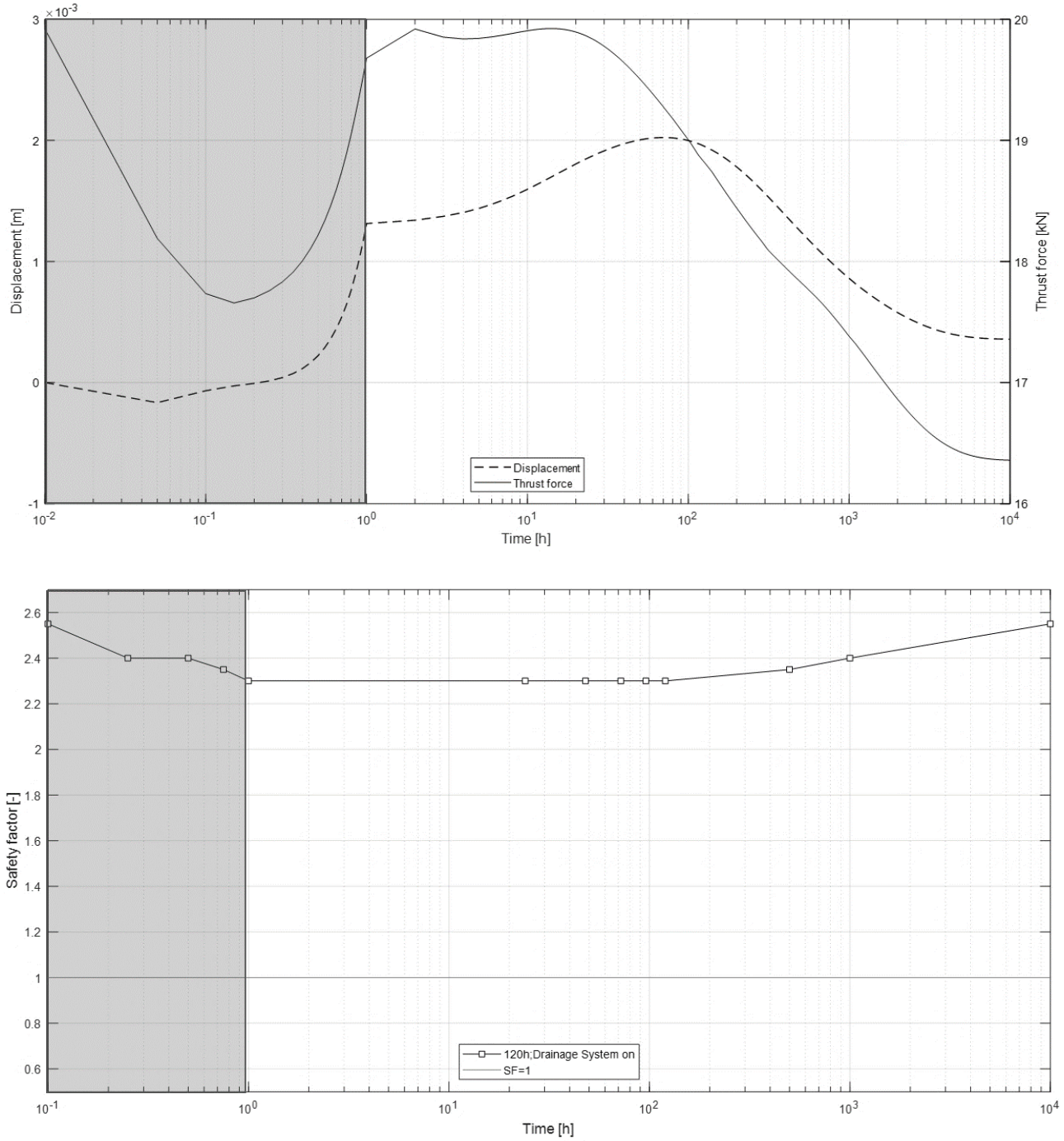


***Figure 6-7;*** *Above: Head horizontal displacements and thrust force acting on the wall (time in logarithmic scale) ; Below: Safety factor (time in logarithmic scale) for intense rainfall of one hour (operative case)*

Referring to the **Figure 6-7**, the displacement and the thrust force have a similar trend, with the exception of the first 6 minutes ($10^{-1}$h), where the force decrease, this strange behaviour is explained with some initial assessment of the model. In spite of this the maximum force exerted is of 20 kPa, while the maximum displacement is of 2mm almost completely recovered, it means with some exception the stress field didn't touch the critical state line (the stress remained in the elastic field).

Finally, the safety factor that from the initial value of 2.6 lowered till 2.3 at the end of the rain event and subsequently recovered after remaining constant for a hundred hour, show a global reliability of the structure under those conditions.

Follows the results for the scenario without a drainage system with the one-hour intense rainfall event.

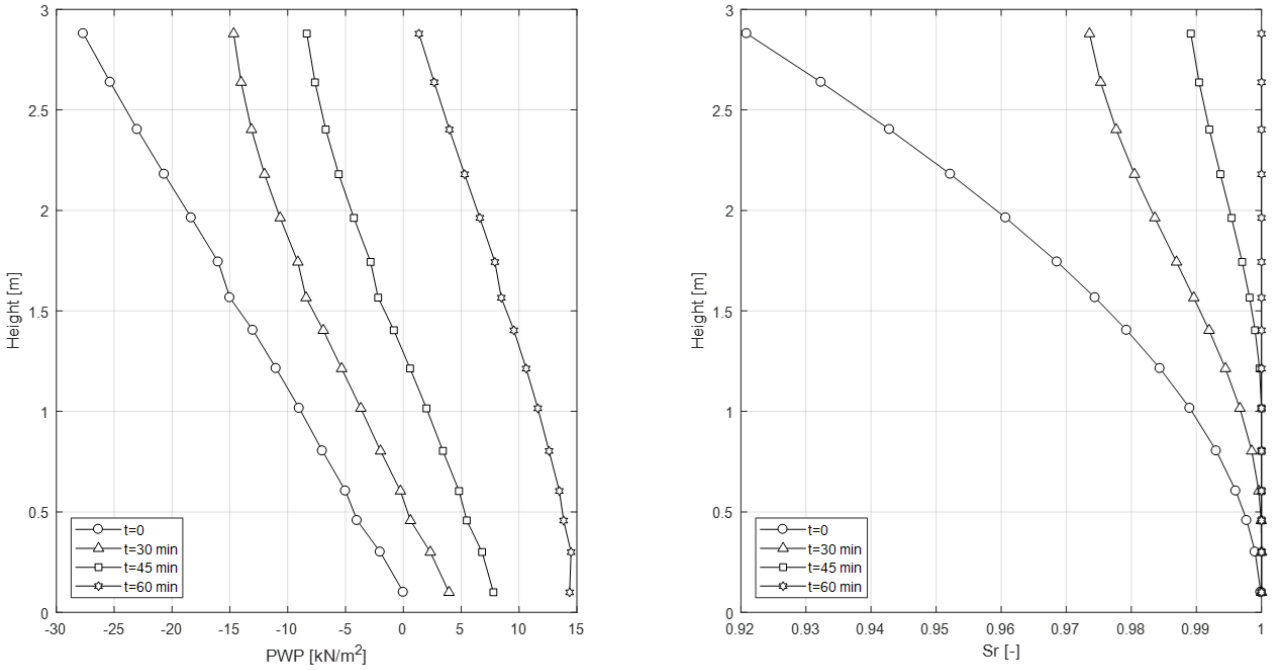


*Figure 6-8; Pore water pressure and saturation ratio for intense rainfall of one hour (No drainage system case)*

In this case (**Figure 6-8**), there is a big change of the pore pressure, that at the head of the wall passed from the hydrostatic suction of -30 kPa till reaching the null value that can be obtained when the soil get saturated. This is confirmed by the saturation ratio that from the initial value of 0.92 became 1 after one hour. With respect the other case, where the initial $S_r$ was 0.65, is clear the different behaviour of the two soils. Indeed while for the sand, for those values of suctions (-30 kPa) we are in the middle of the soil water retention curve, for the silt we are still in a range close to the AEV. Those differences that do not respect the AEV criteria are due of the model used here for the SWRC that by using only one parameter cannot well fit the experimental values. Furthermore, the saturation ratio is reached since the silt has a saturated hydraulic permeability three orders of magnitude smaller than the sand one, that is 0.36 mm/h instead of 360 mm/h and the rain intensity, as before, is bigger 29.2 mm/h.

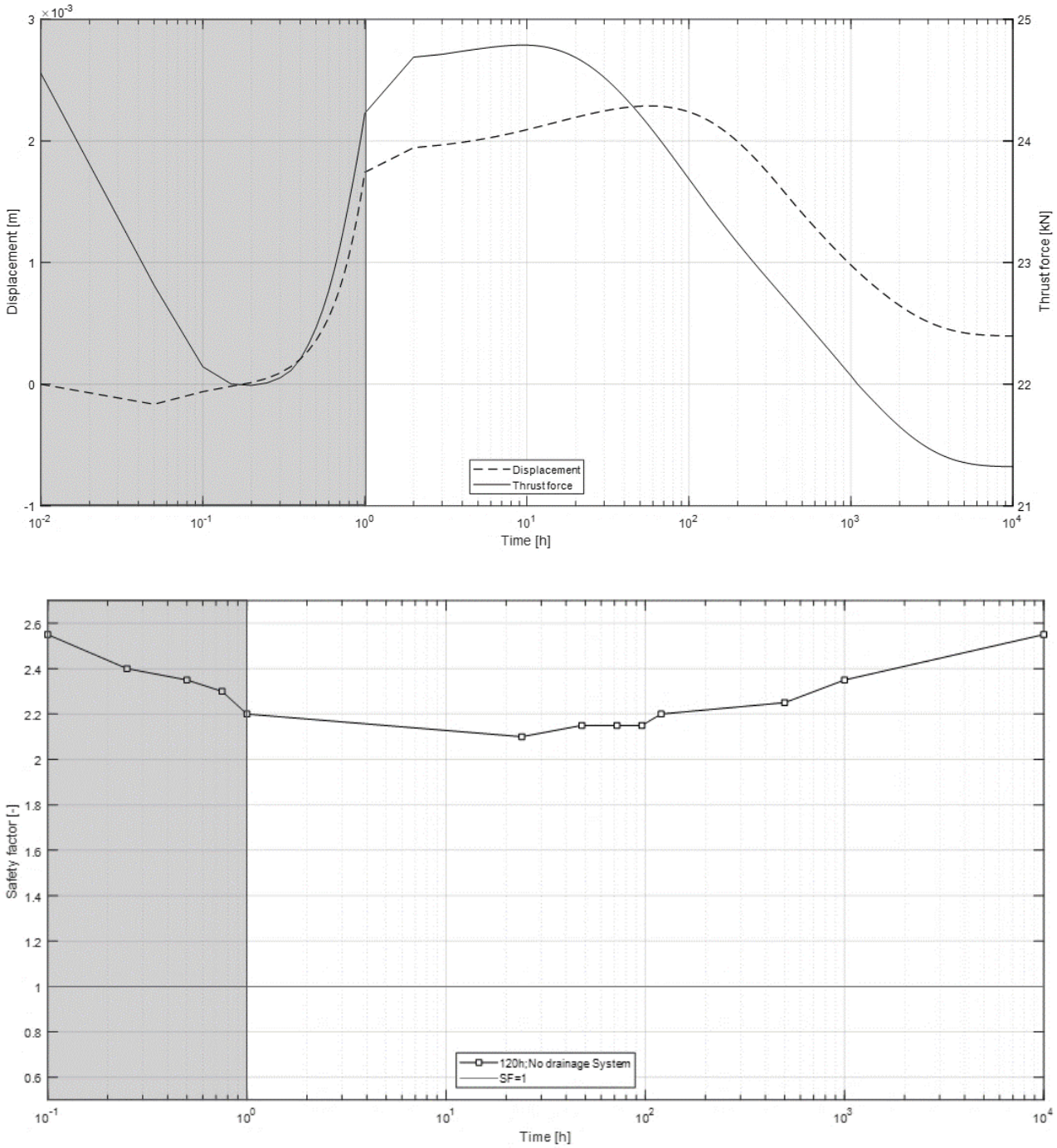


***Figure 6-9;*** *Above: Head horizontal displacements and thrust force acting on the wall (time in logarithmic scale); Below: Safety factor (time in logarithmic scale) for intense rainfall of one hour (No drainage system case)*

As for the same figure of the previous case (**Figure 6-7**), here (**Figure 6-9**), there is an initial decrease of the thrust and both thrust and horizontal displacements have a similar trend. Even though the range of displacement is the same (0-2 mm) the force acting on the wall is a bit higher indeed from the maximum previous value of 20 kPa passed to 25 kPa.

Also in this case the safety factor remined in a safe range indeed it lowered from the initial value of 2.6 to 2.1, differently from the previous case it kept lowering a bit after the rain event, that may be due to the pore water pressure that need to asses further. By considering the pore water pressure distribution at the end of the event and the change in the safety factor steepness's between 0.75h and 1h, should be an awareness. Indeed, if would have been raining for a bit more with the same intensities, it would have probably caused the failure of the structure since a positive hydrostatic pore water distribution would have formed.

Follows the results for the scenario with clogged drain for the one-hour intense rainfall event.

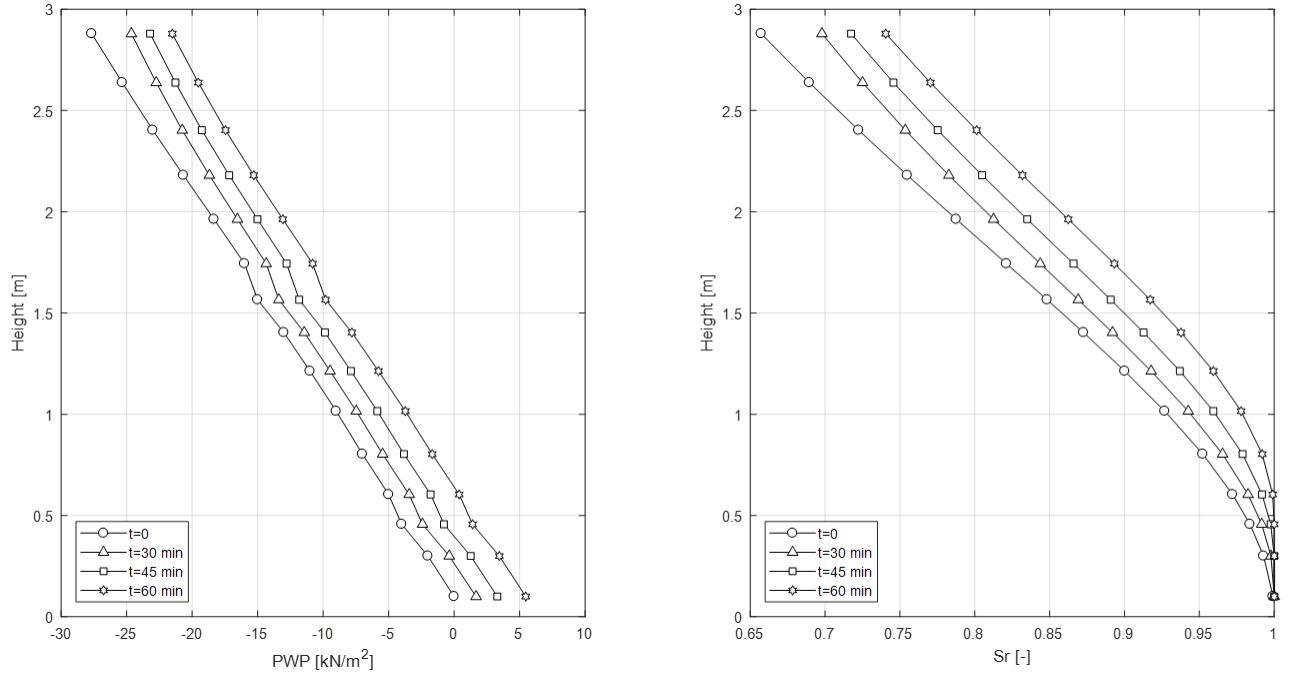


*Figure 6-10; Pore water pressure and saturation ratio for intense rainfall of one hour (Clogged drain case)*

In this case the results of **Figure 6-10**, show that the rain event hasn't modified a lot the hydraulic condition behind the wall. Indeed, as for the operative case (**Figure 6-6**) the pore water pressure decreased of few kPa and the saturation ratio changed of ten percentual point. No relevant differences are expected from the operative case.

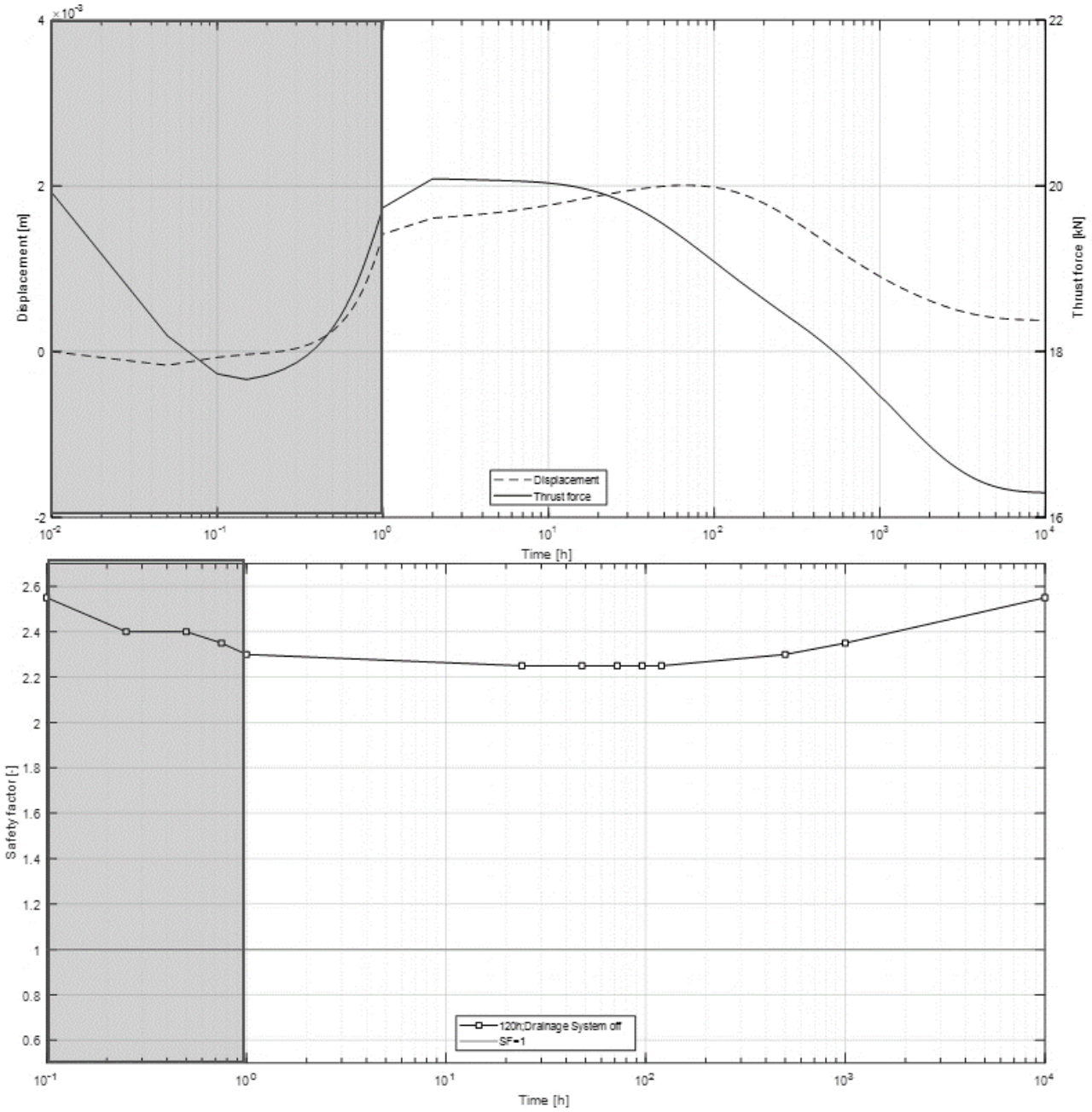


*Figure 6-11; Above: head horizontal displacements and thrust force acting on the wall (time in logarithmic scale); Below: Safety factor (time in logarithmic scale) for intense rainfall of one hour (clogged drain case).*

As expected, the range of the displacement is still of 0-2 mm and the maximum thrust is equal to the one obtained in the operative case. With regard the safety factor lowered to till value of 2.2 exactly as the operative case previous case (cf.  and **Figure 6-7**).

Follows the results for the operative scenario with the 5-day rainfall event.

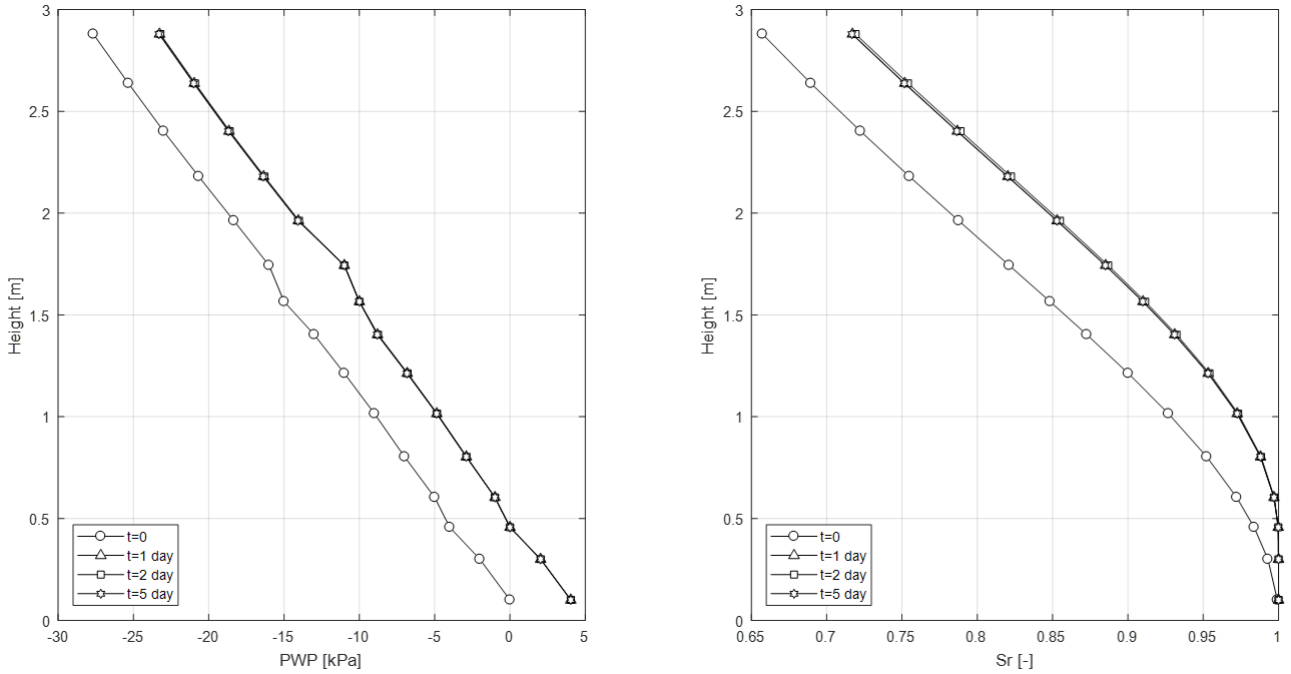


*Figure 6-12; Pore water pressure and saturation ratio for a five-day rainfall (operative case)*

The hydraulic conditions for the operative scenario reach a steady state, indeed how is possible to infer by looking at **Figure 6-12**, both the pore water pressure and the saturation ration didn't change after one day of rain and their range is the same of the clogged and operative case for the on-hour rainfall event (**Figure 6-6** and **Figure 6-10**). The reason can be explained by the achieving of the natural steady state profile or is a steady profile artificially induced by the drain.

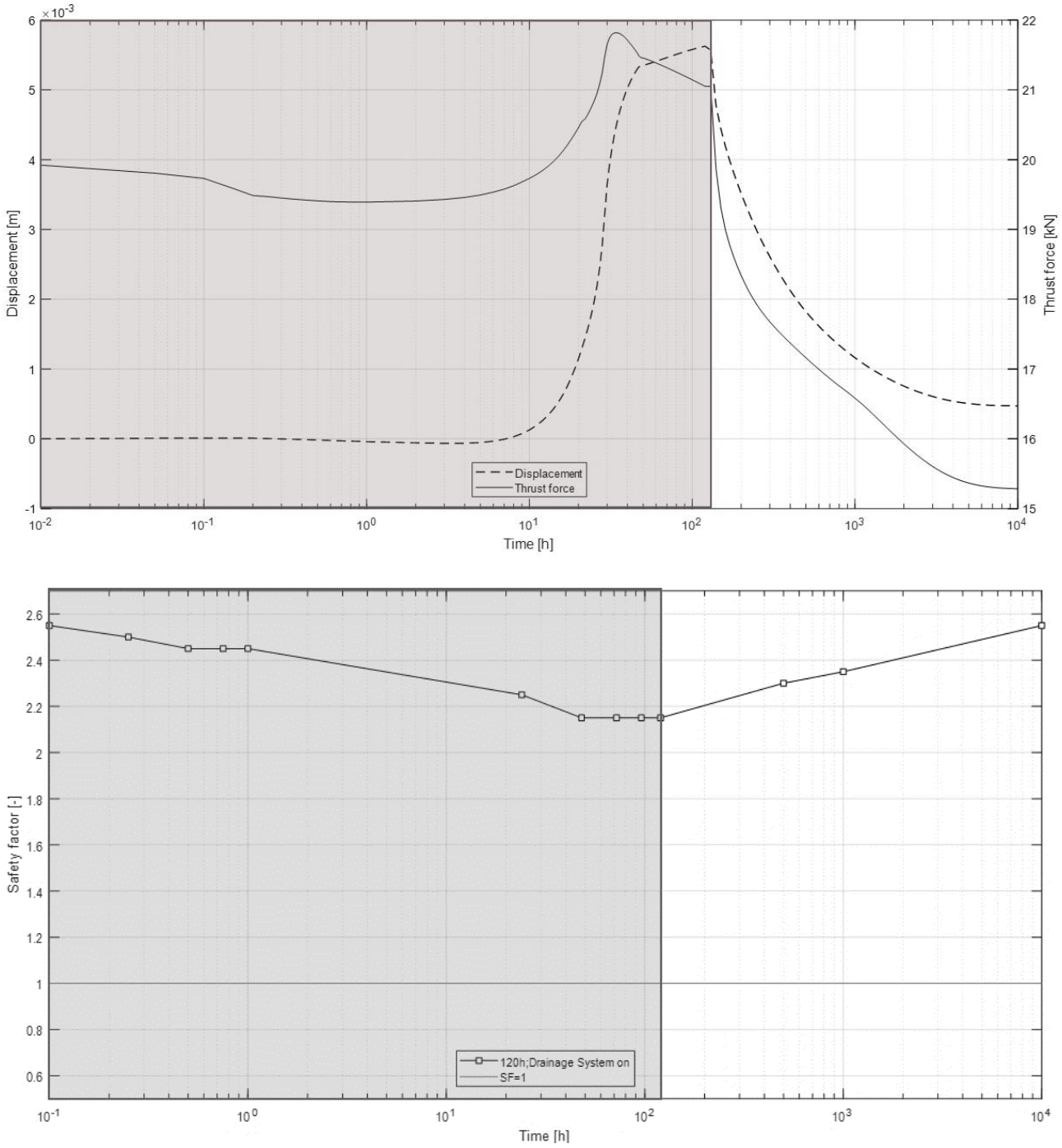


***Figure 6-13**; Above: Head horizontal displacements and thrust force acting on the wall (time in logarithmic scale) ; Below: Safety factor (time in logarithmic scale) for a five-day rainfall (operative case).*

Also this case (**Figure 6-13**) the stress behind the wall didn't change, indeed the thrust force reached a maximum value of 22kN, but really different are the displacements, that during the first day reached 4mm and reaching the maximum value of 5.5mm, this displacement can be considered acceptable especially if at the end the deformation are mostly recovered. The decrease of the force after the first day might be due to the release of the stress, previously accumulated in the soil, by the wall displacement.

Here (**Figure 6-13**), even though the relatively high displacement (5mm) the safety factor spanned from the 2.6 initial value to 2.15 remaining in to a safe interval. by looking at the results showed for the clogged drain (Figure 6-16) is clear that the above-mentioned stationarity is caused by the drain that efficiently withstood the long rain event.

Follows the results for the scenario without a drainage system with the 5-day rainfall event.

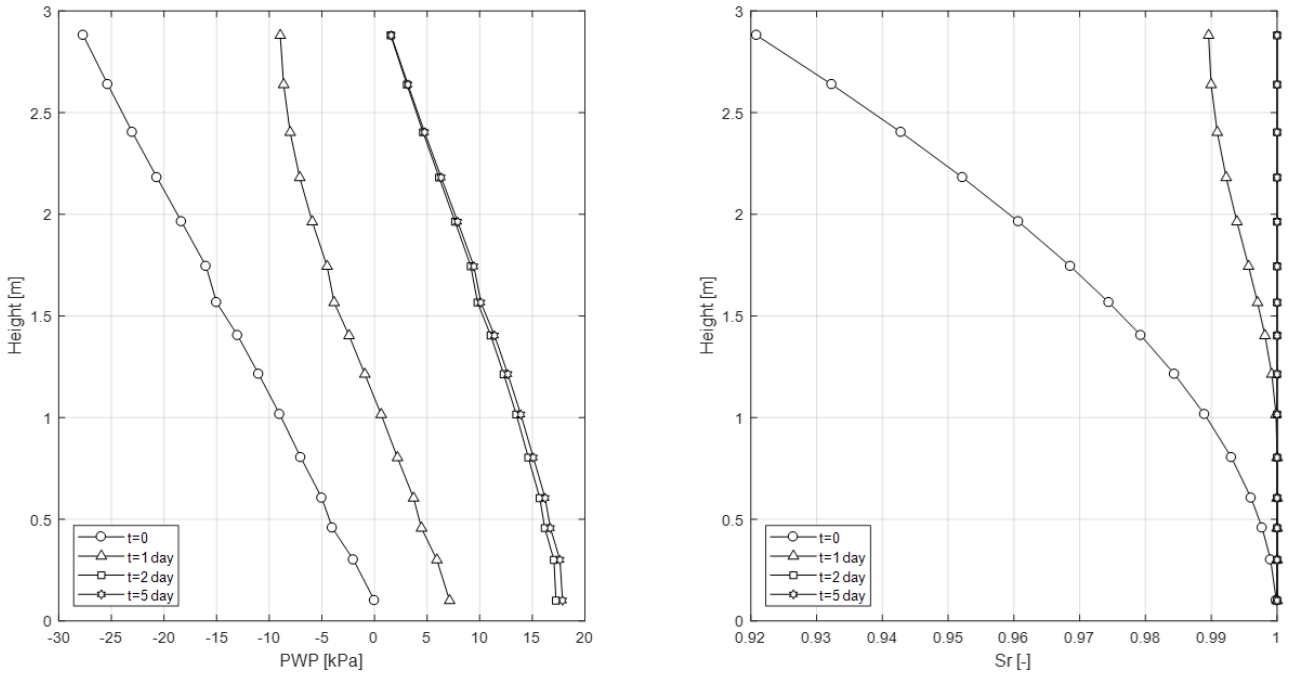


***Figure 6-14;*** *Pore water pressure and saturation ratio for a five-day rainfall (No drainage system case)*

**Figure 6-14** shows a big increase of the water pressure behind the wall, that from the negative hydrostatic initial condition passed to quasi hydrostatic positive one, this is due to a rain event of 1.36 mm/h an thus bigger than the soils hydraulic conductivity (0.36 mm/h). the soil reached the saturation after the second day. Despite that is not reached a full hydrostatic water distribution indeed the value of the pore water pressure at the base of the wall is approximately 18 kPa and do not reach the 30 kPa.

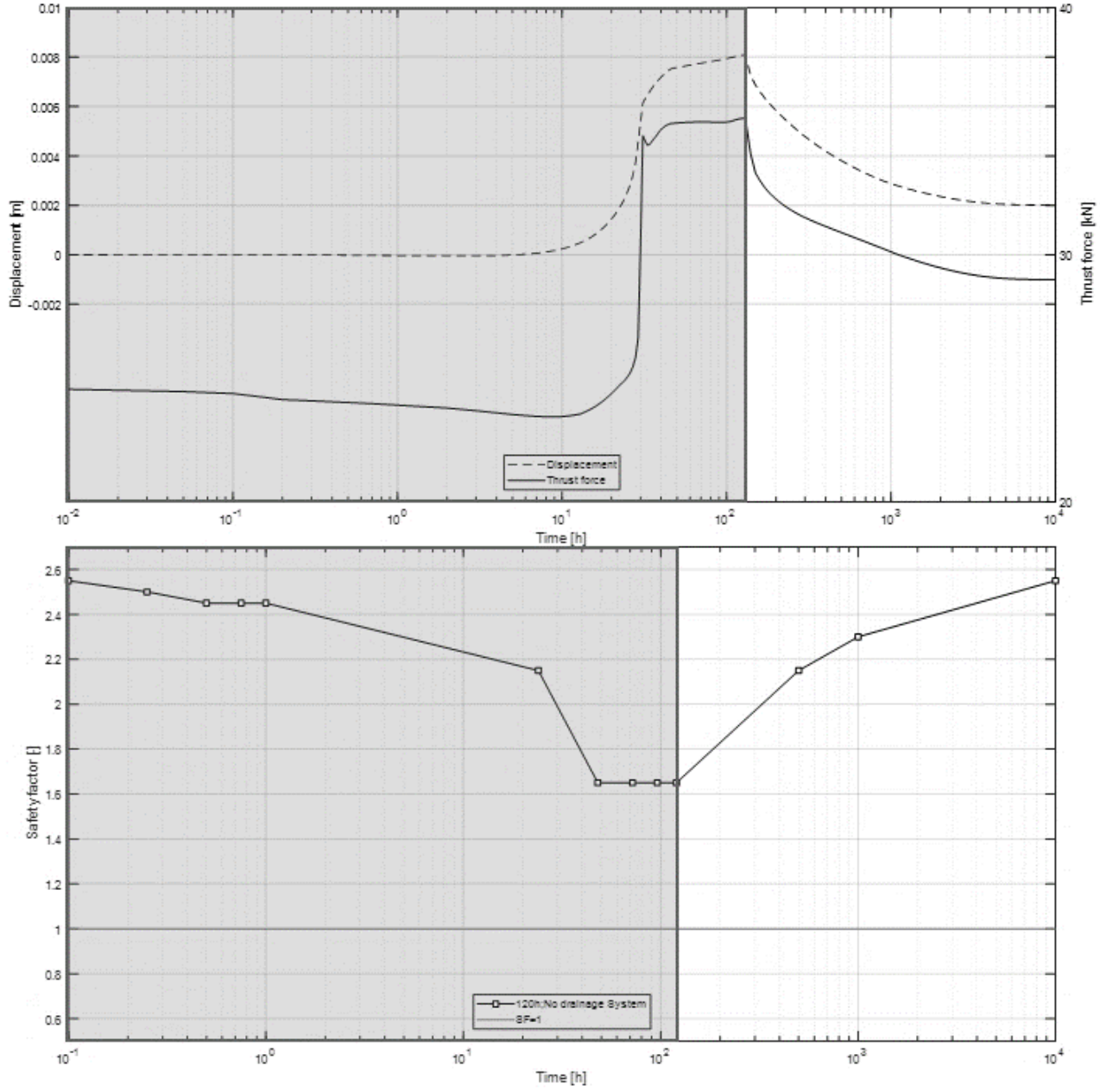


*Figure 6-15; Above: head horizontal displacements and thrust force acting on the wall (time in logarithmic scale); Below: Safety factor (time in logarithmic scale) for a five-day rainfall (No drainage system case).*

For this case (**Figure 6-15**) the maximum displacement have been of 8 mm and is caused by a thrust force of 35 kN here the effect of the positive water pressure is relevant: displacement close to the centimetre and safety factor that decrease of two unitary value, passing from 2.6 to approximately 1.6.

If for the same case but for the shorter rain event a critical condition was supposed, here it is clear: a leak of an efficent drainage system drives to dangerous situation.

Follows the results for the scenario with clogged drain for a 5-day rainfall event.

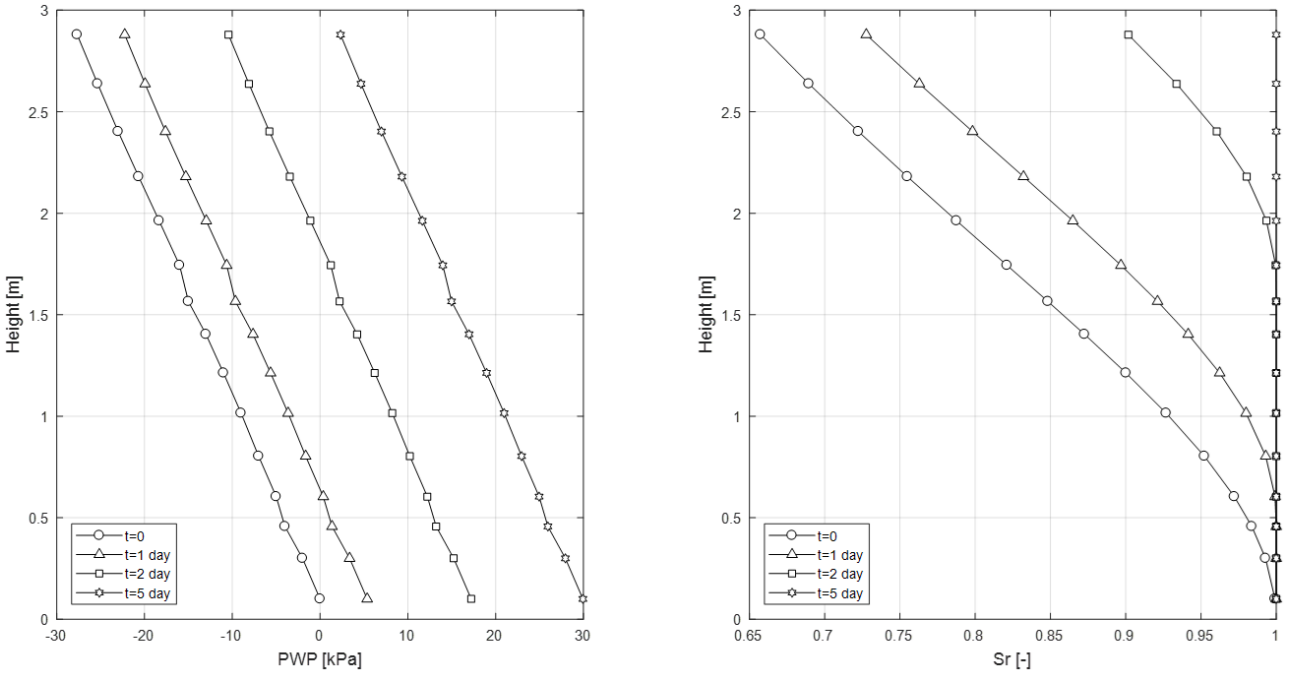


*Figure 6-16; Pore water pressure and saturation ratio for a five-day rainfall (clogged drain case)*

Here (Figure 6-16), show a dramatically rise of the pore water pressure a positive hydrostatic water distribution is reached. Comparing this case with the previous one, unfurnished of a drainage system (**Figure 6-14**), one can observe that the saturation of the soil is reached only the fifth day while in the other after the second day. This difference is due to the different soil hydraulic conductibility (360 mm/h against 0.36 mm/h). All those aspects can be explained by considering the formation of a suspended water table at the sand silt interface. Indeed, the whole precipitation (1.36 mm/h) flowed inside the sand and accumulated on the silt that has a saturated hydraulic conductibility lower that the precipitation values. The water that cannot infiltrate in to the silt, start accumulating and finish to generate the above mentioned suspended water table.

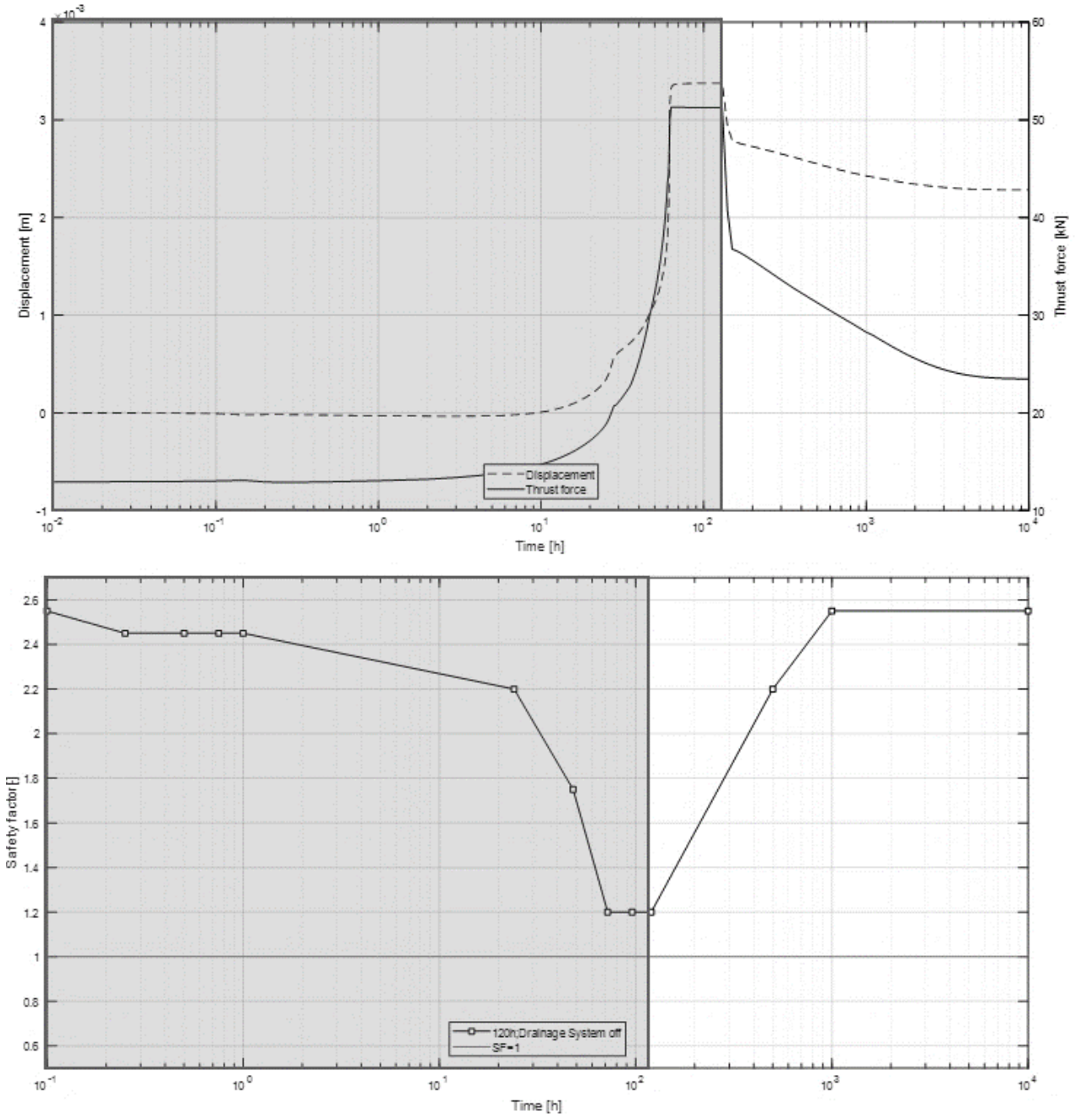


***Figure 6-17;*** *Above: head horizontal displacements and thrust force acting on the wall (time in logarithmic scale); Below: Safety factor (time in logarithmic scale) for a five-day rainfall (clogged drain case).*

The force that developed behind the wall is here pretty high, indeed it passed the 50 kN, but in response the displacements have been fairly contained, the maximum on was approximately 3 mm. That is caused by the reaching of the plastic domain, indeed the final displacement remained of 2 mm. Already those evidences are enough to consider the general failure of the structure, those last are remarked by looking at the safety factor that is more halved by reaching the value of 1.2.

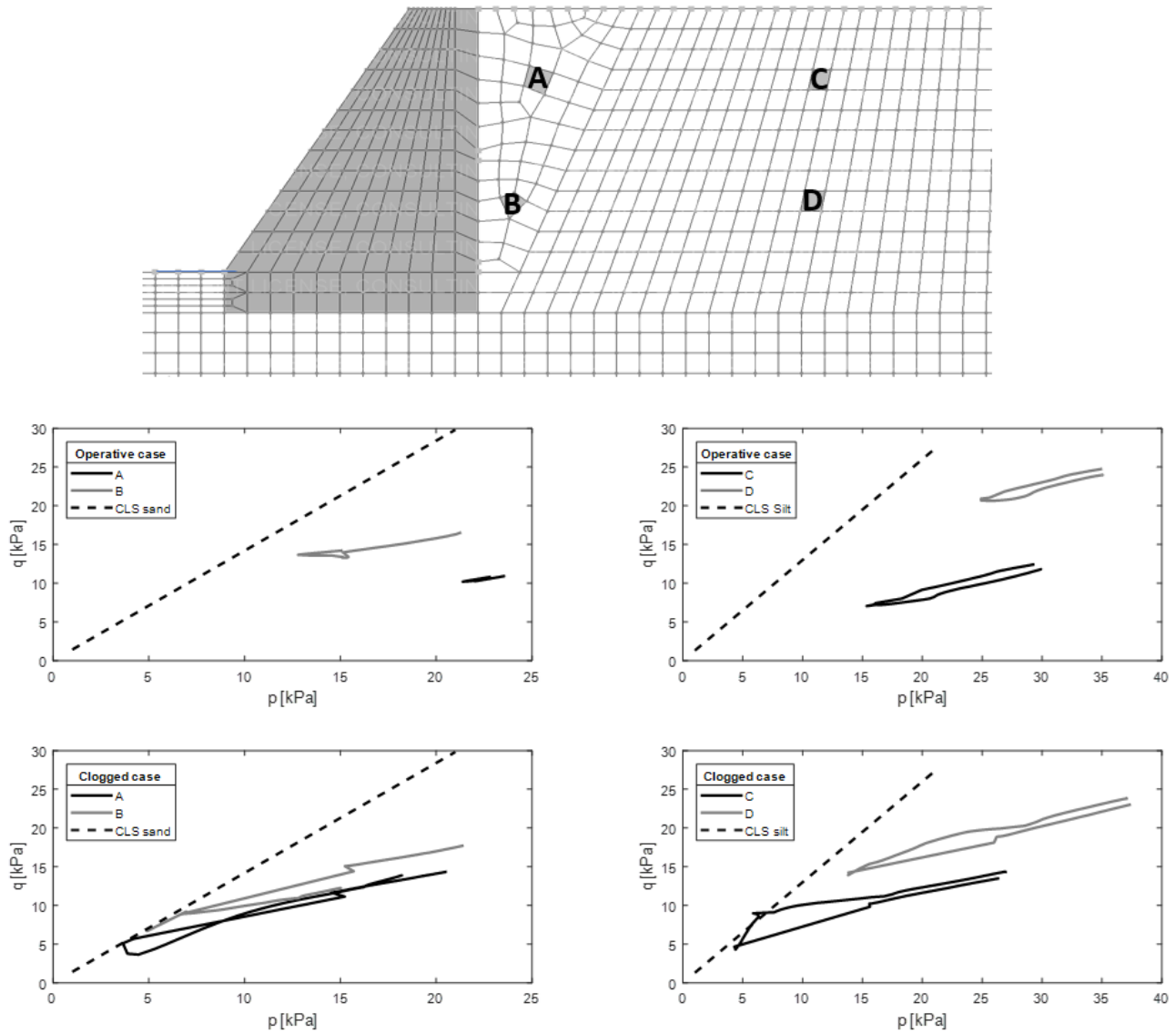


***Figure 6-18**; Effective tress path of the point A, B, C and D and their position: Above position of the point; middle operative case; below clogged drain case (for the 5-day rainfall event)*

The observation done for the two last cases are here (**Figure 6-18**) confirmed, indeed three of the point A, B and C touch the critical state line, it means that passed from the elastic domain to the elastic one. All the represented path starts from the higher extremity of the line, for decreasing in both the components of mean stress and deviatoric stress, reached a peak value that correspond approximately to the fifth day it goes back to the initial values. Since the three-principal components of stress are all different, is quite difficult to understand their behaviours, but by observing the different behaviours of the three principal component is possible to infer that the decrease of the deviatoric stress is due to the decrease of the compression soils caused by the wall's displacement.

For all the six scenarios the software always found a solution (never diverged), that means that also if the stability driver wasn't run the factor of safety never went below the unitary

value. In order to conclude let's report here below (**Figure 6-19**), the classical surface of failure induced by the tan(phi)-c' reduction algorithm. In the specific case the absolute displacement intensities of the 5-day operative scenario are shown, but despite this, all of them are characterized by the same rot-translational movement and slip surface.

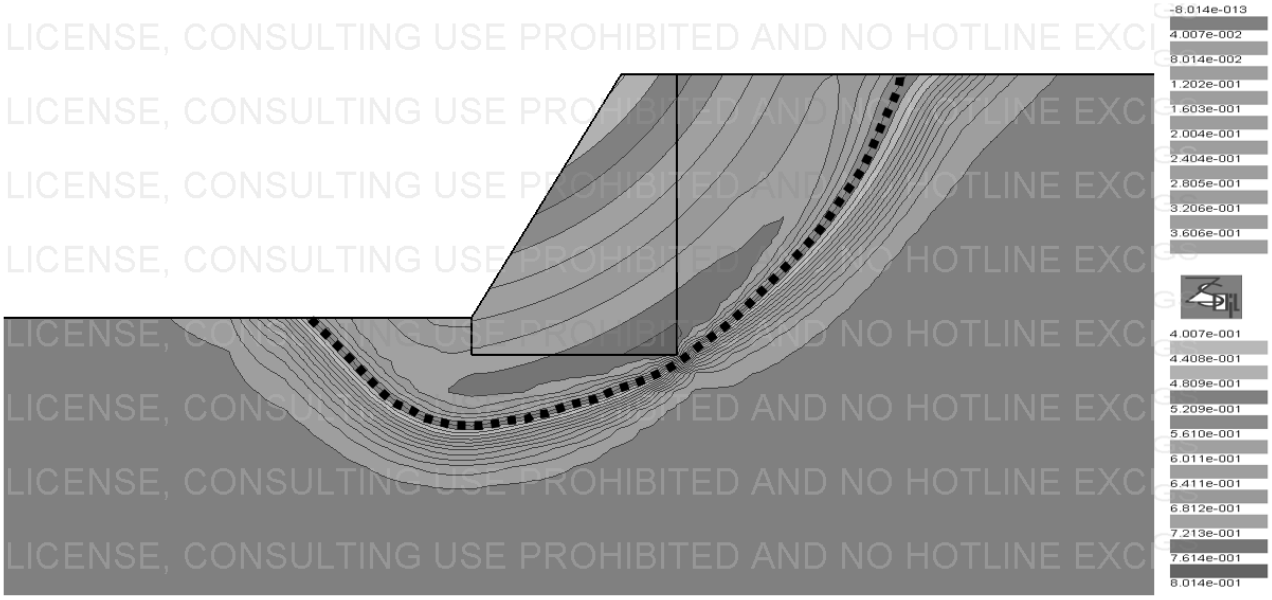


*Figure 6-19; General failure surface induce by the tan(phi)-c' reduction: the dotted line is the slip surface and displayed values are the absolute displacement intensities.*

# Chapter 7 Conclusions

The object of study of this work was the interaction between unsaturated soils and retaining walls during rainfall events. In order to analyse the problem by an engineering scale, the hydromechanical principles of those soils, have been studied. The soil water retention curve surely represents one of the most important parameters to describe their behaviour. Indeed, its comprehensive study allowed to implement the classical geotechnical analysis, in order to take into account their hydromechanical behaviour.

The uncoupled steady hydromechanical analysis, provided reasonable results. LEP solutions, allowing to neglect the tension stress that develop at the ground surface, furnish more reliable results. But them does not allow to take in to account geometry that fall outside the standard case (frictionless straight wall and horizontal backfill). LEM solutions resulted to under evaluate the lateral earth thrust $P_a(k_s)$ = 12.40 kN against the $P_a(k_s)$ = 14.79 kN of the LEP ones. That's because suctions are considered to act all along the failure plane, without reducing their contribute when tensions stress develop. Despite this lack, that can be handled by introducing the tension crack effect (SAHOO & GANESH, 2017), LEM solutions have the potentiality consider more complicated geometry. Thus, their implementation in to the computational code, is surely to achieve. With regard LEM and LEP transitory solutions, are surely a useful tool to evaluate the time required, for a given flux, to nullify the suction component and thus to understand, within a preliminary study the effect of a certain rain event.

By the analysis of the Italian and European standards, resulted clear the necessity to assess the reliability of a retaining structure. The proposed methodological procedure allowed to identify two different rainfall events, characterized by a 100 years' period of return. A short and intense of one-hour, characterized by the critical precipitation $I_c$ =29.2 mm/h and a long one of five-day, characterized by the critical precipitation $I_c$ =1.36 mm/h. This procedure, together with a simulation of a efficiency loss of the drainage system, is fundamental to subsequently asses the reliability of the retaining structure.

The global stability and the displacement of the gravity wall have been verified in the cases of exceptional rainfall event and the obstruction of the drain. This have been done by mean of coupled hydromechanical analysis on a Finite Element Model. The Software *Zsoil* have been used to implement the model and three different cases: operative, clogged drain and

no drainage system. Those cases have been simulated for the two different rain intensities, for a total of six scenarios.

The results showed a good response for all the three cases when subjected to the one-hour rainfall event, indeed the safety factor never went below 2.15, while the residual displacements where of 0.4mm.

Is shown a good response of the wall, in to his operative condition, also when subjected to the 5-days rain event. Indeed, the global stability analysis, showed that the safety factor never went below the value of 2.15. And the displacement remained in to an acceptable range, since after a maximum displacement of 5mm, those have been elastically recovered at the end of the rainfall events showing a residual displacement of 0.5 mm. Instead, the clogged drain case, subjected to the same rainfall event, exhibit the reaching of failure conditions: safety factor on 1.2 and residual displacement of 2.3 mm. Concerning the no drainage system case it showed an intermediary condition: safety factor on 1.65 and residual displacement of 2.0 mm.

The results showed that is possible to evaluate the active earth thrust by mean of the analytical solutions. Although this is a reasonably good approach for preliminary analysis, is surely suggested the use of more complicated methods, that allows to perform 3D or 2D coupled hydromechanical analysis. It is further fundamental to evaluate the behaviour of the structure, considering exceptional precipitation event and a loss of efficiency of the drainage system. Indeed, as shown, drainage system might be a double-edged sword, since wen clogged, can cause a development of positive pressure, higher than the one that could occur without a drainage system.

Thus, when a drainage system is adopted to maintain the soil in to unsaturated condition a careful planning of their maintenance is fundamental.

# Chapter 8 References

AVERSA, S., 2011. *Il progetto dei muri di sostegno.* s.l., s.n.

BEAR, J., 2013. *Dynamics of fluids in porous media.* s.l.:Courier Corporation.

BERARDI, R., 2009. *Fondamenti di geotecnica.* II éd. Novara: Città studi.

BISHOP, A. W., 1959. The principle of effective stress. *Teknisk ukeblad,* Volume 39, pp. 859-863.

BOND, A. J. e. a. .., 2013. *Eurocode 7: geotechnical design worked examples.* Ispra: Joint Research Centre.

CHOW, V. T., MAIDMENT, D. R. & Maidment, L. W., 1988. *Applied Hydrogeology.* s.l.:McGraw-Hill.

CHU, S.-C., 1991. RANKINE'S ANALYSIS OF ACTIVE AND PASSIVE PRESSURES IN DRY SANDS. *Soils and Foundations,* Volume 31.4, pp. 115-120.

COMMEND, S. et al., 2016. *Computational Geomechanics on PC.* IV éd. Lausanne: Zace Services.

DAS, B. M. & SOBHAN, K., 2013. *Principles of geotechnical engineering.* s.l.:Cengage learning.

DI MOLFETTA, A. & SETHI, R., 2012. *Ingegneria degli acquiferi.* s.l.:Springer Science & Business Media.

DM-17/gennaio/2018, 2018. Norme Tecniche per le Costruzioni. *Gazzetta Ufficiale della Repubblica Italiana,* 42(6).

EICHENBERGER, J., 2013. *Geomechanical modelling of rainfall-induced landslides in partially saturated slopes.* s.l.:s.n.

EN1997, 2006. Eurocode 7-Geotechnical Design - General rules. *European Committee for Standardization (CEN).*

FREDLUND, D. G., MORGENSTERN, N. R. & WIDGER, R. A., 1978. The shear strength of unsaturated soils. *Canadian geotechnical journal,* Volume 15.3, pp. 313-321.

FREDLUND, D. G., RAHARDJO, H. & RAHARDJO, H., 1993. *Soil mechanics for unsaturated soils.* s.l.:John Wiley & Sons.

GARDNER, W. R., 1958. Some steady-state solutions of the unsaturated moisture flow equation with application to evaporation from a water table.. *Soil science,* Volume 85.4, pp. 228-232.

GEISER, F., 1999. *Comportement mécanique d'un limon non saturé.* s.l.:s.n.

HAINES, W. B., 1930. *On the existence of two equilibrium series in soil capillary phenomena.* Leningrad, Proc. Int. Congr. Soil Sci., 2nd.

HARRIS, A. & BOND, A. J., 2006. *Decoding eurocode 7.* s.l.:CRC Press.

JAKY, J., 1944. *J. of the Society of Hungarian Architects and Engineers,* pp. 355-358.

KEVORIKAN, J., 1993. *Partial Differential Equations: Analytical Solution Techniques.* s.l.:Springer Verlag.

LÓPEZ MARTÍN, L. Y., 2016. *Estudio del comportamiento tenso-deformacional de suelos parcialmente saturados en Cuba. Aplicaciones al cálculo de las deformaciones de las bases de las cimentaciones..* s.l.:PhD Thesis. Universidad Central “Marta Abreu” de Las Vil.

LU, N. & LIKOS, W. J., 2004. *Unsaturated soil mechanics.* s.l.:Wiley.

MAIONE, U., 1999. *Le piene fluviali.* s.l.:La Goliardica Pavese.

MENDES, J. e. a., 2018. On the development of an Ultra-High Capacity Tensiometer capable of measuring water tensions to 7 MPa. *Géotechnique,* Volume 1-5.

MeteoSwiss, 2016. *Federal Office of Meteorology and Climatology MeteoSwiss.* [En ligne] Available at: https://www.meteoswiss.admin.ch/home/climate/swiss-climate-in-detail/extreme-value-analyses/standard-period.html?station=sio

MUÑOZ-CASTELBLANCO, J. A. e. a., 2010. *Suction measurements on a natural unsaturated soil: A reappraisal of the filter paper method.* s.l., CRC Press, pp. 707-712.

RHOADES, J. D., RAATS, P. A. C. & PRATHER, R. J., 1976. Effects of Liquid-phase Electrical Conductivity, Water Content, and Surface Conductivity on Bulk Soil Electrical Conductivity 1. *Soil Science Society of America Journal,* Volume 40.5, pp. 651-655.

SAHOO, J. P. & GANESH, R., 2017. Active Earth Pressure on Retaining Walls with Unsaturated Soil Backfill. Dans: *In: International Congress and Exhibition "Sustainable Civil Infrastructures: Innovative Infrastructure Geotechnology".* s.l.:Springer, Cham, pp. p. 1-19.

SALAGER, S., NUTH, M., Ferrari, A. & LALOUI, L., 2013. Investigation into water retention behaviour of deformable soils. *Canadian Geotechnical Journal,* 2(50), pp. 200-208.

SHARMA, R. S. & MOHAMED, M. H. A., 2003. Patterns and mechanisms of migration of light non-aqueous phase liquid in an unsaturated sand. *Geotechnique,* Volume 53.2, pp. 225-239.

SIEMENS, G. A., 2017. Thirty-Ninth Canadian Geotechnical Colloquium: Unsaturated soil mechanics—bridging the gap between research and practice. *Canadian Geotechnical Journal,* Volume 55.7, pp. 909-927.

SPEIGHT, J. G. e. a., 2005. *Lange's handbook of chemistry.* New York: McGraw-Hill.

TERZAGHI, K., 1936. The shearing resistance of saturated soils and the angle between the planes of shear. *First international conference on soil Mechanics,* Volume 1, pp. 54-59.

TERZIS, D., 2017. *Mechanics and Micro-structure of Bio-cemented Soils Kinetics.* Lausanne: EPFL.

TOLL, D. G. e. a., 2008. *Unsaturated Soils: Advances in Geo-Engineering: Proceedings of the 1st European Conference on Unsaturated Soils.* Durham, UK, Taylor and Francis.

TRUTY, A. & OBRZUD, R., 2011. *The Hardening soil model–a practical guidebook.* Lausanne: Zace Services Ltd, Software engineering.

VAN GENUCHTEN, M. T., 1980. A closed-form equation for predicting the hydraulic conductivity of unsaturated soils. *Soil science society of America journal,* Volume 44.5, pp. 892-898.

VANAPALLI, S. K., 2009. *Shear strength of unsaturated soils and its applications in geotechnical engineering practice.* New Castle, Australia, Keynote Address. Proc. 4th Asia-Pacific Conf. on Unsaturated Soils.

YUAN, F. & LU, Z., 2005. Analytical solutions for vertical flow in unsaturated, rooted soils with variable surface fluxes. *Vadose Zone Journal,* Volume 4.4, pp. 1210-1218.

ZAPATA, C. E. & HOUSTON, W. N., 2008. *Calibration and validation of the enhanced integrated climatic model for pavement design..* s.l.:Transportation Research Board.

# Annex A) Used codes for LEM and LEP steady state analysis

```
%% computation of the active force exerted on a retainig wall by unsaturated
soil by adopting the Rankine method
%results are contained in the A vector (active force exerted on the wall)
%and on the YG vector (cointaining the y axis of the centroid)

%%
clear all
close all
clc
%% SOIL PARAMETERS:
gamma_sat=21;       % specifc saturated weight [kN/m^2]
gamma_dry=17;          % specifc dry weight [kN/m^2]
ks=1*10^-7;            % saturated hydraulic conductivity [m/s]
phi=32*pi/180;         % soil effective internal friction angle [rad]
c=5;                   % soil effective cohesion [kN/m]
%%
%% SUCTION STRESS PARAMETERS:
ua=0;                % pore aire pressure [kPa]
gamma_water=9.806;   % specific weight of water [kN/m^2]
alpha=2.26*10^-2;    % approximate the inverse of the air entry value [kPa^-1]
n=6.34;              % related to soil's pore size [-]
m=0.13;              % related to soil's pore size close to 1-1/n [-]
q=-(1*10^-7);        % flow rate (one dimension) [m/s]
%%
%% GEOMETRIC PARAMETERS:
H=3;     % wall height [m]
H0=0;    % depth of water table below the base of the wall [m]
%%
%% CALCULATION OF SUCTION STRESS:
Y=0:(H/100):H; % y-axis zero placed at the bottom of the wall [m]
suction=(-1/alpha)*(log((1+(q/ks))*exp(-gamma_water*alpha*(H0+Y))-(q/ks)));
%suction (ua-uw)[kN/m^2]
chi=(1./(1+(alpha*(suction)).^n)).^m; %effective stress [-]
sig =chi.*suction; %suction stress [kN/m^2]
%%% creating a sigma vector(New_sig function of different flux (q1)
q1=-[0 100 1000 2500 5000 7500 9999.99]*10^-11; %flux vector that goes from -
10^-6 to -10^-10
New_sig=zeros(length(q1),length(Y)); %initzializing the New_sig matrix
for ii=1:length(q1)
    New_sig(ii,:)=(-1/alpha)*((log((1+(q1(ii)/ks))*exp(-
alpha*gamma_water*(H0+Y))-(q1(ii)/ks))./((1+(-log((1+(q1(ii)/ks))*exp(-
gamma_water*alpha*(H0+Y))-(q1(ii)/ks))).^n).^m)); %suction stress [kN/m^2]
end
%%% creating a sigma vector(Nsig function of different water table depth (H0)
HH0=[0 0.5 1 2 4 8]; %depth of the water table [m]
Nsig=zeros(length(HH0),length(Y)); %initzializing the Nsig matrix
for a7=1:length(HH0)
    Nsig(a7,:)=(-1/alpha)*((log((1+(q/ks))*exp(-alpha*gamma_water*(HH0(a7)+Y))-
(q/ks))./((1+(-log((1+(q/ks))*exp(-gamma_water*alpha*(HH0(a7)+Y))-
(q/ks))).^n).^m)); %suction stress [kN/m^2]
end
%% CALCULATION OF HORIZONTAL STRESS:
Ka=tan(pi/4-phi/2)*tan(pi/4-phi/2); % active earth pressure when c'=0 [-]
ssw=((gamma_sat*(H-Y))-ua)*Ka; %soil self weight [kN/m^2]
mc=2*c*sqrt(Ka); % mobilized cohesion [kN/m^2]
hs=ssw-mc-sig*(1-Ka); %horizontal stress [kN/m^2]
```

```
hs_neg= hs(hs >= min(hs) & hs <=0); %vector containing negative values of hs
hs_pos= hs(hs > 0 & hs <= max(hs)); %vector containing positive values of hs
%horizontal stress for different flux
hs1=zeros(length(q1),length(Y));
for a1=1:length(q1)
hs1(a1,:)=ssw-mc-New_sig(a1,:)*(1-Ka);%horizontal stress [kN/m^2]
end
%horizontal stress for different watwer tabel depth
hs2=zeros(length(HH0),length(Y));
for a2=1:length(HH0)
hs2(a2,:)=ssw-mc-Nsig(a2,:)*(1-Ka);%horizontal stress [kN/m^2]
end
%creating hs1 & hs2 positive matrix
hs1_pos=zeros(length(q1),length(Y));
for a3=1:length(q1)
    for a4=1:length(Y)
        if hs1(a3,a4)>0
           hs1_pos(a3,a4)=hs1(a3,a4);
        end
    end
end
hs2_pos=zeros(length(HH0),length(Y));
for a5=1:length(HH0)
    for a6=1:length(Y)
        if hs2(a5,a6)>0
           hs2_pos(a5,a6)=hs1(a5,a6);
        end
    end
end

%% CALCULATION OF YG fore the positive value of hs (hs_pos)
Ai=zeros((length(hs_pos)-1),1); %initzializing the Ai vector (area of the
trapezoid)
ygi=zeros((length(hs_pos)-1),1); %initzializing the ygi vector (centroid of Ai)
yi=zeros((length(hs_pos)-1),1); %initzializing the yi vector (distance of the
lower side of Ai from the bottom of the wall)
%computation of Ai, ygi and yi
for t2=1:(length(hs_pos)-1)
    Ai(t2)=(((hs_pos(t2)+hs_pos(t2+1))*(H/100)/2));
    ygi(t2)=((H/300)*((hs_pos(t2)+hs_pos(t2+1)))/(hs_pos(t2)+hs_pos(t2+1)));
    yi(t2)=H/100*(t2-1);
end
Sy=sum(Ai.*(ygi+yi)); %First moment of area
A=sum(Ai) %total area of the trpezoids (active pressure force on the wall)
YG=Sy/A; %y value of the crentroid (the axis is placed at the bottom of the wall
and pointing upward)




%% computation of the active force exerted on a retainig wall by unsaturated
soil by adopting the LEM method
% the results are given in the vectors sol1 sol2 sol3;
%sol(1,1) contain the active force in kN, while sol(1,2) the angle that maximize
the sol(1,1).
%%
clear all
close all
```

```
clc
%% SOIL PARAMETERS:
gamma_sat=21;     % specifc weight [kN/m^2]
gamma_dry=17;        % specifc weight [kN/m^2]
ks=1*10^-7;          % saturated hydraulic conductivity [m/s]
phi=32*pi/180;       % soil effective internal friction angle [rad]
c=5;                 % soil effective cohesion UNSATURATED [kN/m]
cc=5;                % soil effective cohesion [kN/m]
%%
%% SUCTION STRESS PARAMETERS:
gamma_water=10;   % specific weight of water [kN/m^2]
alpha=2.26*10^-2;     % approximate the inverse of the air entry value [kPa^-1]
n=6.34;               % related to soil's pore size [-]
m=0.13;               % related to soil's pore size close to 1-1/n [-]
q=-(9*10^-8);         % flow rate (one dimension) [m/s]
ua=0;                 %air pressure [kPa]
%%
%% GEOMETRIC PARAMETERS:
i=0*pi/180;      % angle between the wall and the vertical counterclockwise [rad]
b=0*pi/180;      % (only for non horizontal backfill) angle between the backfill
and horizontal clockwise [rad]
H=3;             % wall height [m]
H0=0;            % depth of water table below the base of the wall [m]
%% OTHER PARAMETER:
delta=0*pi/180;       % soil-wall friction angle [rad]
Cw=0;                 %tangential adhesive force acting at soil-wall interface
[kN]
%% CALCULATION OF THE WEDGE WEIGHT:
o=0.0175:0.0175:90*0.0175; % angles between horizontal and failure surface
counterclockwise [rad]
W=((gamma_sat*(H^2))/2)*((cos(o-i))./(cos(i)*sin(o)));  % saturated wedge weight
[kN]
Wd=((gamma_dry*(H^2))/2)*((cos(o-i))./(cos(i)*sin(o))); % dry wedge weight [kN]
imult=[0.0175*0,0.0175*5,0.0175*10,0.0175*15,0.0175*20];% different wall
inclination [rad]
Wi=zeros(length(imult),length(o));                      % initzialaizing weight
matrix #imult rows #o columns [kN]
for as=1:length(imult)
Wi(as,:)=((gamma_sat*(H^2))/2)*((cos(o-imult(as)))./(cos(imult(as))*sin(o)));
end
%% CALCULATION OF SUCTION STRESS:
Y=0:(H/100):H; % y-axis zero placed at the bottom of the wall [m]
suction=(-1/alpha)*(log((1+(q/ks))*exp(-gamma_water*alpha*(H0+Y))-(q/ks)));
%suction (ua-uw)[kN/m^2]
chi=(1./(1+(alpha*(suction)).^n)).^m; %effective stress [-]
sig =chi.*suction; %suction stress [kN/m^2]
Sig=(-1/alpha)*((log((1+(q/ks))*exp(-alpha*gamma_water*(H0+Y))-(q/ks))./((1+(-
log((1+(q/ks))*exp(-gamma_water*alpha*(H0+Y))-(q/ks))).^n).^m)); %suction stress
[kN/m^2]
%%% creating a sigma vector(New_sig function of different flux (q1)
%4000 5000 6000 7000 8000 9000 9999.99 0 100 1000 2500 5000 7500 9999.99
q1=-[4000 5000 6000 7000 8000 9000 9999.99]*10^-11; %flux vector that goes from
-10^-7 to -10^-11
New_sig=zeros(length(q1),length(Y)); %initzializing the New_sig matrix
for ii=1:length(q1)
    New_sig(ii,:)=(-1/alpha)*((log((1+(q1(ii)/ks))*exp(-
alpha*gamma_water*(H0+Y))-(q1(ii)/ks))./((1+(-log((1+(q1(ii)/ks))*exp(-
gamma_water*alpha*(H0+Y))-(q1(ii)/ks))).^n).^m)); %suction stress [kN/m^2]
end
%%% creating a sigma vector(Nsig function of different water table depth (H0)
HH0=[0 0.5 1 2 4 8]; %depth of the water table [m]
```

```
Nsig=zeros(length(HH0),length(Y)); %initzializing the Nsig matrix
for a7=1:length(HH0)
    Nsig(a7,:)=(-1/alpha)*((log((1+(q/ks))*exp(-alpha*gamma_water*(HH0(a7)+Y))-
(q/ks))./((1+(-log((1+(q/ks))*exp(-gamma_water*alpha*(HH0(a7)+Y))-
(q/ks))).^n).^m)); %suction stress [kN/m^2]
end
%% CALCULATION OF ACTIVE EARTH FORCE(by discretizing suction stress):
PSig=zeros((length(sig)-1),1); %initzializing the PSig vector
for t=1:(length(sig)-1)
    PSig(t)=((sig(t)+sig(t+1))*(H/100)/2);
end
Cf=c*H./sin(o);  % tangential cohesive force along failure surface UNDRAINED[kN]
Cv=cc*H./sin(o); % tangential cohesive force along failure surface [kN]
PSIG=sum(PSig)./sin(o);
Pa1=(W.*sin(o-phi)-Cw*sin(o-phi-i)-Cf*cos(phi)-PSIG*sin(phi))./(cos(-i-delta-
phi+o)); %active earth force [KN]
[PaMax1,I]=max(Pa1);
%computing different Force by changing the flux (q1)
New_Psig=zeros(length(q1),(length(Y)-1)); %initzializing the New_Psig vector
for tt=1:length(q1)
    for jj=1:(length(Y)-1)
   New_Psig(tt,jj)=((New_sig(tt,jj)+New_sig(tt,jj+1))*(H/100)/2);
    end
end
Neew_PSIG=zeros(length(q1),(length(o))); %initzializing the New_PSIG vector
for ff=1:length(q1)
    Neew_PSIG(ff,:)=sum(New_Psig(ff,:))./sin(o);
end

% NEW_PA=(W.*sin(o-phi)-Cw*sin(o-phi-i)-Cf*cos(phi))./(cos(-i-delta-phi+o));
NEW_PA=(W.*sin(o-phi)-Cw*sin(o-phi-i)-Cf*cos(phi)-Neew_PSIG*sin(phi))./(cos(-i-
delta-phi+o));

%computing different Force by the water table depth (HH0)
NPsig=zeros(length(HH0),(length(Y)-1)); %initzializing the NPsig vector
for a8=1:length(HH0)
    for a7=1:(length(Y)-1)
   NPsig(a8,a7)=((Nsig(a8,a7)+Nsig(a8,a7+1))*(H/100)/2);
    end
end
NPSIG=zeros(length(HH0),(length(o))); %initzializing the NPSIG vector
for a9=1:length(HH0)
    NPSIG(a9,:)=sum(NPsig(a9,:))./sin(o);
end
NWPA=(W.*sin(o-phi)-Cw*sin(o-phi-i)-Cf*cos(phi)-NPSIG*sin(phi))./(cos(-i-delta-
phi+o));

%% CALCULATION OF ACTIVE EARTH FORCE:
Fsig=@(y) (-(log((1+(q/ks))*exp(-alpha*gamma_water*(H0+y))-
(q/ks))./(alpha*((1+(-log((1+(q/ks))*exp(-alpha*gamma_water*(H0+y))-
(q/ks))).^n)).^m)); %function of Sig
Psig=integral(Fsig,0,H)./sin(o); % computation of the integral divided by sin(o)
Pa2=(W.*sin(o-phi)-Cw*sin(o-phi-i)-Cf*cos(phi)-Psig*sin(phi))./(cos(-i-delta-
phi+o)); %active earth force [KN]
[PaMax2,J]=max(Pa2)
%% CALCULATION OF THE ACTIVE EARTH FORCE SATURATED CASE
PaSat=(W.*sin(o-phi)-Cw*sin(o-phi-i)-
Cv*cos(phi)+((0.5*gamma_water*H^2)./sin(o))*sin(phi))./(cos(-i-delta-phi+o));
%active earth force [KN]
[PaSatMax,K]=max(PaSat);
%% CALCULATION OF THE ACTIVE EARTH FORCE DRY CASE
```

```
PaDry=(Wd.*sin(o-phi)-Cw*sin(o-phi-i)-Cv*cos(phi))./(cos(-i-delta-phi+o));
%active earth force [KN]
[PaDryMax,qq]=max(PaDry);
%% plotted values %%
SIG=zeros(length(q1),length(Y)); %initzializing the SIG matrix
SUCTION=zeros(length(q1),length(Y)); %initzializing the SUCTION matrix
CHI=zeros(length(q1),length(Y));  %initzializing the CHI matrix
for ii=1:length(q1)
    SIG(ii,:)=(-1/alpha)*((log((1+(q1(ii)/ks))*exp(-alpha*gamma_water*(H0+Y))-
(q1(ii)/ks))./((1+(-log((1+(q1(ii)/ks))*exp(-gamma_water*alpha*(H0+Y))-
(q1(ii)/ks))).^n).^m)); %suction stress [kN/m^2]
    SUCTION(ii,:)=(-1/alpha)*(log((1+(q1(ii)/ks))*exp(-
gamma_water*alpha*(H0+Y))-(q1(ii)/ks)));
    CHI(ii,:)=(1./(1+(alpha.*(-1/alpha)*(log((1+(q1(ii)/ks))*exp(-
gamma_water*alpha*(H0+Y))-(q1(ii)/ks)))).^n)).^m;
end
deltass=[0:0.0175:phi]; %soil-wall friction angle [rad]

 PAAA=zeros(length(deltass),length(o)); %initzializing PAAA matrix force exerted
function of (#length(deltass),#length(o))
for II=1:length(deltass)
    PAAA(II,:)=(W.*sin(o-phi)-Cw*sin(o-phi-i)-Cf*cos(phi)-Psig*sin(phi))./(cos(-
i-deltass(II)-phi+o)); %active earth force [KN]
end
PAA=zeros(length(q1),length(o),length(deltass));%initzializing PAA matrix(3D)
force exerted function of (#length(q1),#length(deltass),#length(o))
for aa=1:length(deltass)
PAA(:,:,aa)=(W.*sin(o-phi)-Cw*sin(o-phi-i)-Cf*cos(phi)-
Neew_PSIG*sin(phi))./(cos(-i-deltass(aa)-phi+o));
end
BBB=permute(PAA,[3 2 1]); % permuting PAA so that
(#length(q1),#length(deltass),#length(o))-->
(#length(o),#length(deltass),#length(q1))
Paa=zeros(length(q1),length(deltass));
for a1=1:length(q1)
    for a2=1:length(deltass)
    Paa(a1,a2)=max(BBB(a2,:,a1));
    end
end
AB=zeros(length(q1),length(o),length(i)); %%initzializing AB matrix(3D) force
exerted function of (#length(q1),#length(o),#length(imult)); (imult= deifferent
i angle)
for a3=1:length(imult)
    AB(:,:,a3)=(Wi(a3,:).*sin(o-phi)-Cw*sin(o-phi-imult(a3))-Cf*cos(phi)-
Neew_PSIG*sin(phi))./(cos(-imult(a3)-delta-phi+o));
end
ABi=zeros(length(q1),length(imult)); %%initzializing ABi matrix force exerted
function of (#length(q1),#length(imult))considering the value of o that maximize
the force
for a4=1:length(q1)
    for a5=1:length(imult)
    ABi(a4,a5)=max(AB(a4,:,a5));
    end
end



ACi=zeros(length(imult),length(o)); %%initzializing ACi matrix force exerted
function of (#length(o),#length(imult))considering just one flux (the q)
for a6=1:length(imult)
ACi(a6,:)=(Wi(a6,:).*sin(o-phi)-Cw*sin(o-phi-imult(a6))-Cf*cos(phi)-
Neew_PSIG(3,:)*sin(phi))./(cos(-imult(a6)-delta-phi+o));
```

```
end
ACib=zeros(length(imult),length(o)); %%initzializing ACi matrix force exerted
function of (#length(o),#length(imult))considering just one flux (the q)
for b1=1:length(imult)
ACib(b1,:)=(Wi(b1,:).*sin(o-phi)-Cw*sin(o-phi-imult(b1))-Cf*cos(phi)-
Neew_PSIG(7,:)*sin(phi))./(cos(-imult(b1)-delta-phi+o));
```

# Annex B) Used codes for LEM and LEP transient analysis

```
clear all;
clc
close all

%computing the thrust force exerted on a retaining wall adopting an
%unsteady hydrological model and the LEM model and rankine


%% SOIL PARAMETERS:
gamma_sat=21;        % specifc weight [kN/m^2]
gamma_dry=17;        % specifc weight [kN/m^2]
ks=1*10^-7;          % saturated hydraulic conductivity [m/s]
phi=32*pi/180;       % soil effective internal friction angle [rad]
c=5;                 % soil effective cohesion UNSATURATED [kN/m]
ccc=5;               % soil effective cohesion [kN/m]%%
%% SUCTION STRESS PARAMETERS:
gamma_water=10;        % specific weight of water [kN/m^2]
%alpha=2.26*10^-2;     % approximate the inverse of the air entry value [kPa^-1]
n=6.34;                % related to soil's pore size [-]
m=0.13;                % related to soil's pore size close to 1-1/n [-]
q=-(1*10^-11);          % flow rate (one dimension) [m/s]
ua=0;                  %air pressure [kPa]
%%
%% GEOMETRIC PARAMETERS:
ib=0*pi/180;     % angle between the wall and the vertical counterclockwise [rad]
b=0*pi/180;      % (only for non horizontal backfill) angle between the backfill
and horizontal clockwise [rad]
H=3;             % wall height [m]
H0=0;            % depth of water table below the base of the wall [m]
%% OTHER PARAMETER:
delta=0*pi/180;        % soil-wall friction angle [rad]
Cw=0;                  %tangential adhesive force acting at soil-wall interface
[kN]
%% CALCULATION OF THE WEDGE WEIGHT
o=0.0175:0.0175:90*0.0175; % angles between horizontal and failure surface
counterclockwise [rad]
We=((gamma_sat*(H^2))/2)*((cos(o-ib))./(cos(ib)*sin(o)));
Cf=c*H./sin(o);  % tangential cohesive force along failure surface UNDRAINED[kN]
Cv=ccc*H./sin(o); % tangential cohesive force along failure surface [kN]
Wa=((gamma_sat*(H^2))/2)*((cos(o-ib))./(cos(ib)*sin(o))); % wedge weight [kN]
Wd=((gamma_dry*(H^2))/2)*((cos(o-ib))./(cos(ib)*sin(o))); % dry wedge weight
[kN]
%% Hydrological transient Input data for Sion Silt
alpha = 0.006/(10.1974); %1/cm
n_SWRC = 6.34;
m_SWRC = 0.13;
ksat = 0.036; %cm/h
l = 300; %cm
teta_sat = 0.35; %porosity n
teta_res = teta_sat*0.17; % n*Sr,res
fi = 32*pi/180;
kA = (tan(pi/4-fi/2))^2;
rain_time = 1000;% ore
D = ksat/(alpha*(teta_sat-teta_res));
q0 =0;%cm/h
q1 = -ksat;
```

```
countz = 0;
for asd = 0 : 0.1 : l/100
    countz = countz + 1;
    vertical(countz,1) = asd;
end

%% Zero Function
count = 0;
time_count = 0;

z_count = 0;
h=zeros(1, 5001);
for i = 0 : 0.002 : 10

            count = count + 1;

            h(count) = fzero(@(x)fun(x,l,alpha),i);

end

cc=unique(round(h*10000000000))/10000000000;
%% Sum

for z = 0 : 10: l

    z_count = z_count + 1;

    for time = 0 : 10 : rain_time

        time_count = time_count + 1;

        for i = 1 : size (cc,2)

            x = cc(i);

            W (i, z_count) =
(sin(l*x)*sin(z*x))/((alpha^2)*l+2*alpha+4*l*(x)^2);

%             Q(i, time_count) =
integral(@(tau)Q_integrand(tau,x,alpha,q0,k,delta,D,time),0,time);

              Q(i, time_count) = exp(-D*(x^2+(alpha^2)/4)*time);

            prodotto (i, z_count, time_count) = W (i, z_count)*Q(i, time_count);
        end

        count = 0;

    end

    time_count = 0;

end

z_count = 0;
```

```
sommatoria = sum(prodotto,1);

 for z = 0 : 10: l

     z_count = z_count + 1;

     phi_s (z_count) = ksat*exp(alpha*(-z))/alpha + q1 /alpha*(exp(-alpha*z) -
1);
     A (z_count) = -8*(q0-q1)*exp(alpha*(l-z)/2);

 end
 %% Tot_Potential, Suction and volumetric water content


 for t = 1 : size(sommatoria,3)
     for z = 1 : size(sommatoria,2)

         total_potential(z,t) = phi_s(1,z) + A(1,z)*sommatoria(1,z,t);
         hydraulic_head (z,t) = +1/alpha*log(alpha/ksat*total_potential(z,t));
         teta(z,t) = teta_res+(teta_sat-
teta_res)*exp(alpha*hydraulic_head(z,t));

         shear_stress_parameter (z,t) = (teta(z,t)-teta_res)/(teta_sat-
teta_res);
         degree_of_saturation (z,t) = (1/(1+(alpha*(10.1974)*(-
hydraulic_head(z,t))/100*9.80638)^n_SWRC))^m_SWRC;


     end
 end

%% LEM
% (New_sig) suction stress at different time --> (31=depth,101=time) [kPa]
%shear_stress_parameter--> Sr [-]
%hydraulic_head/100*9.80638*(-1)--> PWP [kPa]
New_sig=shear_stress_parameter.*hydraulic_head/100*9.80638*(-1);
Pwp=hydraulic_head/100*9.80638*(-1); % [kPa]
SR=shear_stress_parameter; % [-]
%initzializing the (New_Psig) matrix --> areas for the computation of the
integral (31,100)
New_Psig=zeros((length(vertical)-1),(size(New_sig,2)));
for tt=1:(size(New_sig,2))
    for jj=1:(length(vertical)-1)
   New_Psig(jj,tt)=((New_sig(jj,tt)+New_sig(jj+1,tt))*(0.1)/2);
    end
end
%initzializing the (New_PSIG) vector --> sum of the areas;
for ff=1:size(New_Psig,2)
    New_PSIG(1,ff)=sum(New_Psig(:,ff));
end
%initzializing the (NAA) matrix --> placing (New_PSIG) in each  rows (90)
NAA=zeros(length(o),size(New_Psig,2));
for iii=1:length(o)
    NAA(iii,:)=New_PSIG;
end
% computing the active suction force on each failure surface
NAA=(NAA')./sin(o);
% computing (NEW_PA) the force exerted on the wall for each failure surface
% and at each time step flux [kN];
```

```
NEW_PA=(We.*sin(o-phi)-Cw*sin(o-phi-ib)-Cf*cos(phi)-(NAA)*sin(phi))./(cos(-ib-
delta-phi+o));
% computing the max value of the force for each time
NEW_PA_max=zeros(1,size(New_Psig,2));
for a7=1:size(New_Psig,2)
    NEW_PA_max(a7)=max(NEW_PA(a7,:));
end
%% sat stationary
PaSat=(Wa.*sin(o-phi)-Cw*sin(o-phi-ib)-
Cv*cos(phi)+((0.5*gamma_water*H^2)./sin(o))*sin(phi))./(cos(-ib-delta-phi+o));
%active earth force [KN]
PaSatMax=max(PaSat);

%% dry stationary
PaDry=(Wd.*sin(o-phi)-Cw*sin(o-phi-ib)-Cv*cos(phi))./(cos(-ib-delta-phi+o));
%active earth force [KN]
PaDryMax=max(PaDry);


%% RANKINE %%

% CALCULATION OF HORIZONTAL STRESS:
Ka=tan(pi/4-phi/2)*tan(pi/4-phi/2); % active earth pressure when c'=0 [-]
ssw=((gamma_sat*(H-vertical))-ua)*Ka; %soil self weight [kN/m^2]
mc=2*c*sqrt(Ka); % mobilized cohesion [kN/m^2]

%horizontal stress for different flux
hs1=zeros(length(vertical),size(New_Psig,2));
for a1=1:size(New_Psig,2)
hs1(:,a1)=ssw-mc-New_sig(:,a1)*(1-Ka);%horizontal stress [kN/m^2]
end
%creating hs1 & hs2 positive matrix
hs1_pos=zeros(length(vertical),size(New_Psig,2));
for a4=1:size(New_Psig,2)
    for a3=1:length(vertical)
        if hs1(a3,a4)>0
           hs1_pos(a3,a4)=hs1(a3,a4);
        end
    end
end
%computing the integral of hs1_pos along the vertical
hs1_pos_areas=zeros(length(vertical),size(New_Psig,2));
hs1_pos_integral=zeros(1,size(New_Psig,2));
for a5= 1:1:size(New_Psig,2)
    for a6=1:(length(vertical)-1)
        hs1_pos_areas(a6,a5)=((hs1_pos(a6,a5)+hs1_pos(a6+1,a5))*0.05);
        hs1_pos_integral(a5)=sum(hs1_pos_areas(:,a5));
    end
end
%% sat stationary
SAT=0.5*(gamma_sat-gamma_water)*H*H*Ka+((gamma_water*H^2)/2)-2*ccc*sqrt(Ka)*H;
rsat=ones(1,length(o))*SAT;
%% dry stationary
DRY=0.5*(gamma_dry)*H*H*Ka-2*ccc*sqrt(Ka)*H;
rdry=ones(1,length(o))*DRY;
```